Thermodynamic Performance Evaluation and Experimental Study of a Marnoch Heat Engine

By

Pooya Saneipoor

A Thesis Submitted in Partial Fulfillment

of the Requirements for the Degree of

Master of Applied Science in Mechanical Engineering

Faculty of Engineering and Applied Science

University of Ontario Institute of Technology

October 2009

© Pooya Saneipoor, 2009

Abstract

The Marnoch Heat Engine (MHE) is a recently patented type of new heat engine that produces electricity from lower temperature heat sources. The MHE utilizes lower temperature differences to generate electricity than any currently available conventional technologies. Heat can be recovered from a variety of sources to generate electricity, i.e., waste heat from thermal power plants, geothermal, or solar energy. This thesis examines the performance of an MHE demonstration unit, which uses air and a pneumatic piston assembly to convert mechanical flow work from pressure differences to electricity. This thesis finds that heat exchangers and the piston assembly do not need to be co-located, which allows benefits of positioning the heat exchangers in various configurations. This thesis presents a laboratory-scale, proof-of-concept device, which has been built and tested at the University of Ontario Institute of Technology, Canada. It also presents a thermodynamic analysis of the current system. Based on the MHE results, component modifications are made to improve the thermal performance and efficiency. The current configuration has an efficiency of about thirty percent of the maximum efficiency of a Carnot heat engine operating in the temperature range of 0^{o}C to 100^{o}C. The analysis and experimental studies allow future scale-up of the MHE into a pre-commercial facility for larger scale production of electricity from waste heat.

Key Words

Marnoch Heat Engine; Heat Recovery; Energy; Exergy; Efficiency, Power Cycle; Carnot Cycle.

Dedication

This research is dedicated to Ian Marnoch.

Acknowledgments

I am highly indebted to several people for their extended help given to me during the work of this entire thesis. This would not have been possible without them. It is a pleasure to thank those who made this possible and I would like to express my sincere gratitude and appreciation to my co-advisors: Professor Greg Naterer and Professor Ibrahim Dincer for providing me the unique opportunity to work in this research area under their expert guidance. I owe my deepest gratitude to Mr. Ian Marnoch who has helped me all the way. He made available his support in a number of ways. The most valuable source was his wealth of knowledge that helped me in completing this thesis.

Also, support of this research from Marnoch Thermal Power, the Ontario Centres of Excellence and OPA is gratefully appreciated.

I am also indebted to many of my colleagues: O. Jaber, P. Bahadorani, S. Garmisiry, P. Regulagada, H. Nojoumi, R. Rashidi, V. Balah, and A. Odukoya who have helped me in terms of guidance and moral support.

In the end, I would like to express my honest and eternal gratitude towards my parents: Darab and Masoudeh, to my siblings: Parya, Peyman, and also to Hamid and Shervin who have been really influential. They have shown everlasting and unconditional love, support and encouragement. Thank you for your concerns, which gave me a chance to prove and improve myself through all phases of my life.

Table of Contents

List of Tables

List of Figures

Nomenclature

A	=	area [m^2]
AD	=	angular distance [^{o}]
c	=	specific heat capacity [J/kg.K]
C	=	constant
D	=	diameter [m]
f	=	force [N]
F	=	friction factor
Ex	=	exergy [J]
G	=	gravitational acceleration [m/s^2]
h	=	head loss [m]
Jm	=	rotational mass moment of inertia [$kg.m^2$]
k	=	loss coefficient
K	=	radius of gyration [m]
KE	=	kinetic energy [J]
L	=	Length [m]
m	=	mass [kg]

P = pressure [Pa]

Re = Reynolds number

RT = rotational time [s]

RPM = number of revolutions per minute

R = gas constant for dry air [J/kg.K]

SRDR = shaft rotation per revolution [^{o}]

T = temperature [K]

V = velocity [m/s]

Vol = volume [m^3]

X = piston length [m]

Z = height [m]

$\dot{m}$ = mass flow rate [kg/s]

Greek Letters

Γ = exergetic temperature factor

τ = torque (N.m)

η = efficiency

Δ = change

Subscripts

0	=	dead state (ambient condition)
1, 2,...	=	state 1, 2, ...
a	=	air
apl	=	all piston losses
d	=	destroyed
e	=	electric
fa	=	from air
fpc	=	friction between the sealing and the cylinder body
frp	=	friction between rack and pinion
fw	=	from water
gen	=	generated
i	=	point number
in	=	inlet
out	=	outlet
p	=	piston
Q loss	=	heat loss

t	=	total
ta	=	to air
tw	=	to water
w	=	water

Acronyms

DAQ	=	Data Acquisition System
OCE	=	Ontario Centres of Excellence
OPA	=	Ontario Power Authority
UOIT	=	University of Ontario Institute of Technology
IDB	=	International Data Base
MHE	=	Marnoch Heat Engine
NSP	=	Number of strokes per minute
LTD	=	Low-temperature differential
PLC	=	Programmable Logic Controller
PVC	=	Polyvinyl chloride

Chapter 1:

Introduction

1.1 Energy and Its Importance

The population around the world is rapidly growing. Even though many countries have initiated new policies to reduce this growth rate, which averages 2% per annum, the issue still persists [1]. It is predicted that the population will double by the year 2050 [2]. This population growth will create a huge demand for energy. World energy demand in 2003 had increased by 20% in comparison to the nineties. More than half of the world's energy was consumed by around 950 million people in industrialized countries [3]. Oil has been considered as a major source of energy ever since. Total world oil demand is expected to increase from 77 million barrels in 2003 to about 119 million barrels in 2025, a 55% increase [3]. Uneven distribution of world resources and the resulting dependence of many countries on politically unstable nations, raise concerns about energy security [3].

In 2004, a research study by the Pembina Institute in Canada showed that electricity consumption during peak hours by the year 2020 could be reduced to 30% below the 2004 levels, through a series of energy efficiency and demand reduction policies [4]. Energy is one of the key needs of modern society. Since the Industrial Revolution, developed nations have primarily relied on fossil fuels for their energy needs. This fossil fuel consumption has contributed to environmental pollution and carbon dioxide emissions. Carbon dioxide comprises 82.3% of greenhouse gases and it is considered to be the main greenhouse gas, which is linked to climate change and

global warming [5]. Furthermore, there are limited fossil fuel resources in the world, which will eventually be exhausted [6].

Global warming is a major issue that has to be considered in regards to energy production. Clean and sustainable energy resources are now preferable, together with the more efficient use of fossil fuels. Renewable energy resources are one of the most promising solutions for this energy demand. World contributions of coal, oil, gas, nuclear and biomass in the current energy supply are shown in Figure 1.1. From this figure and information from the International Energy Agency (IEA), more than 60% of the total required global energy is being supplied by fossil fuels [7]. These statistics differ from one region to another. For instance presently, the USA is nearly as dependent on fossil fuels (85% in 2007) as it was 93% in 1973 [8].

Figure 1.1 shows significant continual growth of nuclear energy after year 2020. Nuclear technologies have been safe and reliable when used with precaution. Some countries may be unwilling to employ nuclear power on a larger scale [9]. The demand for these nuclear power plants and their capacity has to be increased, to satisfy our ever growing energy demands. Since nuclear power plants require large amounts of water for cooling, the majority of these power plants are built beside lakes, rivers or seas. Hence, this water that cools the reactors will be drained to the surroundings. As a result, it increases the surrounding temperature and has effects on natural habitats [11]. One strong benefit of nuclear fuels is their high energy content. This energy is generated during the nuclear fission process. This process is initiated by a chain reaction using Uranium fuel. A nuclear reaction with U-235 releases more than 1.6 million times as much energy per gram in comparison to a chemical oxidation reaction of CH_4 [12].

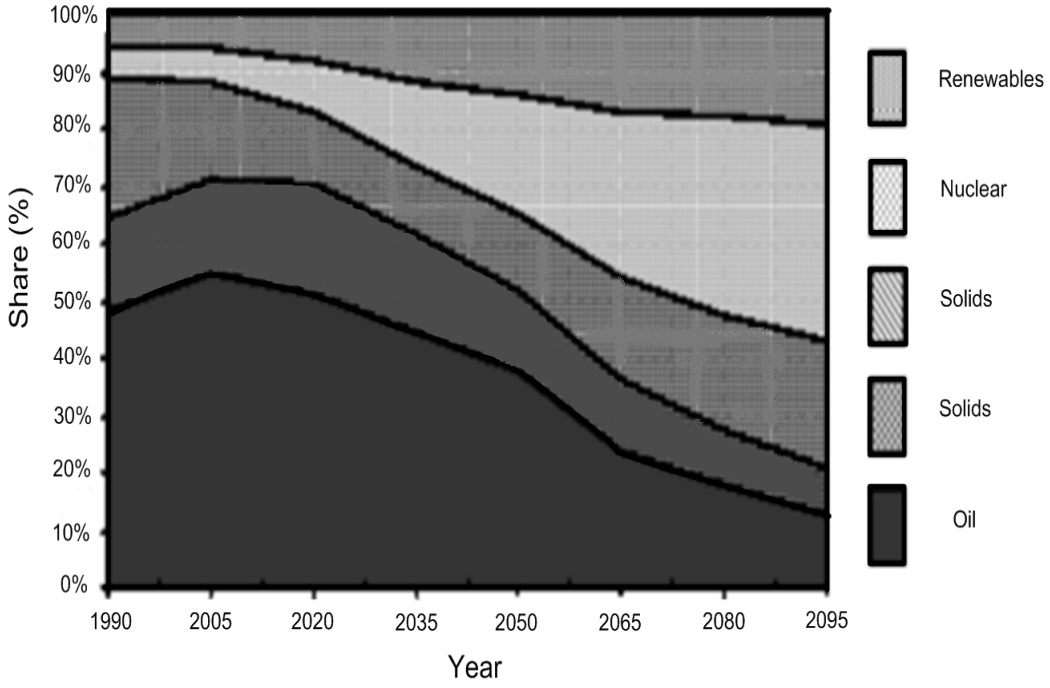

Figure 1.1: Distribution of energy from 1990 to 2095 (from [10]).

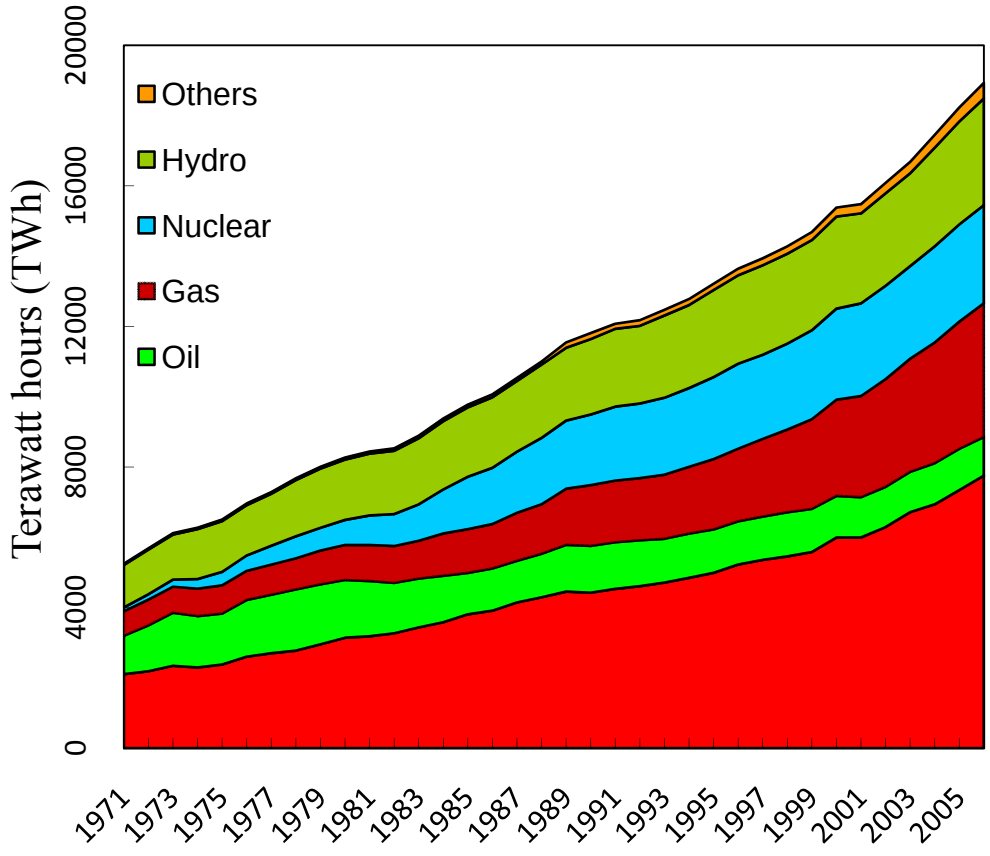

Figure 1.2: World electricity generation by source of energy (from [13]).

Figure 1.2 illustrates the world electricity generation by fuel type. The lowest region in the figure shows that coal power plants have a steady and vital share of electricity production in the world. The amount of coal in some countries like China and the United states is abundant and their energy demand is high, thus, these countries are building new coal power plants to meet this energy demand in the future. Coal power plants are the single largest source of some of the worst air pollutants, including deadly particulate matter, acid-rain-formation by sulfur dioxide, and toxic mercury [14]. In power plants, several methods are being applied to increase the efficiency and also capture released greenhouse gasses. In order to increase the efficiency of these power plants, one way is to apply combined power generation cycles. This solution can increase the efficiency of these plants by almost 60% [15]. Another method to increase the power plant efficiency is to operate these power plants under higher pressures and temperatures, in comparison to conventional power plants [16, 17]. An example of a power plant working over the normal regulated pressure and temperature conditions is a power plant called the AD700 in Europe [18]. Commencement of this project AD700 took place in 1998 in Europe. In cases like these, the efficiency of a steam power plant can reach up to 55% [18]. Safety is one of the main concerns regarding these projects. Most of the advanced materials that are used incur large expenses and are hard to fabricate. Examples of such materials are different stainless steels, Inconel alloys, high-temperature ceramics, and coatings [19, 20]. Engineers have been trying to develop the most appropriate material for such projects. However, corrosion is still one of the main concerns in power plants [21, 22]. By increasing the efficiency of a power plant by even one percent, it can have significant gains for the reduction of greenhouse gas emissions to the environment.

Another process for reducing greenhouse gases is to use alternate renewable sources of energy. In the transportation sector, this can be achieved by electric vehicles powered with batteries, fuel cells on board, the combination of internal combustion engines with renewable energy sources in hybrid cars, or in aircraft [23, 24]. By using renewable sources of energy, it will be possible to generate the electricity in large quantities, to power different sectors of society. The most common renewable energy systems are hydroelectric, solar panels, wind turbines, tidal turbines, and geothermal heat sources.

Wind energy is a prime example of a sustainable energy resource. Because it is a non-polluting source of energy during power generation, it has no emissions or residues to burden society. However, it is limited by its site and intermittency; it stands out as a viable alternative to fossil fuels [25]. Some analysts estimate that wind energy will be limited to a maximum of 20% of the total installed generating capacity from all sources. Its role would be confined to displacing higher cost fossil fuels for electric generation [26].

Oceans are a major source of mechanical and thermal energy. Their energy can be converted to electricity using different methods. Ocean mechanical energy is quite different from ocean thermal energy. Even though the sun affects all ocean activities, tides are primarily driven by the gravitational pull of the moon and waves are driven by the winds. A barrage is typically used to convert tidal energy into electricity by forcing the water through turbines, thereby driving a generator. In favourable locations, wave energy density an average is 40 MW per kilometre of coastline [27].

Renewable sources of energy are not uniformly available everywhere. Some power generation systems like fuel cells are expensive and heavy in some applications

[28]. Fluctuations of energy sources in some cases are so high that we cannot rely on these resources for critical usage. Some of them require huge capital costs and it takes many years to repay that investment. For this reason, some countries stay with their old energy systems for power production. Hence, one of the best solutions to solve the problem of energy demand and pollution in the world is to increase the efficiency of major power generation systems like power plants. This is possible by effective use of energy recovery systems.

1.2 Motivation and Objectives

Marnoch heat engine can be used as an individual energy system or as a heat recovery system for producing green energy. Currently, there is a great demand for research and development of heat engines, which can produce electricity in industrial scales. Increasing the amount of electricity produced by the heat engines and their lifetime are two main goals of the researchers in this area.

This thesis performs a comprehensive thermodynamic performance investigation of the current Marnoch heat engine at UOIT. The main objectives of thesis are (i) energy and exergy analyses of the MHE, and (ii) experimental performance and data acquisition.

Furthermore, suggestions are made for the mechanical configuration of the future MHE prototype by using different components such as multiple tank pairs, and hydraulic systems.

Chapter 2:

Literature Review

Heat recovery systems recover the heat during exchange with other systems. In some cases, it converts and captures the heat in different forms of energy such as electricity. Energy recovered from such systems can be used after its recovery, or it can be stored for use during peak periods. In a number of other applications, cold thermal energy storage is applied for energy savings [29].

Energy recovery systems exist in several forms. In one method, energy is recovered in the form of compressed air [30, 31]. Compressed air energy storage gives the opportunity to increase the efficiency of wind powered energy systems. Such a recovery system stores energy, when in excess and subject to availability. It can then be used as backup during energy consumption peaks [32].

With pumping storage systems, it is possible to store energy at a lower consumption rate by pumping water onto an elevated reservoir during off-peak hours. During peak hours, hydropower energy can be produced by the release of this water to a lower level reservoir through a water turbine [33]. In such a pumping storage system cycle, electricity is converted to mechanical energy and back again to electricity. During these processes, some part of the stored energy is lost because of irreversibility within the energy conversion and storage systems.

Another category that can be used as a heat recovery system to produce electricity is heat engines. These systems can produce electricity using temperature differentials. In the next chapter, different heat engines and their operation will be discussed in detail.

2.1 Background

A heat engine system converts thermal energy to mechanical energy, using temperature gradients between the heat source and the heat sink. Cengel and Boles [34] outlined four main characteristics of heat engines as follows:

1. Heat engines receive heat from a high-temperature source.
2. These engines convert part of the heat to work (usually in the form of a rotating shaft).
3. They reject the remaining waste heat to a low-temperature sink (Environment).
4. They operate on the basis of a power-cycle.

The term heat engine is often used in a broader sense to include work-producing devices that operate in a thermodynamic cycle. Engines that involve internal combustion such as gas turbines and car engines fall into this category. These devices operate in a mechanical cycle, but not a closed thermodynamic cycle. The working fluid (combustion gases) in these heat engines do not go through a complete cycle. In these systems, instead of cooling the exhaust gases, fresh gas originates within the system.

All thermodynamic systems require a working substance. Generally working fluids are considered as the fluids moving through the equipment, often as gases. These gases can expand and compress easily. Common examples of working fluids in a thermodynamic system are air, steam and hydrogen.

Daley [35] reported that hydrogen, as a working fluid, permits the most compact engine design among any other working fluids (for a given power output and efficiency). Therefore, hydrogen has been the choice of Stirling development programs for automotive applications where engine size is a major concern. Daley

[35] stated that, systems using helium or air as a gaseous working fluid can be used where size is not an important factor.

Due to the molecular weight and size of hydrogen, those systems which use hydrogen as a working fluid have to be well contained. Hydrogen molecules can penetrate through most containment vessels that are available [36]. Air in the form of a working fluid has certain limitations, like poor heat conductivity as compared to hydrogen, in heat engines [37]. However, air as a working fluid is more preferable in many systems because it is freely available and it is not reactive.

2.2 Gas Power Cycles

Some important gas powered cycles are discussed in this section. Most gas power-cycles were originally developed in the nineteenth century [38]. Table 2.1 shows comparisons of processes for twelve different gas power-cycles.

These power-cycles consist of compressions and expansions of working fluids. The working fluid in a cylinder can be compressed by pushing a piston.

To calculate the work output from a heat engine system, the cyclic-work has to be calculated. Typically, gas power-cycles consist of four processes [39].

- Isothermal process: This process takes place at constant temperature.
- Isobaric process: During this process, pressure is constant.
- Isovolumetric process: A constant volume process is Isovolumetric.
- Adiabatic process: In this process, no heat is removed from the system and no heat is added to the system.

To calculate the work values of Equation (2.1), the area under the process line in Figure 2.1 has to be calculated. This value represents the work performed during each process.

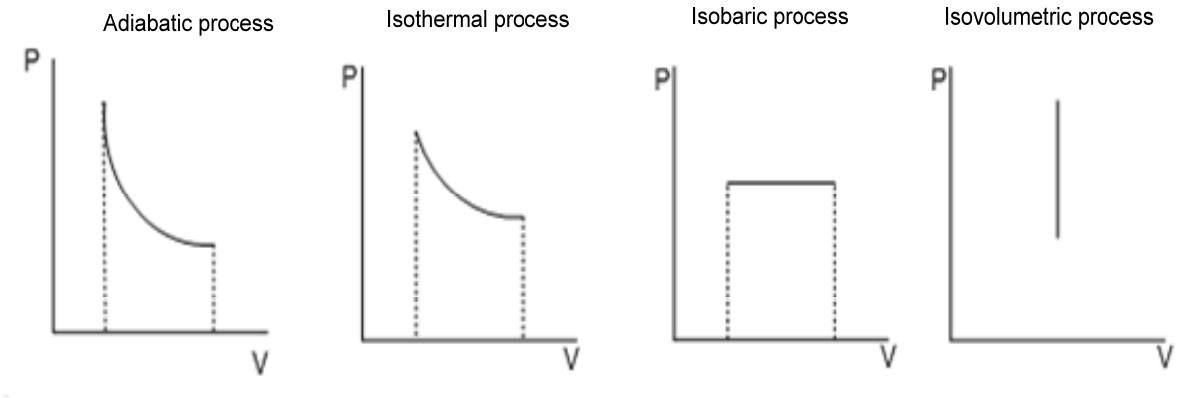

Figure 2.1: Four main thermodynamic processes in power-cycles.

2.2.1 The Carnot Cycle

In this section, essential details about the Carnot cycle are illustrated. This cycle is an ideal cycle and cannot be achieved in practice. Figure 2.2 shows the power-cycle of a Carnot heat engine. In a Carnot cycle, the system executing the cycle undergoes a series of four internally reversible processes. This includes two adiabatic processes and two isothermal processes.

Table 2.1 defines the steps for a Carnot heat engine. During the isothermal expansion process 3-4, referring Figure 2.2, the temperature of the reservoir is constant, and to keep this process reversible, the temperature difference between the heat reservoir and gas is small. The same condition exists for process 1-2 in Figure 2.2. In this process, isothermal compression takes place. The amount of heat that is being absorbed by the heat sink has to be exactly equal to the heat generated as a result of compression. Process 2-3 shows that the gas is compressed adiabatically. Process 4-1 in Figure 2.2 shows that the system is insulated, and the gas is allowed to continually expand adiabatically until the temperature reaches the heat sink temperature.

Table 2.1: Comparison of processes for different gas power-cycles

Cycle name	Process 1-2	Process 2-3	Process 3-4	Process 4-1
Atkinson cycle	Constant pressure	Adiabatic	Constant Volume	Adiabatic
Brayton cycle	Isobaric	Adiabatic	Isobaric	Adiabatic
Cayley cycle	Constant Pressure	Polytropic	Constant Pressure	Polytropic
Carnot cycle	Isothermal	Adiabatic	Isothermal	Adiabatic
Crossley cycle	Polytropic	Constant Volume	Polytropic	Constant Volume
Diesel cycle	Adiabatic	Constant Pressure	Adiabatic	Constant Volume
Ericsson cycle	Constant Pressure	Isothermal	Constant Pressure	Isothermal
Otto cycle	Adiabatic	Constant Volume	Adiabatic	Constant Volume
Rankine cycle	Isentropic	Isobaric	Isentropic	Isobaric
Reitlering cycle	Isothermal	Polytropic	Isothermal	Polytropic
Stirling cycle	Isothermal	Constant Volume	Isothermal	Constant Volume
Stoddard cycle	Adiabatic	Constant Pressure	Adiabatic	Constant Pressure

Source: [38, 40]

In each of the four internally reversible processes of the Carnot cycle, work can be represented by the enclosed area in Figure 2.2a. The areas under process lines 3-4 and 4-1 show the work done per unit mass by the gas, as it expands in these processes. The areas under curves 1-2 and 2-3, show the required work for compression in a Carnot cycle.

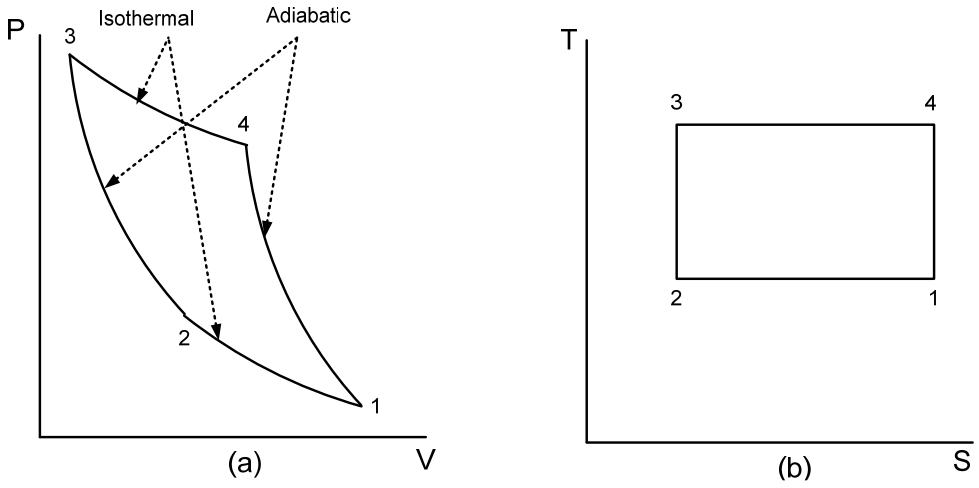

Figure 2.2: Carnot cycle (a) P-V diagram; (b) T-s diagram.

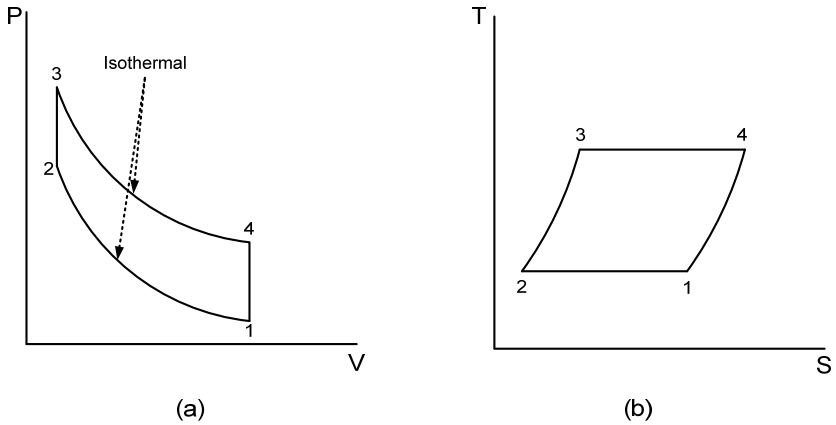

Figure 2.3: Stirling cycle (a) P-V diagram; (b) T-s diagram.

2.2.2 Stirling Cycle

The Stirling cycle is a well known power-cycle that represents the processes in a heat engine. A Stirling cycle uses a regenerator in its cycle. Figure 2.3 shows the related P-V and T-s diagrams for a Stirling cycle. This cycle consists of four internally reversible processes in series: isothermal compression from state 1 to state 2 at the heat sink temperature, constant volume heating from state 2 to state 3, isothermal expansion from state 3 to sate 4 at the heat source temperature, and constant volume cooling from state 4 to state 1. All heat addition and rejection during processes 3-4 and 1-2 occur in the isothermal processes [41].

2.3 Stirling Engines

The Stirling engine was invented by Robert Stirling in the year 1816 [42]. Its purpose was to function as a safer source for generating power than the steam engine. Steam engines had a common problem of having their hot water boilers explode from extreme buildup of pressure. During that time, Stirling engines were used for water pumps and fans. In the late 1800s they had become quite popular due to the fact that they were so dependable, safe, and easy to use [43]. The early 1900s brought a decline

for the Stirling engine as engines running on cheap fossil fuels appeared. In the 1940s and 1950s as gas prices rose, engineers started to see the first environmental effects of fossil fuel engines, so research and development on heat engines started again [44].

One of the most important features of a heat engine is that many fuel sources can be used to operate them. They can use renewable energy sources as solar energy. For example, some Stirling engines that are being used in the United States are using solar energy, or when there is not enough energy available, they can use methane instead [45]. Another advantage of using a heat engine is its silent operation. In comparison to Internal Combustion Engines (ICE), heat engines are almost noiseless, since combustion does not need to take place inside the engine and compression ratios are generally less than that of ICEs. Below, some of the advantages and disadvantages of heat engines are listed.

Advantages:

- Heat engines can operate quietly.
- Heat engines can be environmentally clean, because they can operate on all type of heat sources.
- Heat engines can be made of cheaper materials than the other methods.

Disadvantages:

- A requirement of heat engines is a heat source that is continually available and has almost a constant temperature.
- Heat engines cannot start and stop running as fast as ICEs, thus their usage in vehicles would be ineffective.
- The weight and volume of heat engines, in comparison to ICEs that produce the same amount of power, is generally large.

It can be concluded that Stirling engines have the capability to be used in many applications and it is suitable in the following cases [45].

- Multi-fuelled characteristics are required.
- A very good cooling source is available.
- Quiet operation is required.
- Relatively low-speed operation is permitted.
- Constant power output operation is permitted.
- Slow changing engine power output is permitted.
- A long warm-up period is permitted.

2.4 Different Configurations of Stirling Engines

Four types of Stirling engines are discussed in this section. Based on the availability of the heat source and sink, and simplicity, one of these configurations can be selected. These configurations do not show the designs in detail, but just the key parts are shown in the sketches. In Stirling engines, expansion and compression takes place in a cylinder with a power piston. When they are operating, a displacer transfers the working fluid through the heater, cooler, and regenerator.

2.4.1 Alpha Configuration of the Stirling Engine

Figure 2.4 shows the Alpha configuration of Stirling engines. This assembly has no displacer involved, and the two pistons are working together so that the volume stays constant.

Cold and hot pistons move uniformly in the same direction and they provide constant volume heating and cooling processes of the working fluid. When the majority of gas is in one cylinder, the other piston expands and compresses the working fluid. Expansion takes place on the hot side, and compression occurs in the cold side [45, 47].

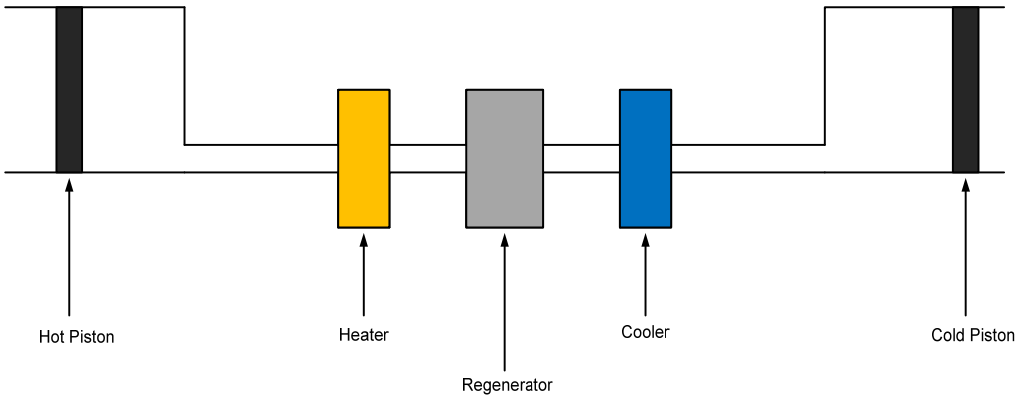

Figure 2.4: Schematic of the Alpha configuration of the Stirling engine (modified from [46]).

2.4.2 Beta Configuration of the Stirling Engine

Another possible assembly for the Stirling engine is a Beta configuration. Figure 2.5 shows the fundamental assembly of a Beta Stirling engine. In this configuration, one displacer and one power piston are installed within the same cylinder [48].

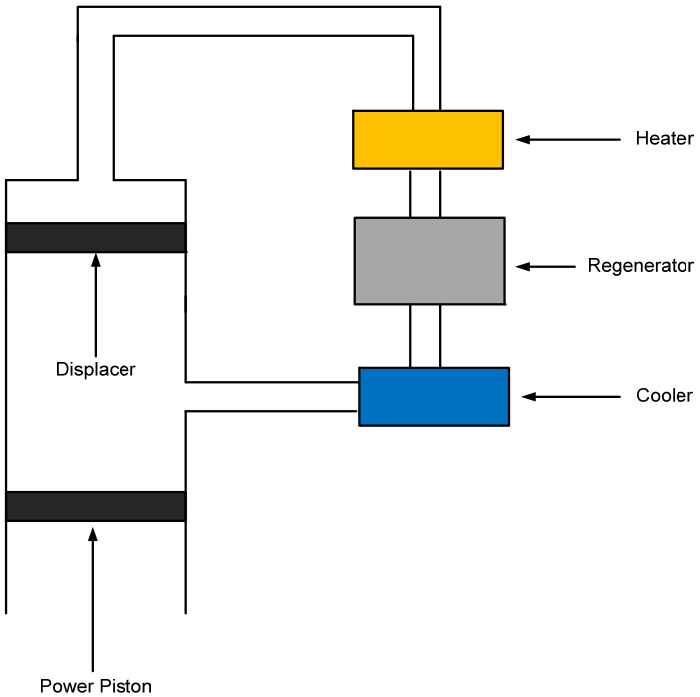

Figure 2.5: Schematic of the Beta configuration of a Stirling heat engine (modified from [49]).

In the Beta assembly, the working fluid between the heat source, sink, and regenerator is moved by the displacer. The power piston and heat sink are located in the same place in the Beta configuration. It compresses the gas when the working fluid comes to the heat sink, and the gas expands when the fluid is moved to the heat source.

2.4.3 Gamma Configurations of the Stirling Engine

Unlike Beta heat engines, in the Gamma configuration of heat engines, two separated cylinders, one for the displacer and the other for the power piston, are used [50].

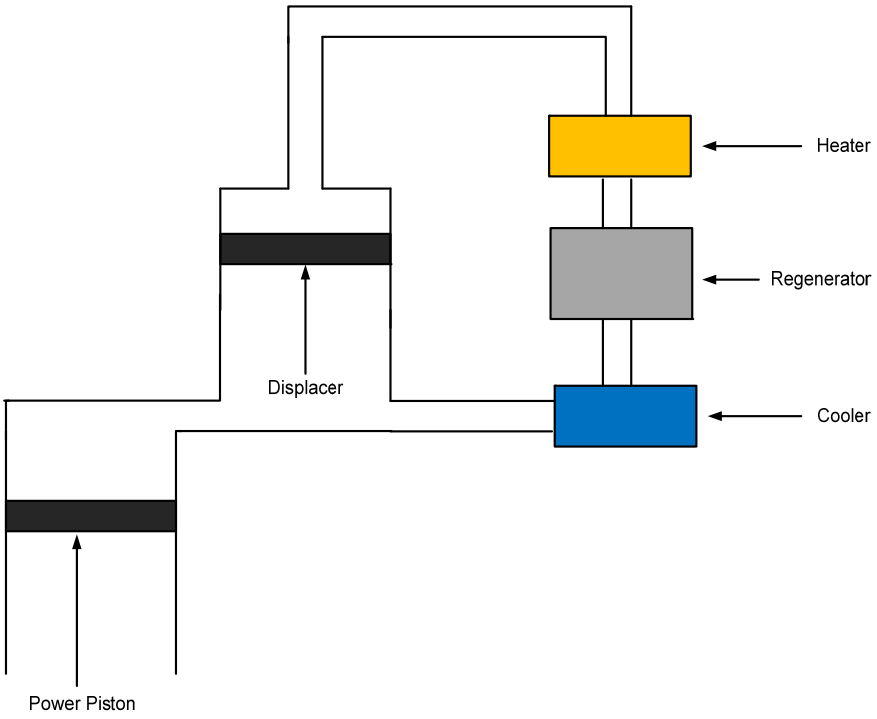

Figure 2.6: Schematic of the Gamma Configuration of the Stirling engine (modified from [49]).

Figure 2.6 shows the fundamental assembly of this heat engine. The configuration and components of this heat engine are similar to the Beta configuration; however, there are numerous differences in mechanical assemblies.

2.4.4 Low-temperature Differential Heat Engines

This special type of heat engine can produce mechanical work from low-temperature differentials. In this design, the mechanical losses are significantly decreased to obtain the maximum possible shaft work output. The performance of Low Temperature Differential heat engines (LTD) built and tested so far have not met the expectations. Most of them produce power less than 100 W [51]. Kongtragool et al. [52] mentioned some characteristics of LTD engines as follows:

- Displacer or power-piston swept volume compression ratio is large.
- Diameters of displacer cylinder and displacer are large.
- Displacer length is short.
- Effective heat transfer surfaces on both end plates of the displacer cylinder are large.
- Displacer stroke is small.
- Operating speed is low.

Low-temperature Differential (LTD) engines have two possible different configurations. One type is called a Ringbom engine. In this type of LTD engine, the power piston is connected to the flywheel. The diameter of the displacer in comparison to the piston in this design is very large, and the piston rod has a small length. The other type of LTD is called a Kinematic Engine. It has a Gamma configuration design; both the power piston and displacer are connected to the flywheel with a 90^{o} phase angle. In both designs, the operation speed is low in comparison to the other types of heat engines. Based on the equipment and fundamental configurations of these heat engines, the torque output of these heat engines is typically not sufficient to run electric generators [53]. The main focus of this thesis is on the Marnoch heat engine. In chapter three, the configuration of this system will be discussed.

Chapter 3:

The Marnoch Heat Engine

This chapter presents a study of the performance and operation of a Marnoch Heat Engine (MHE) prototype unit. The main focus is heat recovery from low-temperature heat sources.

3.1 Energy Conversion Steps and Processes

The Marnoch heat engine functions similar to the other heat engines and converts thermal energy to mechanical work. In the MHE assembly, the mechanical work done by the heat engine is converted to electricity. Figure 3.1 shows the steps of energy conversion in a MHE.

The MHE is able to produce electricity from low-quality energy sources, having temperatures less than 373.15 K. In this novel heat engine, heat exchangers are installed at different locations from the piston cylinder assembly; hence, the heat can be collected from various reservoirs [54, 55].

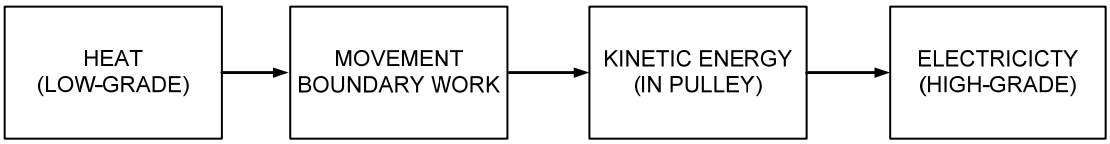

Figure 3.1: The working stages of energy conversion in a Marnoch heat engine.

Air in a Marnoch Heat Engine operates in the gaseous phase. It carries heat from the heat source to a heat sink, and the working fluid passes through the piston assembly of the heat engine and produces shaft work. This gas flow occurs as a result of pressure differentials in hot and cold tanks. In comparison to other heat reservoirs,

and based on the availability of space for this type of engine structure, it is possible to use a different working fluid in MHEs. The required heat for this system can be supplied from power plants, solar energy or waste heat from various sources. Moreover, in some regions, it is possible to use geothermal reservoirs to obtain the required temperature differences [56]. Considering the available temperature differences, it is possible to modify the mechanical design of the MHE to achieve the highest possible efficiency within the system.

3.2 System Operation

This section gives an introduction to the current MHE and its patent [57]. Figure 3.2 shows the schematic of the system and Figure 3.3a is a photograph of the present MHE.

The current prototype of the MHE has two pairs of heat exchangers with helical coils made of copper tubes. All heat exchangers are connected to the heat source and heat sink. Pneumatic valves control the air direction into the piston cylinder assembly. Solenoid valves were employed to control the water direction from the reservoirs, and the two electric valves are switching between the tank-pairs. A two-way piston assembly with a rack and pinion is used to convert the energy of the expanded gases into mechanical work. All the valve motions are controlled by a Programmable Logic Controller (PLC).

A programmable controller is used for automation of the MHE. MHE motions of the pneumatic valves are changed in less than one second, thus, one cannot operate the engine manually. The Marnoch embedded system carries out a pre-defined task repeatedly, while making decisions based on varying physical and logical control parameters. ***C*** language software written for the Marnoch system resides on the ROM (read-only-memory). The Marnoch control system was designed to require minimal

input from the user, so only signals from the pressure and temperature sensors are primary control triggers. Data was processed using the 80 MHz processor, with an address and data bus width of 16-bits.

The transmission system of this prototype converts the reciprocating motions of the piston to a one-way rotary motion. In each movement of the piston, the piston rack rotates the pinion 270 degrees. As shown in Figure 3.3b, using two chains, the clockwise and counterclockwise motions of the system are converted to a one-way clockwise rotary motion. A freewheel in the pulley-center makes the pulley rotations continuous. The pulley is connected to an electric generator by a belt and pulley. The generated electricity is stored in an ionic battery.

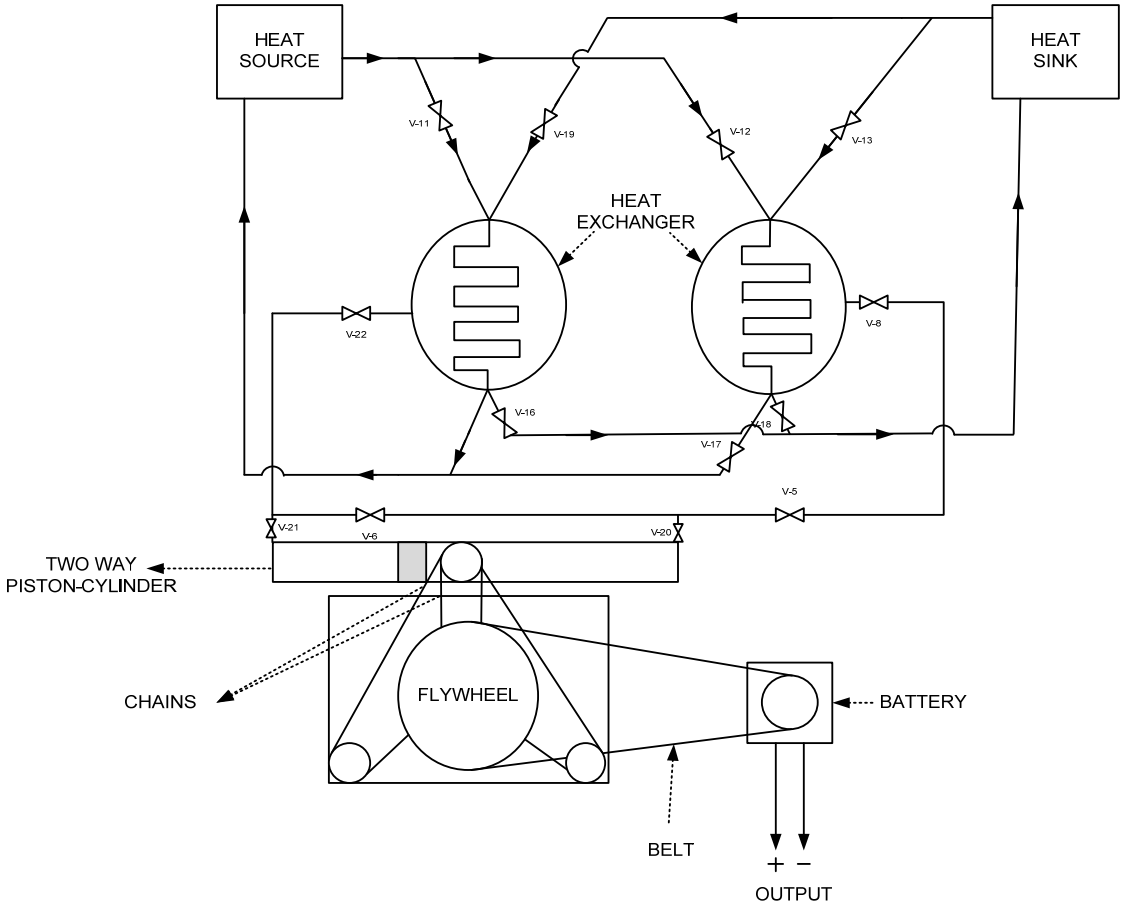

Figure 3.2: Schematic of the MHE configuration with two pairs of tanks (modified from [57]).

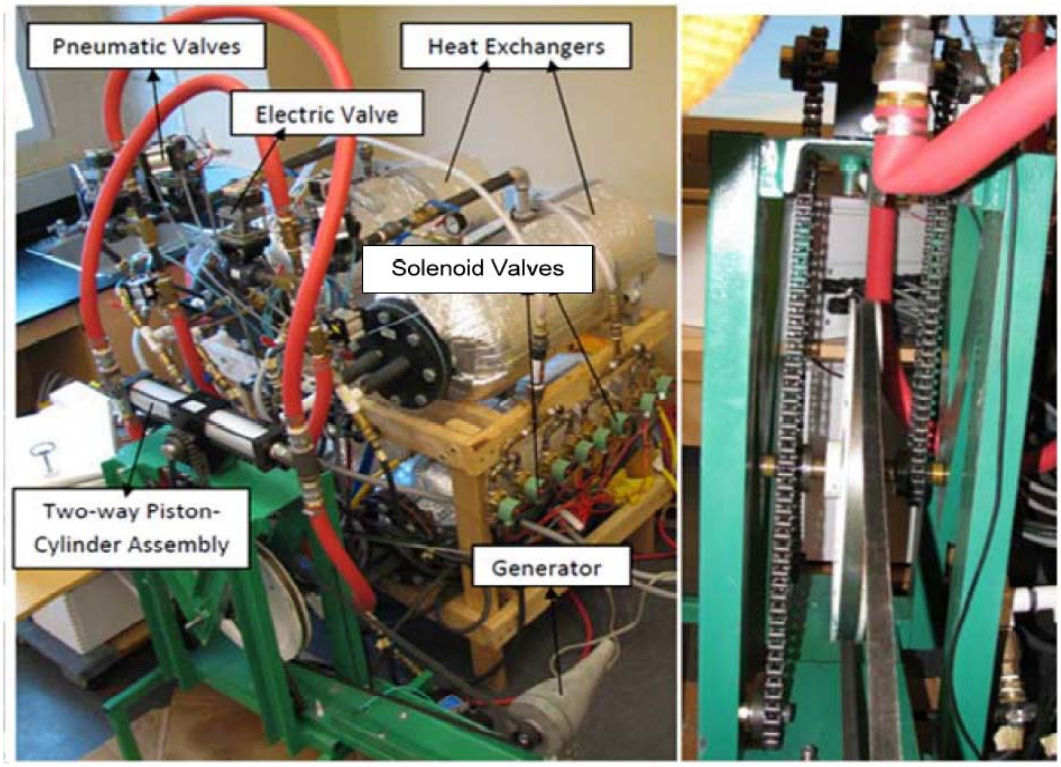

Figure 3.3: Photos of the (a) current prototype and (b) transmission.

Different mechanical configurations of the MHE can have effects on the performance of the engine. In Chapter Six, based on the experimental and theoretical results, some possible and modified designs for the next generation of heat engine will be discussed.

3.3 Description of MHE

In this section, a description of the MHE is presented. First, operation processes will be presented for each operation step. These steps are different from the processes of the Marnoch cycle; however, the processes of the cycle can be defined from these steps. Water is used to transfer heat from the heat source to the system and extract heat from the working fluid in the unmixed-heat exchangers. Moving boundary-work is converted to mechanical work by utilization of a two-way piston-cylinder assembly. The steps of the mechanical operation are discussed below.

Step one: hot water moves from the heat source through heat exchanger 1 and heats up the air inside the heat exchanger. The resulting air inside the tank will expand and increase the pressure in the hot tank. The coolant that comes from the heat sink goes to tank 2. As a result, it reduces the air pressure in the heat-sink.

Step two: when the air temperature inside the tanks reaches the projected temperature, the valves in the vessels will be opened. Consequently, the air goes from the high-pressure tank to the low-pressure tank. Pipes are connected in a way that there is a piston-cylinder assembly in series. Therefore, when air goes from the heat source to the cold source, it moves the piston. When the piston reaches its end position, the pneumatic valves redirect high pressure air to the other side of the piston to push it back to its initial position. The system diagram in Figure 3.5 illustrates the system. The air mass goes from the high-pressure tank to the heat sink, and it is stored in the cold tank.

Step three: by transferring air mass from the high-pressure side and storing it in the cold heat exchanger, the pressure of the cold side increases gradually, and a greater mass of air deposits itself in the cold side. As a result, after a certain number of strokes based on the size of the tanks and pre-charge pressure, the pressures of the cold and hot sides become almost equal. Therefore, the air pressure is not sufficient to push the piston. When the piston stops functioning, the PLC disconnects the first pair of tanks and connects tanks 3 and 4 for the rest of the operation. Two electric valves connect and disconnect the tank-pairs.

Step four: in stage four, the task of tanks 1 and 2 changes in operation. During this time period, the engine is using tanks 3 and 4 to achieve the pressure difference, and the engine operates continuously. Throughout the second mechanical cycle of tanks 1and 2, tank 1 is used as the heat sink and tank 2 will be used as the heat source.

Solenoid valves are changing the direction of water from the heat source and sink, such that hot water goes to tank 2 and cold water goes to tank 1 during this cycle.

When the pressure inside tanks 3 and 4 is almost equalized, the first pair will be reused to get the temperature difference, and step four is repeated for the second pair.

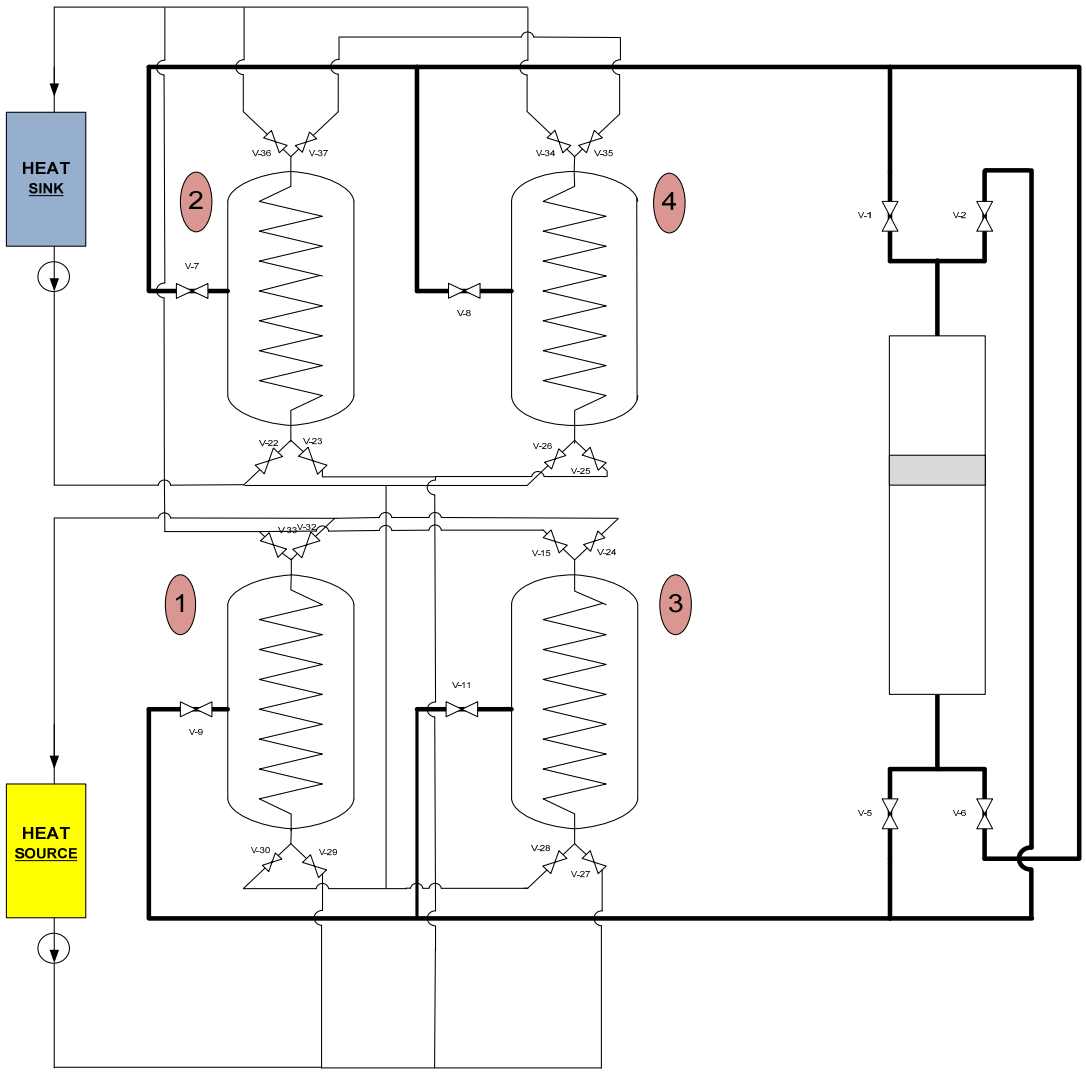

Figure 3.4: Connection diagram of the current prototype of the MHE with two pairs of tanks.

3.4 Comparison of Marnoch and Stirling Engines

In the earlier sections, the working principles of a Stirling engine and MHE were presented. Thermodynamic and mechanical considerations show that there are three major differences between the Stirling engine and the MHE.

1. In Stirling engines, a part of the mechanical work output from the flywheel is used in the compression process. However, in the MHE, all of the energy that comes out of the piston assembly is transferred to the electric generator.
2. In MHEs, cylinders of the power piston and heat exchangers can be located away from each other. However, in the Stirling engine designs, heat exchangers and piston assembly are attached. This feature of the MHE results in the ability to use a variety of sources to create pressure differences from temperature differentials.
3. Unlike Stirling engines, in MHEs, after each stroke, the enclosed area of a P-V diagram changes. This area is reduced because after each stroke, the expansion pressure reduces and the compression pressure increases.

3.5 Materials of Construction for MHEs

An MHE can be designed to operate over different temperature and pressure ranges. Moreover, as discussed earlier, different working fluids in an MHE can be used for the system. Some gases like ammonia are corrosive. Therefore, if this gas is used, all parts in contact with the working fluid should be stainless steel. Some other working fluids, like hydrogen and helium, have very small molecules. Hence gas leakage can occur through small gaps. This is one of the main concerns when the system is operating at high pressures.

At high pressures and temperatures, the materials selection has a significant role in the design and manufacturing process. Safety and durability of the system is strongly dependent on the materials and their properties.

In MHEs, hot and cold heat exchangers are inter-changed after each cycle of operation; hence they are subjected to thermal shocks. On average during one hour of

operation, each tank will be cooled down and heated up 20 times. In the current assembly, the heat engine uses temperatures ranging between 273.15 K to 373.15 K, and energy transfers into the system via water streams. Therefore, for this engine, properties of materials within this temperature range are investigated. In addition, if the heat engine is going to use higher temperatures, around 1000^{o} K, materials like ferrite can incur phase transformation. If phase transformation takes place in materials, the properties of materials will change noticeably.

In the current prototype, polymeric and cupric hoses and joints are used for hot and cold water streams. During the first few hours of system operation, there are no leakages that occur in joints, but after several hours, water leaks were observed in some connections, because of the significant differences in the coefficients of expansion of the materials. Common Teflon tapes are used for sealing joints of water hoses, but for the working fluid section, gas piping seals are used. The same problem is experienced during operation within air pipes. After several hours of operation, air starts to leak from joints of electric valves and metallic hoses. Hence, it is preferable to use materials having a similar coefficient of expansion for joints, hoses and valves.

3.6 Heat Exchanger Specifications

In the current configuration of MHE, four heat exchangers are used to heat up and cool down the air inside the heat engine. Hot water from the reservoir flows through two of the heat exchangers, and simultaneously cold water flows into the other two heat exchangers. In each operation cycle, only one hot and cold heat exchanger is operating.

The power generation of the system can be raised by increasing the heat transfer rate within the heat exchangers. For instance, the water stream enters the

system with a temperature of T_1 and increases the gas pressure from P_1 to P_2 in 60 seconds. If this time period is reduced to 45 sec, this pair of tanks can start the operation 15 seconds faster. Thus, a certain amount of energy will be produced by the heat engine within a shorter time period. Hence, the heat engine power output will have higher values.

The design of the transmission in the MHE is strongly related to the volume and heat transfer rates inside the heat exchangers. For example, if the applied heat exchangers can tolerate high pressures, the speed of the piston can be higher in comparison to low pressure units. Thus, the flywheel has to be heavier. In section 4.2, calculations of the transmission system will be presented and the effect of each term on the system performance is analyzed individually.

In this prototype, two different types of coils were used. For the first prototype, helical tubes inside the shells were used. This configuration of coils has two major advantages. Helical tubes can be fabricated easily. In addition, they have a high heat transfer rate, inside a smaller required space, compared with the length of the tubes.

In the second stage, the heat engine was rebuilt with multi-pass heat exchangers. The same shells were applied in both earlier and later heat exchangers. Figure 3.6 illustrates each configuration and shows the positions of installed valves and sensors. Due to safety regulations, the air gauge pressure inside the shells cannot be more than 1379 kPa in the present prototype. Reaching higher pressures at a constant temperature inside the shells requires more gas inside the system. The heat engine gives a higher torque output from the piston assembly with longer operation. The effects of pressure variations on the performance of the system will be illustrated in the thermodynamic analysis of the system in chapter four.

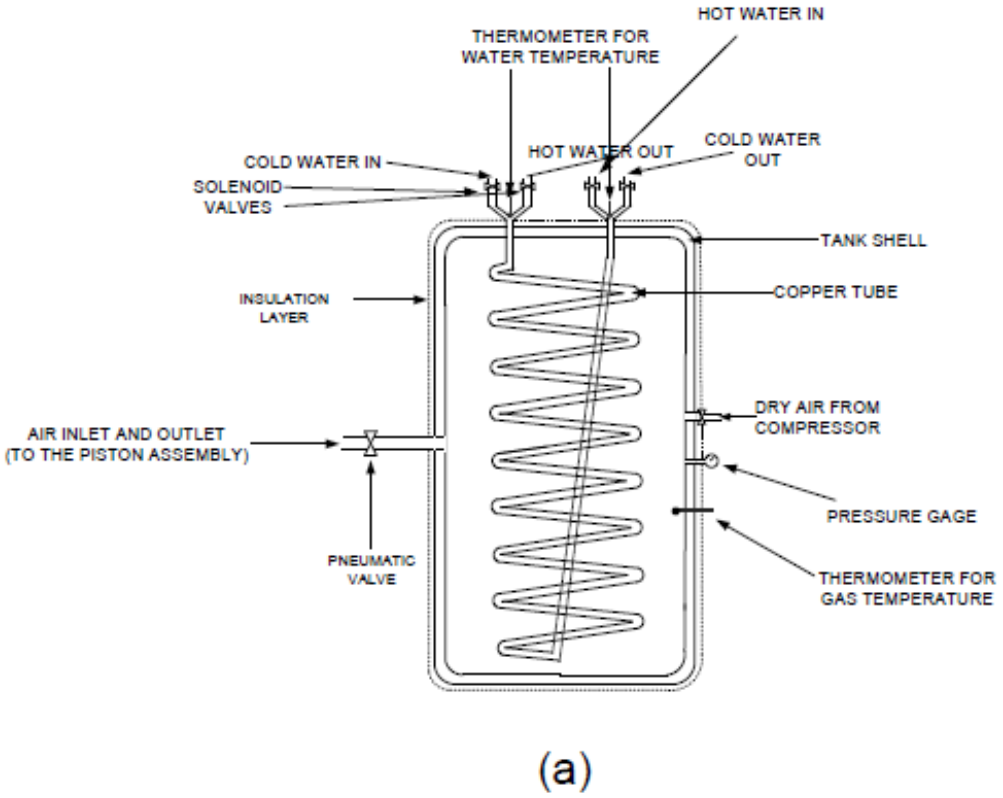

Figure 3.5a: Shell and tube heat exchanger with helical coils.

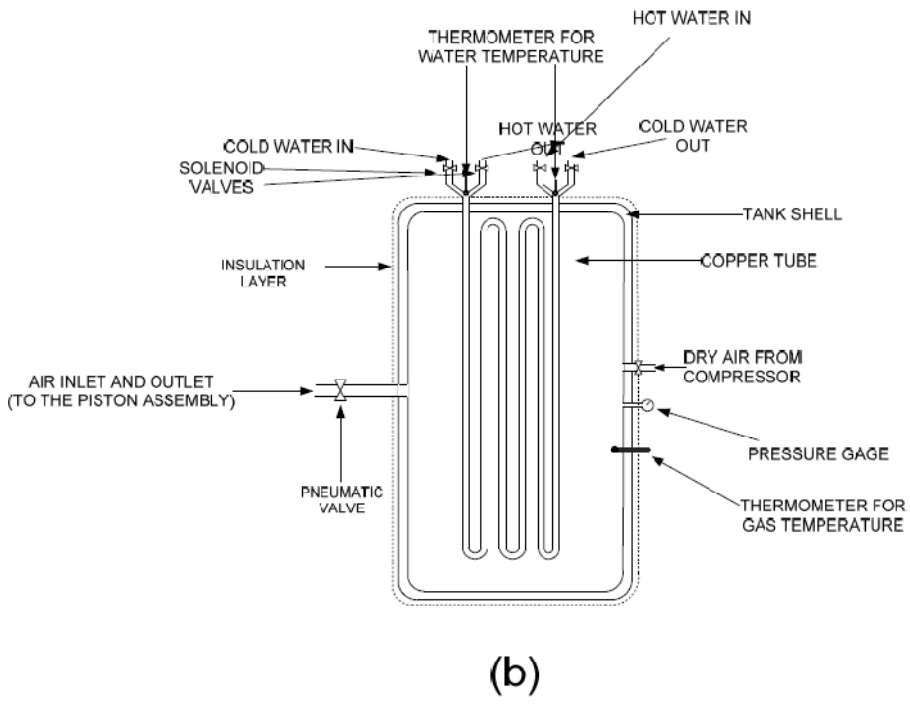

Figure 3.5b: Shell and tube heat exchanger with multi-pass coils.

Several heat exchanger configurations are possible in this design of heat engine. Figure 3.6 shows a current photograph of the shells, which were used for the helical and multi-pass coils. This figure shows the shape of the shells. Specific dimensions of the shells and their flanges are available in Table 3.1.

Figure 3.6 shows the shell before insulation. After the heat engine assembly, heat foil bubble insulation was used to insulate the heat exchangers. Figure 3.7 shows the configuration of the coils inside the heat exchanger. As shown in Figure 3.7a, for helical coils, two 90^{o} elbows are used in the water tubes. Thus, in this configuration the possibility of having leakages from the Copper tubes is not high.

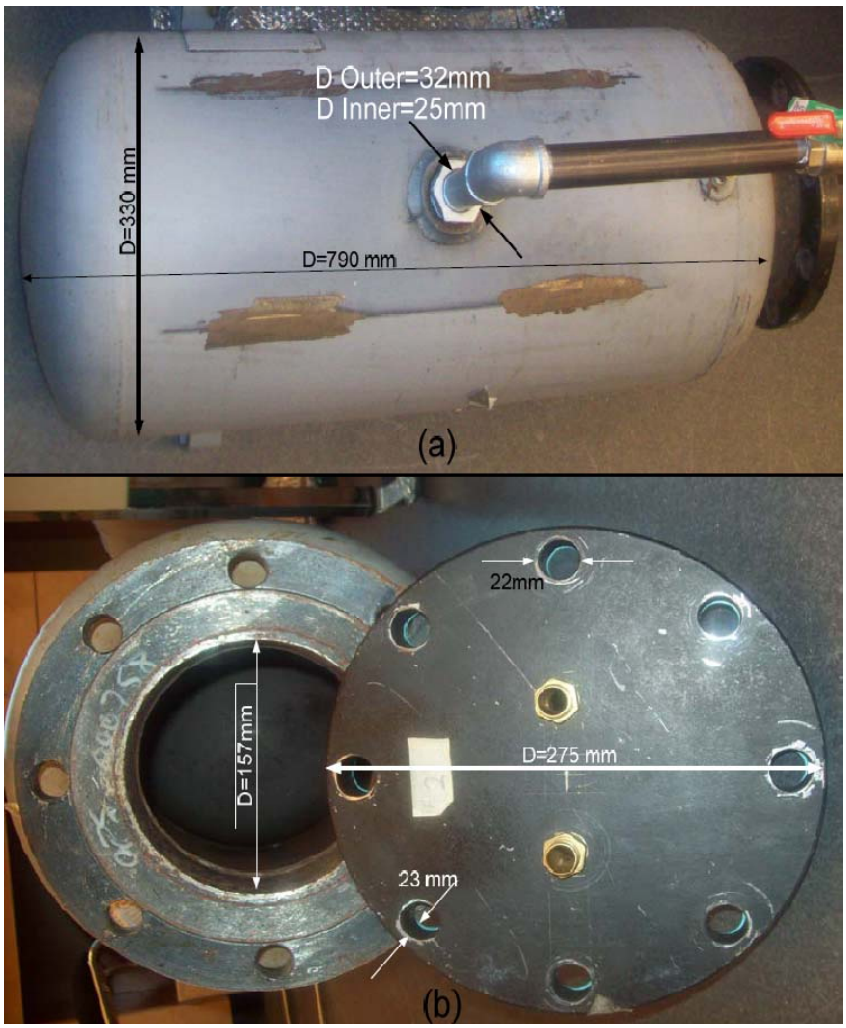

Figure 3.6: Photo of the shell and flanges in the MHE, with dimensions.

Table 3.1: Shell side of seat exchanger specifications

Shell Diameter	330mm
Shell Length	790mm
Thickness of the Metal Sheet in the Body	4mm
Thickness of Flanges	23mm
Number of the Bolts that Tighten the Flanges	8
Bolts Diameters	22mm
Diameter of the Air Inlets and Outlets	25.4mm
Total Volume of the Heat Exchanger	$0.07815m^3$

The challenge during fabrication of the helical section after rolling was tube deformation. As a result of this deformation, the surface area of the tube was reduced and flow rate of the water that comes through the tube was kept constant. Therefore, the pressure drop increased because of the higher fluid velocity.

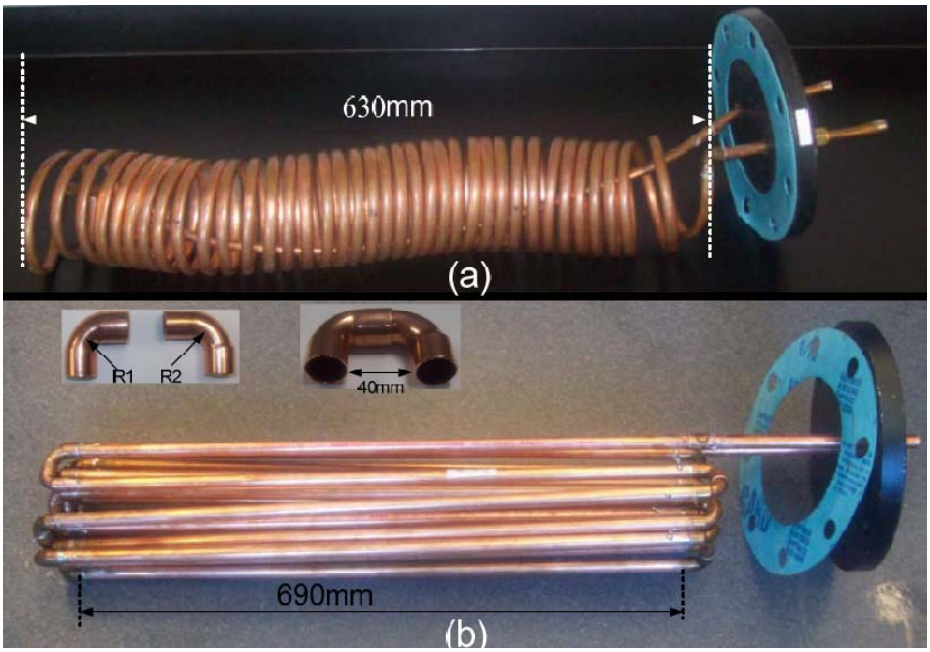

Figure 3.7: Helical and multi-pass heat exchangers.

As demonstrated in Figure 5.3a, another issue with the helical configuration is that the coils are close to each other. Hence, air conduction from the inner part of the coil to the outer part cannot occur easily. The average distance between each coil is 2.7 mm and some coils are joined together. To overcome these problems, another design for helical copper tubes is illustrated in Figure 5.1b.

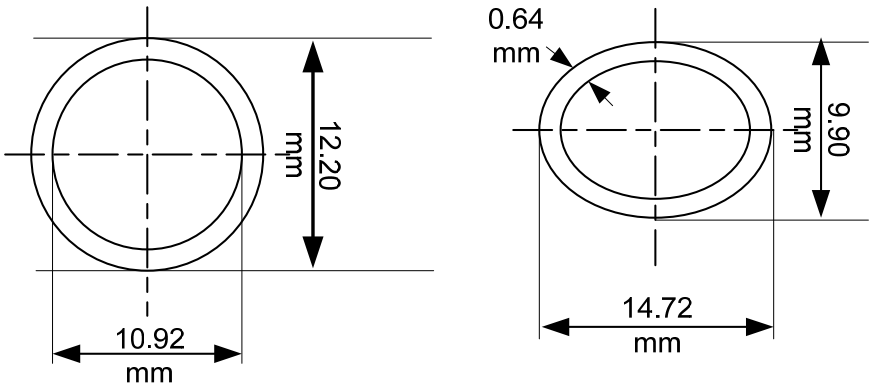

Figure 3.8: Tube deformation in helical coils.

In this configuration, 20 straight tubes were used and 38 short turn 90^{o} elbows were used to make the 180^{o} turns. In the current system, the inner distance between tubes is 25mm. Therefore, heat convection occurs faster than the previous configuration of copper coils. The new diameter of tubes is increased to 14.6mm, and after the fabrication process, no visible deformation took place within the tubes. Table 3.3 shows all related specifications of the multi-pass configuration.

In this step of the experiment, shells were not changed, and the flange inlet diameter of the heat exchangers was 157mm. Therefore, no more than 20 straight tubes could fit into each shell in the current configuration. To find the pressure drop of water through the coils Bernoulli's principle was applied. The pressure drop for the water temperatures of around $4^{o}C$ is about 5 kPa. This is small and it shows that the pressure drop for water in the current system is not a major concern.

Table 3.2: Helical coil specifications

Tube Outer Diameter after Deformation	a= 9.90mm, b=14.72mm
Thickness of Tube	0.64mm
Inner Diameter before Deformation	10.92mm
Outer Diameter before Deformation	12.20mm
Number of Coils	37
Length of Heat Exchanger Coils	630mm
Radius of Bends	65mm
Total Length of Tubes	17350mm
Total Occupied Volume by Tubes	$2006.23(10^{-6})$
Percentage of Occupied Shell Volume by Tubes	2.57%

Table 3.3: Straight pass tubes specifications

Thickness of Tube	0.64mm
Inner Diameter	14.61mm
Outer Diameter	15.90mm
Number of Passes	20
Length of Each Pass	690mm
Radius of Bends	22mm
Total Length of Tubes	15150mm
Total Occupied Volume by Tubes	$3044.54(10^{-6})$
Percentage of Occupied Shell Volume by Tubes	4.40%

3.7 Piston Cylinder Description

In the current prototype, a two-way piston cylinder assembly is utilized. The body of the cylinder is made of aluminum. This aluminum is hard-coat anodized and permanently sealed for wear resistance, and more endurance. The sealing in the system is critical to avoid leakages from the piston assembly to the surroundings, and from one side of the piston to the other side. At the same time, the friction loss between the piston and cylinder must be minimized.

The piston in this prototype has the diameter of 63.30 mm. Figure 3.9 shows the piston assembly and its elements. This assembly has a coupled rack and pinion mechanism, and it is hardened by chrome in the alloy.

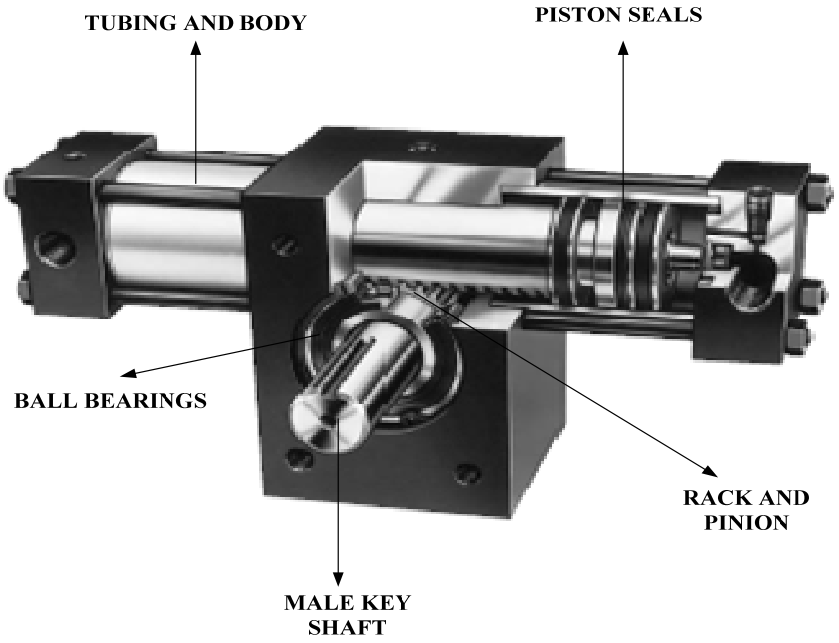

Figure 3.9: Two-way piston assembly in the MHE (modified from [59]).

In this equipment, the maximum operating pressure is 1723.7 kPa, with a breakaway pressure of 34.5 kPa. Rotation of the shaft by each complete stroke is 270 degrees. The displacement per degree of rotation in the cylinder is 1.23 cm^3. Therefore, in each stroke, 331.83 cm^3 of the working fluid is transferred to the low-

pressure tank. Seals in the piston are designed for continually running between temperatures ranging from 255.45 K to 355.35 K [59].

The torque outputs of the piston-cylinder, in four pressure differences, are shown in Table 5.1 for two different diameters. These values specifically belong to a piston-cylinder with a diameter of 63.30 mm, which is currently used in the MHE. These values are compared with the torque output from a piston assembly with a diameter of 81.21 mm. They are proposed to be used in the next prototype.

As Table 3.4 shows, the higher torque output of the system requires higher pressure differences. Based on the manufacturer's specification of the piston, friction losses in the assembly are about 20% of theoretical output torque. The actual torque output of the piston in the specification sheet with a diameter of 63.3 mm, and pressure difference of 689.47 kPa, is about 42.37 N.m [59].

Table 3.4: Torque output of the piston

Pressure Difference (kPa)	344.74	517.11	689.475	1723.69
Torque Output (N.m) (Piston Diameter: 63.30mm)	24.29	36.38	48.58	121.35
Torque Output (N.m) (Piston Diameter: 81.21mm)	64.40	96.04	128.92	322.23

Source: [59].

Figure 5.2 shows the variations between the torque outputs of a piston with different diameters. The difference between the diameters of these pistons is 17.91 mm, and the differences between torque outputs are noticeable.

There are several aspects to be considered for piston sizing of the MHE. If the volume of the cylinder is large, consequently the amount of working fluid that is transferred from one tank to the other is high, per stroke. Hence, if the volume of the heat exchangers does not match the piston size after a few of strokes, the engine

operation will be stopped and another pair of tanks must be charged for operational use. The charging mode is time consuming, and delays in piston operation can happen when tanks are being switched.

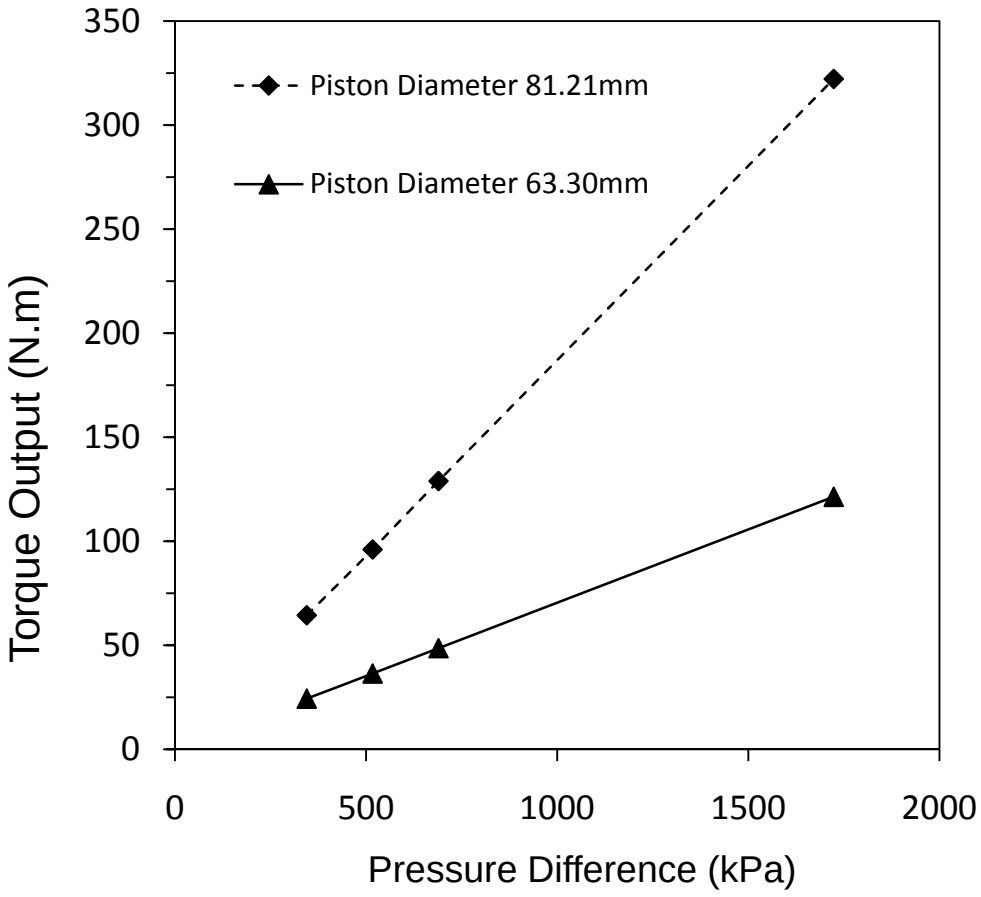

Figure 3.10: Comparison of torque outputs of two piston assemblies with different diameters [59].

An advantage of having cylinders with larger diameters and volumes is that when a larger piston cylinder is used, less time is spent for changing the direction of the piston by the valves. Thus, the power output from the piston assembly will have higher values. Moreover, the torque output is more than the output of smaller pistons. When smaller pistons are used, the direction is changed more frequently. Changing direction by the valves is time consuming, thus certain amounts of energy are produced in longer durations. Therefore, the output power of the piston will reduce.

The other concern about using large cylinders is the amount of required heat to keep the process isothermal. For large volumes, this amount at the start and end of the stroke is noticeably different. Practically, it is hard to keep the gas at the same temperature in this condition for isothermal processes.

3.8 Control Valves

There are three types of valves utilized in the current prototype. In order to change the water direction, 16 solenoid valves were installed on the water hoses. The body of these valves are made of brass and the temperature of the fluid through these valves cannot be more than 82 ^{o}C. The power that is consumed by these solenoid valves is about 6.1W. They use power when the valves are open. Thus, a considerable amount of energy output from the engine is consumed by these valves.

Figure 3.11: Ball valves (a) PVC ball valve and 4 RPM electromotor, (b) Iron ball valve with electromotor and speed controller.

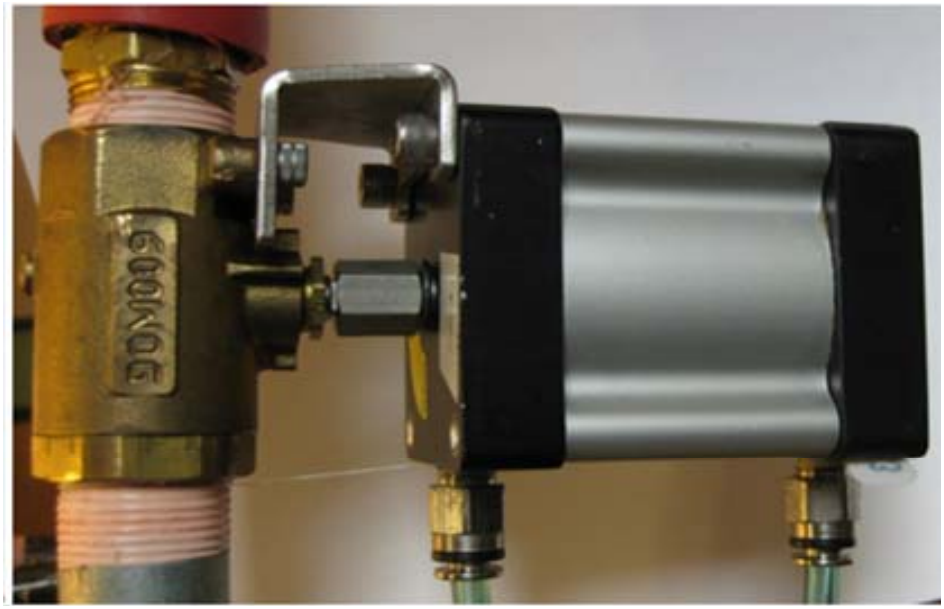

Figure 3.12: Pneumatic ball valves to change the air direction through the piston assembly.

Four PVC ball valves connect and disconnect the tank pairs and they operate with an electromotor and gearbox (Figure 3.11a). The maximum speed of these valves is 4 RPM. Slow functioning of these valves was a problem that was initially observed during the operation of the heat engine. During this time period, no energy from the piston is transferred to the flywheel

Four ball valves change the air direction through the cylinder. During each revolution the motion of theses valves change by 90^{o}. The direction of these valves changes with pneumatic motors (Figure 3.12). Even though they operate very fast, the noise that they produce is a major drawback. The other concern about these valves is the energy required for operation. These valves use compressed air to open and close. To maintain this compressed air, an air compressor is required and consequently some energy is consumed therein. Moreover, the ball valves are well sealed and stiff. To overcome these problems, the pneumatic ball valves were replaced with the electric ball valves. The electric motor that is used in their structure has two poles and it has a power output of 30W. The head gear ratio is 30:1, thus, the maximum speed cannot be

more than 100 RPM. These valves are connected to electric controllers. These controllers change the valve speeds between 1 and 100 and control the required delays during the operation.

Chapter 4:

Performance Analysis

4.1 Thermodynamic Analysis

Thermodynamic analysis is necessary to evaluate the performance of the MHE. All major components of the MHE will be analysed separately, to determine the parameters that have the most significant impact on the performance and efficiency of the MHE. Thus, in future prototypes, particular attention will be given to these parameters.

In order to perform a proper energy and exergy analysis on the MHE, a boundary is defined for the system and its components. The time period for analyzing this heat engine is also specified, since the same components perform different tasks at different periods of the cycle. For instance, the first operation cycle operates for about 29 to 60 seconds. Within this period, heat exchanger 1 transfers heat from the hot reservoir and heats up the air inside the heat engine. At this time, tank 2 is connected to the heat sink, and cools the air that is coming from the piston. Hence, if this period is analysed, tank 1 and tank 2 are the heat source and heat sink, respectively. In the next cycle, the functions of tank 1 and 2 will be reversed. In order to present the analysis coherently, calculations for charging and discharging periods of the heat exchangers are done separately.

The schematic of the system is shown in Figure 4.1. This figure represents the first operation cycle in two different stages (charging and discharging). In Figure 4.1a, both valves are closed and initially both tanks have the same pressure. When water

flows through the heat exchangers, tank 1 is heated to raise the pressure, and at the same time, tank 2 is cooled and its pressure is decreased.

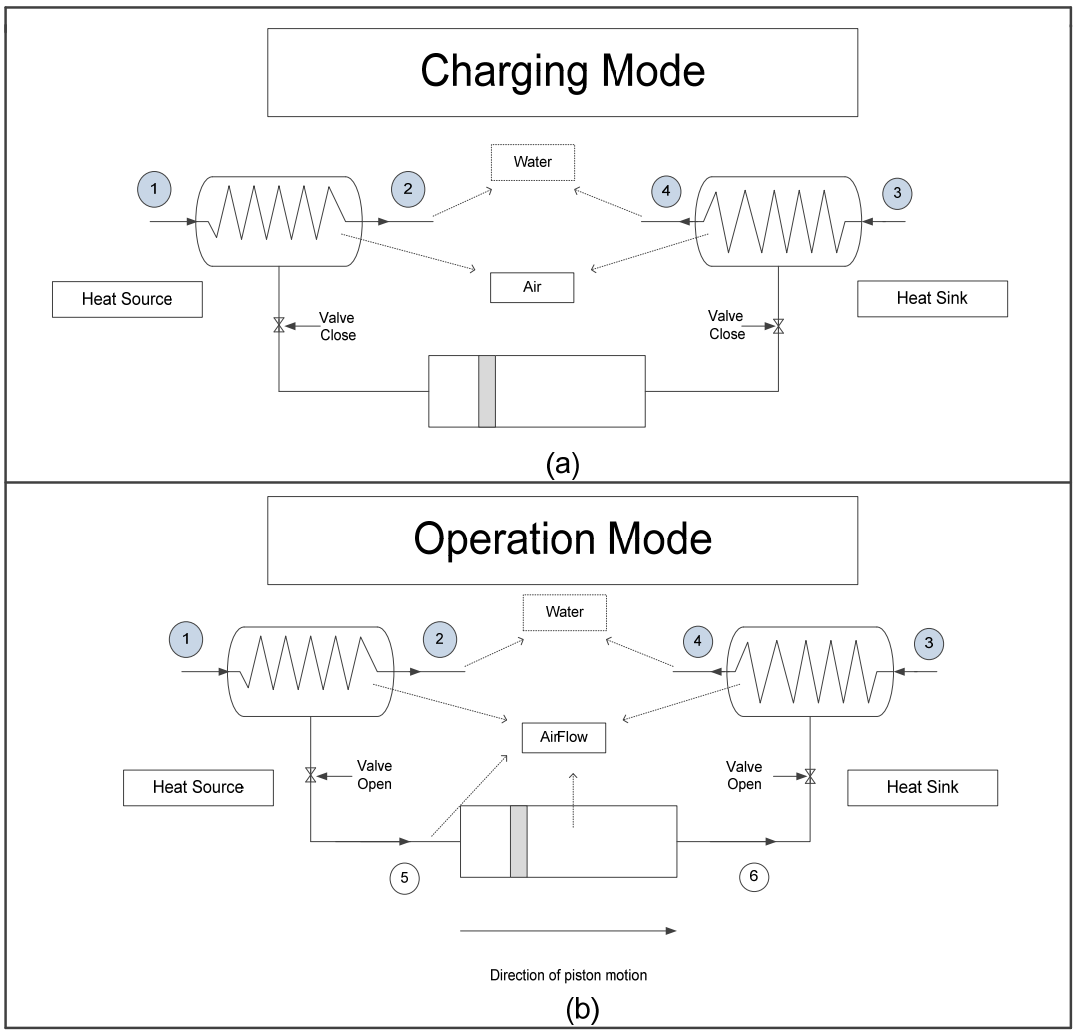

Figure 4.1: Schematic of a MHE with one pair of tanks for thermodynamic analyses; section (a) is for the charging period and section (b) is for the discharging (operation) period.

Figure 4.1b demonstrates the second step of the operation. In this step, the air temperatures inside both heat exchangers are close to the temperatures of the water streams. In step 2, air vales are open and this set of tanks and piston start the operation. Operation of this set continues until the air pressures inside both heat exchangers equalize. During charging and discharging periods, water flows through the tanks continuously and it does not shut off until the last stroke. This occurs to achieve near isothermal expansion and compression strokes of the piston.

In Figure 4.1, the setup and flow connections for one piston revolution is shown. This figure is sufficient to conduct the thermodynamic analysis. However, for continuous operation, all of the components shown in Figure 3.4 are required. In the first part of the thermodynamic analysis, only the thermal energy balance is considered, and the transmission system is analysed subsequently.

In this system, all properties of the working fluid are time dependent. It is assumed that the water-flow from the reservoir is steady state. When the valves are closed, it is assumed that no leakage takes place within the system, and air leakages from the joints and hoses to the surroundings are neglected. Changes in volume of the tanks, due to changes in heat exchanger temperatures and pressures are negligible, and heat exchanger shells are assumed as rigid bodies. Fluid friction losses in the heat exchangers are assumed to be negligible, and air is assumed to behave as an ideal gas.

In order to analyze the transient behaviour, the readings from the installed sensors were used. The shortest period (dt) for the experimental readings cannot be less than one second. In the theoretical analyses of the system, (dt) is the required time for each revolution. This value is very close to one second in the current system. The equations are solved by calculating the air properties after each stroke.

The three major components to be analyzed in the thermal energy analysis are given as follows,

1. Tank 1: Connected to a heat reservoir;
2. Piston Assembly: A two-way piston assembly between the heat source and sink;
3. Tank 2: Connected to a heat sink.

A general balance equation for any conserved quantity in a system can be written as:

$$Input + Generation - Output - Consumption = Accumulation \quad (4.1)$$

Therefore, the general mass, energy, entropy, and exergy balance equations can be written as:

Mass inflow – Mass outflow = Mass accumulation (4.2)

Energy inflow – Energy outflow = Energy accumulation (4.3)

Entropy input + Entropy generation – Entropy output = Entropy accumulation (4.4)

Exergy input – Exergy output – Exergy destroyed = Exergy accumulation (4.5)

In this analysis, Equations (4.2)- (4.5) will be used for each component separately to conduct the thermodynamic analysis as shown below.

4.1.1 Mass Balance of Tank 1

Tank 1 is a shell and tube heat exchanger with both fluids unmixed. A heating fluid (hot water) flows through the tubes and exchanges heat with the working fluid (air) in the shell. The overall mass balance can be written as:

$$\Delta\dot{m} = \sum \dot{m}_{in} - \sum \dot{m}_{out} \quad (4.6)$$

Equation (4.6) is written separately for water as

$$\Delta\dot{m} = 0 \Rightarrow \dot{m}_{w1} = \dot{m}_{w2} \quad (4.7)$$

Equation (4.7) shows that the water flow rate in tank 1 is steady state and the mass of water inside the copper coils is constant. For air, the system is not at steady state.

$$\sum \dot{m}_{Air,in} - \sum \dot{m}_{Air,out} = \Delta\dot{m} \quad (4.8)$$

As mentioned earlier in section 4.1, air leakages from the valves and joints are negligible. In Equation (4.8), the values of the parameters for heating and cooling modes for a set of tanks are equal to zero, because all air valves are closed, and no air can enter and leave the tank. At the start of the piston operation, air leaves tank 1 and no air mass will enter the tank. The air mass flow rate in Equation (4.8) for this condition can be shown by negative values.

$$\Delta\dot{m} = -\dot{m}_5 \tag{4.9}$$

where $\dot{m}_5$ is the mass flow rate at point 5 (Figure 4.1) and it is a function of time. The value of $\dot{m}_5$ is calculated by Equation (4.10). After each piston stroke, the amount of air mass that is transferred from the heat source to the heat sink decreases.

$$\dot{m}_5 = \frac{m_{Air,out}}{dt} \tag{4.10}$$

The time step does not have a constant value even during one operation cycle. When the pressures of both heat exchangers are equal, no air mass will be transferred from tank 1, and again all parameter values in Equation (4.8) will be zero.

To perform the thermodynamic analysis, Uniform State Uniform Flow (USUF) equations are used. In USUF processes, all properties are uniform within the system at any instant in time. In addition, the flow is uniform so all mass flow properties at each inlet and outlet are uniform. If tank 1 is assumed as a control volume and the overall process occurs during time *t* , at any instant of time during the process, the continuity equation is given by

$$\frac{m_{Air,out}}{dt} + \sum \dot{m}_5 = 0 \tag{4.11}$$

where the summation is over all areas on the control surface through which the flow occurs. In tank 1, only the exit point area is considered for Equation (4.11). Integrating over *t* gives the changes of mass in tank 1 during the overall process:

$$\int_0^t \left(\frac{m_{Air,out}}{dt}\right) dt = m_{initial} - m_{final} \tag{4.12}$$

Where, $m_{initial}$ denotes the initial air mass in tank 1, and m_{final} denotes the air mass that remains in tank 1 after one operation cycle.

Thus, the final and initial properties of the gas inside the heat exchanger allow the value in Equation (4.12) to be calculated. This equation can be solved for the whole period of the discharging process. To find the performance of the engine

between these periods Equation (4.11) is integrated over appropriate time periods, Equation (4.13) shows this integration. The total mass leaving tank 1 during time *(t1)-(t2)* is:

$$\int_{t1}^{t2}(\sum \dot{m}_5)\, dt = \sum m_5 \tag{4.13}$$

Therefore, for the whole operation, over a period of time *(t),* the continuity equation for the transient process can be written as:

$$(m_{initial} - m_{final}) = -\sum \frac{\dot{m}_5}{dt} \tag{4.14}$$

4.1.2 Energy Analysis of Tank 1

In the first cycle of operation, as shown in Figure 4.1, tank 1 is connected to the heat reservoir. Equation (4.15) shows the general energy balance equation for this control volume.

$$\Delta \dot{E} = \sum \dot{E}_{in} - \sum \dot{E}_{out} \tag{4.15}$$

This includes energy transfer by water streams and air. This equation is used for tank 1 in two different modes: charging and discharging modes. In this equation, $\sum \dot{E}_{in}$ is the summation of total energy input to the heat exchanger 1, and $\sum \dot{E}_{out}$ is the energy that leaves heat exchanger 1. In the first step, heat is transferred into the system by the hot water stream. A portion of its energy is transferred to the gas inside the heat exchanger. A fraction of $\sum \dot{E}_{in}$ goes back to the ambient by the exit water stream, and the rest is lost to the surroundings. Figure 4.2 shows the system boundary for the hot water stream that is entering tank 1. This figure is an illustration for Equations (4.15) - (4.18).

Thus for the water stream:

$$\dot{m}_{w1} h_{w1} = \dot{m}_{w2} h_{w2} + \dot{Q}_{ta} + \dot{Q}_{loss} \tag{4.16}$$

here the values of $\dot{m}_{w1}$and $\dot{m}_{w2}$ are obtained from Equation (4.6), and h_{w1} and

h_{w2} denote the enthalpy of the water that enters and exits the heat exchanger, respectively. Thus, $\dot{m}_{w1}h_{w1}$ gives the flow rate of energy that is entering the system by the water stream. The temperature of the water that is entering the system is assumed to be constant during charging and operation. Hence, there will be no change in the value of $\dot{m_{w1}}h_{w1}$. Unlike $\dot{m}_{w1}h_{w1}$, $\dot{m}_{w2}h_{w2}$ (energy flow to the ambient via the outlet water stream) changes over time and its value depends upon $\dot{Q}_{ta}$ (heat transfer rate from the water to the working fluid). This rate is reduced over the period of time during charging, because the temperature of the gas approaches the water temperature. Also $\dot{Q}_{loss}$ is the amount of heat that is rejected to the ambient from the hot stream tubes, and it varies with time because the average temperature of the stream changes with time. In the current system, the water temperature sensors are positioned close to the tanks and the entire section is insulated. Thus, in the calculations, $\dot{Q}_{loss}$ can be neglected.

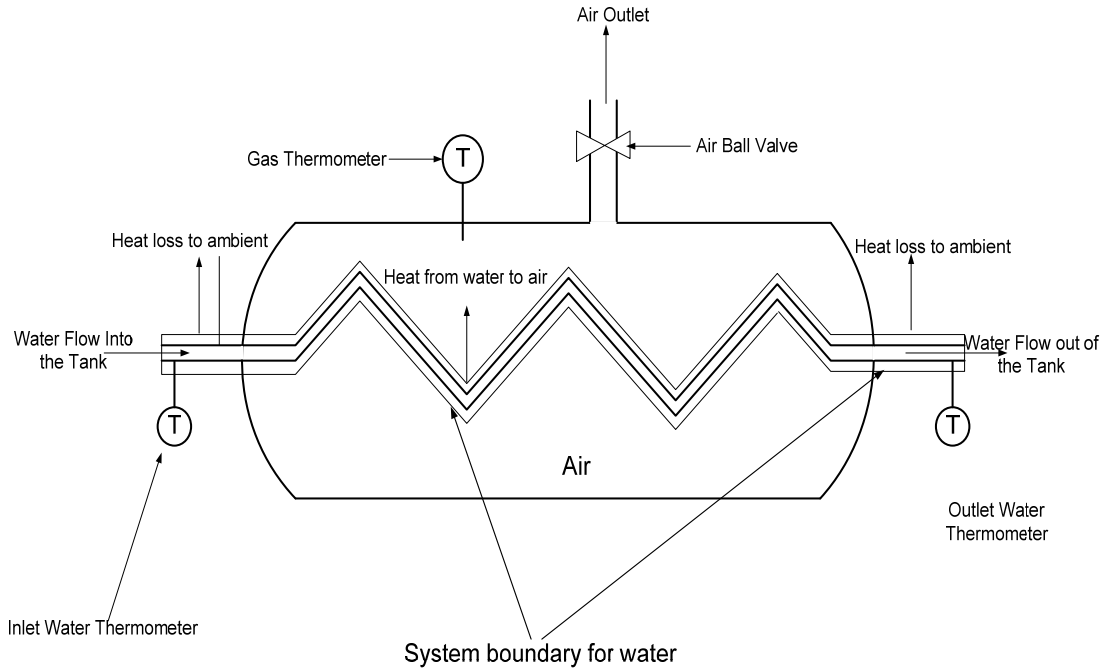

Figure 4.2: Schematic of tank1 with a water system boundary.

The heat transfer rate ($\dot{Q}_{ta}$) from the water stream to the air, in a given time, can be expressed as:

$$\int_0^t \dot{Q}_{ta}\ (dt) = mc_v\Delta T \tag{4.17}$$

When Equation (4.17) is used for the charging period, the air mass (m) is constant inside the tank, and its value is $m_{initial}$ in Equation (4.12). Temperature differences shown by ΔT have major effects on the heat transfer rates. When this equation is solved for the water streams, ΔT is the temperature difference between the water inlet and exit, and the value of c_v is the value of c at that specific temperature.

At the end of the charging period, the thermometers that are installed at the water inlet and water exit do not show the same temperatures; however, after a certain time, the pressure of the hot gas will remain constant. From the changes in temperature and pressure, it is understood that the heat loss from the heat exchanger to the ambient occurs, although the tank shell is insulated. When the piston operation starts, considering Figure 4.1, it is assumed that

$$T_1 = T_2 = T_5 \tag{4.18}$$

where $T_1$and T_2 are the water inlet and outlet temperatures respectively, and T_5 is the gas temperature inside the hot heat exchanger. It should be noted that heat loss from the pipe, which connects tank 1 to the piston assembly, is neglected. Hence, air temperatures at point 5 (Figure 4.1) and inside tank 1 are the same. This assumption is appropriate in experimental conditions when the system is well insulated, or when the ambient temperature is close to the hot stream temperature.

When the piston operation starts, heat is transferred by mass through the piston assembly, and afterwards it is transferred into tank 2. When the air mass is leaving the hot tank, the pressure of the tank will decrease. However, the expansion process in this heat engine should be isothermal to obtain maximum work output.

Water flows through the heat exchangers during piston operation, so when the gas is expanded, it is being heated up simultaneously.

The amount of heat that for the first revolution to keep the expansion isothermal, is not equal to the required heat for the last expansion. In the current system, the mass flow rate and temperature of the water that flows into the system is constant. Hence, there is a variation between the actual expansions and isothermal expansions, from theory.

The energy balance equation inside tank 1 during the operation mode can be expressed as:

$$\Delta \dot{E} = \dot{Q}_{ta} - \dot{m}_5 h_5 \tag{4.19}$$

where $\Delta \dot{E}$ is the change in energy rates in tank 1 that occurs due to heat and mass transfer. The value of $\dot{Q}_{ta}$ is from Equation (4.17), $\dot{m}_5$ is calculated in Equation (4.10), and h_5 is the enthalpy of the air at the outlet.

4.1.3 Exergy Analysis of Tank 1

To find the performance of the system in different ambient conditions, an exergy analysis was also performed. In the current system, no chemical reaction occurs with air, or water that brings and removes heat from the system.

When no chemical reaction exists within the system, the physical exergy of each point Ex_i can be calculated by:

$$Ex_i = (H_i - H_0) - T_0(S_i - S_0) \tag{4.20}$$

where H_0 , T_0 and S_0 are enthalpy, temperature and entropy of dry air under ambient conditions, respectively. Also H_i and S_i are the enthalpy and entropy at each point within the system boundary.

If the tank is considered as a control volume, to find the flow exergy ($\dot{E}x_Q$), which is associated with the heat transfer to the system $\dot{Q}$, Equation (4.21) can be used.

$$\dot{E}x_Q = \int_i^f \left(1 - \frac{T_0}{T}\right) dQ \tag{4.21}$$

where dQ is the incremental heat transfer, and the integral is taken from the initial state (i) to the final state (f). This thermal exergy is the minimum work required by the combined mass and environment in bringing the control mass to the final state from the dead state. In the MHE prototype, in most of the conditions, heating the tank starts from the dead state. But in situations where the temperature of the heat sink is lower than the ambient, the initial state has negative values.

The dimensionless quantity $\left(1 - \frac{T_0}{T}\right)$ is called the exergetic temperature factor, and denoted as [60]:

$$\Gamma = \left(1 - \frac{T_0}{T}\right) \tag{4.22}$$

For heat transfer across a segment (r) of the control surface, for which tank 1 is charged initially, the thermal exergy associated with heat transfer is

$$\dot{E}x_Q = \int_r q_r . \Gamma \, dA_r \tag{4.23}$$

where q_r is the heat flow per unit area at a region on the control surface, and the temperature is denoted as T_r. The dimensions of the copper tubes inside the heat exchanger are used to find the surface area (Table 3.2 and 3.3).

Equation (4.24) can be used instead of Equation (4.23) when the value of $\dot{Q}_{ta}$ is known. This equation gives certain values, whereby if the temperature T of the control mass is constant, the thermal exergy transfer associated with the heat transfer is:

$$\dot{E}x_Q = \left(1 - \frac{T_0}{T}\right) \dot{Q}_{ta} = \Gamma \dot{Q}_{ta} \tag{4.24}$$

where T_0 is the ambient temperature and T is the working fluid temperatures at certain times during discharging mode.

4.1.4 Mass Balance of the Piston Assembly

As discussed in section (3.7), a two-way piston assembly was used to convert thermodynamic work to mechanical work. No mass accumulation exists in the piston assembly. All mass that enters through the piston cylinder from tank 1 of one revolution is transferred to the cold heat exchanger in the next revolution. Equation (4.25) is used as the mass balance equation for the piston assembly,

$$\dot{m}_5 = \dot{m}_6 \tag{4.25}$$

where $\dot{m}_5$ is the mass that enters the piston from tank 1 and its value is obtained from Equation (4.10). Also $\dot{m}_6$ is the mass that leaves the piston to the heat sink. It is assumed that the piston assembly is well sealed, and there is no leakage to the surroundings. The values of Equation (4.25) are not constant throughout the operation cycle. When the operation starts, $\dot{m}_5$ and $\dot{m}_6$ have higher values than the values of the last strokes. This occurs because the amount of remaining mass in tank 1 is reduced and the back pressure inside tank 2 is increased.

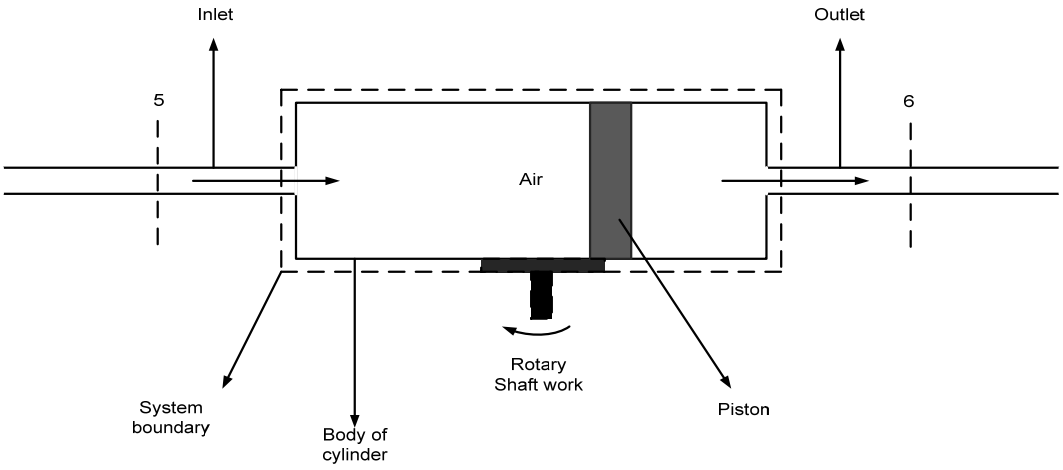

Figure 4.3: Schematic of the two-way piston cylinder assembly.

4.1.5 Energy Analysis of the Piston Assembly

The piston assembly converts the heat exchanger pressure differences to shaft work. Energy input enters by the expanded gas from the heat source, displaces the piston and flows to the heat sink after work extraction. Equation (4.26) shows the energy balance for the piston,

$$\dot{W}_{shaft} = \dot{m}_5 h_5 - \dot{m}_6 h_6 - \dot{Q}_{loss} - \dot{E}_{fpc} - \dot{E}_{frp} \quad (4.26)$$

where $\dot{W}_{shaft}$ is the total actual work output from the piston assembly, and $\dot{E}_{fpc}$ is the friction loss between the piston sealing and the inner body of cylinder. In the current calculations, $\dot{E}_{fpc}$ is a combination of static and dynamic frictions. This friction loss is released in the form of heat and some fraction will be transferred to the gas inside the piston, and a portion will be lost to the ambient. Also $\dot{E}_{frp}$ is the second part of the friction loss. It occurs between the rack and pinion that converts the revolutions to rotary motions. $\dot{Q}_{loss}$ is the heat loss rate that is rejected from the gas to the body of the cylinder, and afterwards to the ambient.

It is assumed that the temperature of the body of the cylinder is the average temperature of the heat source and sink, because the inlet and outlet of the cylinder is changed frequently. In the calculations for the piston assembly, $\dot{Q}_{loss}$, $\dot{E}_{fpc}$, and $\dot{E}_{frp}$ were not calculated separately. All were considered as piston assembly losses ($\dot{E}_{apl}$), and values were found from the manufacturer catalogue. In the current setup this loss is estimated between 10-20% of energy output of the piston assembly [59].

$$\dot{E}_{apl} = \dot{Q}_{loss} + \dot{E}_{fpc} + \dot{E}_{frp} \quad (4.27)$$

Substituting Equation (4.27) into Equation (4.26) gives

$$\dot{W}_{shaft} = \dot{m}_5 h_5 - \dot{m}_6 h_6 - \dot{E}_{apl} \quad (4.28)$$

The installed pressure sensors on this heat engines has to respond in less than one second. The reason is because of inlet and outlet of the piston change more than 50 times per minute. For instance, under 649.48 kPa of pressure difference, the inlet and outlet switch occurs about 50 times in 58 seconds.

To find the shaft work output of the piston, the pressure differences in both sides of the piston assembly were applied. From the pressure difference and piston specifications, the torque output of the piston is obtained. By this method, the pressure drops inside the valves and tubes are not considered in the calculation. It is a source of error in the current experimental calculations.

4.1.6 Exergy Analysis of the Piston Assembly

Exergy that enters the piston cylinder assembly is carried by the air flow from tank 1, and rejected to tank 2. To perform an exergy analysis, Equation (4.20) is used to find the exergy at each point. With regards to Figure 4.1, it can be shown that:

$$\dot{W}_{shaft} = E\dot{x}_5 - E\dot{x}_6 - \dot{E}x_{Q-loss} - \dot{E}x_d \tag{4.29}$$

where $\dot{W}_{shaft}$ is the work extracted from the pressure differences. $E\dot{x}_5$ and $E\dot{x}_6$ are the exergy of the air flow at the inlet and outlet of the piston, respectively. $\dot{E}x_{Q-loss}$ is the exergy lost because of heat transfer to the ambient, and from one side of the piston to the other side. $\dot{E}x_d$ is the exergy destroyed within the system from irreversibility. The value of $\dot{E}x_d$ can be found by calculation of the entropy generation. The relationship between entropy generation and exergy destroyed is defined as:

$$\dot{E}x_d = \dot{I} = T_0\, \dot{S}_{gen} \tag{4.30}$$

where $\dot{I}$ is the irreversibility rate, T_0 is the ambient temperature and $\dot{S}_{gen}$ is the value of entropy generated based on mass flow of the air in the piston assembly. Practically, it is difficult to find the exact values for $\dot{E}x_{Q-loss}$ and $\dot{E}x_d$ separately, so in the

calculation, the combination of them can be used.

To find the work output per unit mass, both sides of Equation (4.29) should be divided among the mass flow rate of the working fluid,

$$\dot{w}_{shaft} = e\dot{x}_5 - e\dot{x}_6 - (\dot{e}x_{Q-loss} + \dot{e}x_d) \quad (4.31)$$

where $\dot{w}_{shaft}$ is the shaft work output of the piston per unit air mass. Also $e\dot{x}_5$ and $e\dot{x}_6$ are the exergy of the air flow through the inlet and outlet of the piston per unit mass, respectively. Also $(\dot{e}x_{Q-loss} + \dot{e}x_d)$ shows all internal and external irreversibilities per unit of working fluid mass.

4.1.7 Calculation of Shaft Work Output of the Piston Assembly

There are several ways to calculate the shaft work output from the piston assembly, with regards to the current configuration of the MHE. As mentioned in the previous section, one way to calculate the shaft work output is to find the gas enthalpy at different points and performing energy and exergy analyses. The other way to find this value is to focus on the thermodynamic cycle of the heat engine. The results of the analysis will show how the system can be improved. In this section, the analysis was performed by considering the thermodynamic cycle of the MHE.

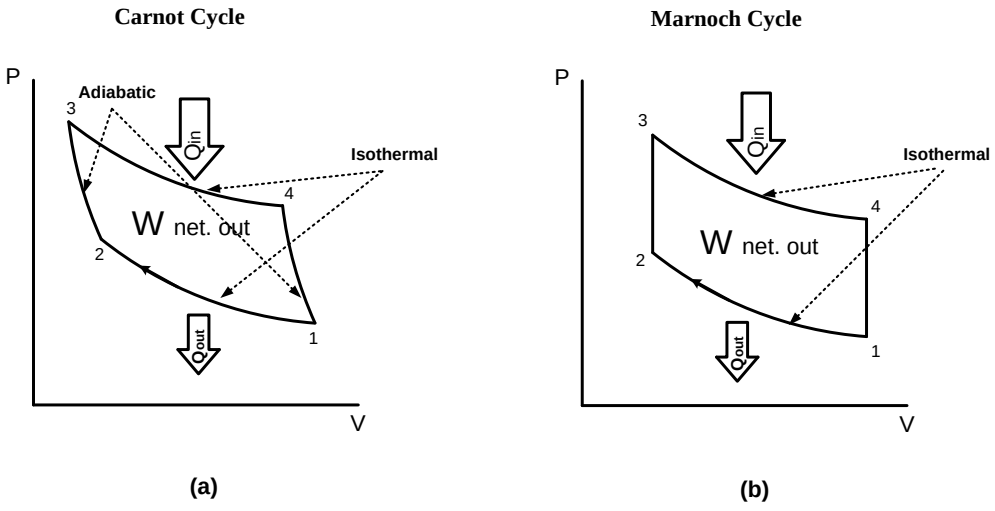

Figure 4.4: Comparison of Carnot cycle and Marnoch cycle.

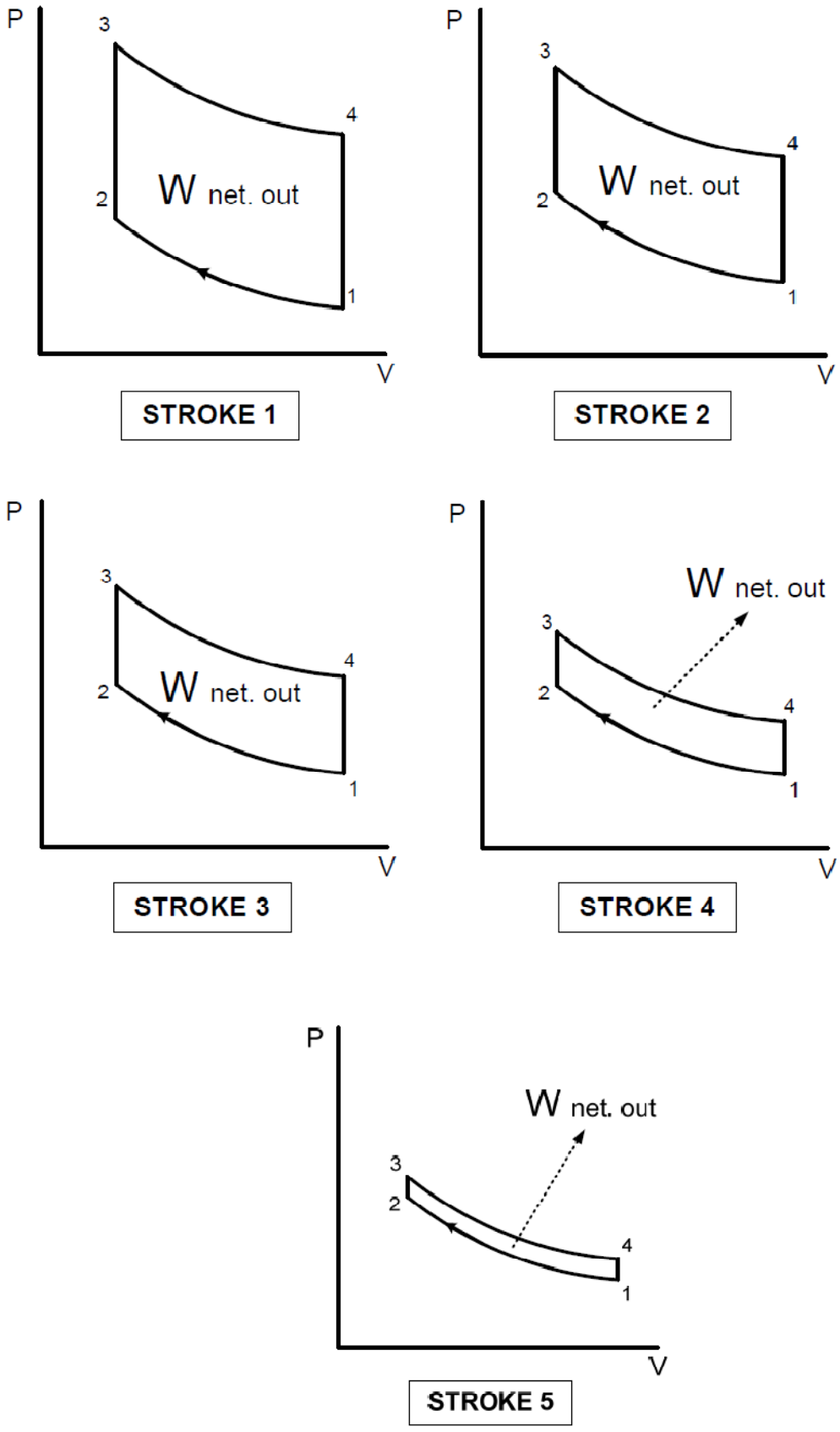

Figure 4.5: Five power-cycles of the MHE for five piston revolutions.

In Figure 4.4, the related thermodynamic power-cycle of the MHE [60] is shown and compared with an ideal Carnot cycle. Figure 4.4b shows that the power-cycle of the MHE is similar to the Stirling cycles. However, unlike the Stirling cycle, the enclosed area of the MHE is reduced after each stroke during the operation of one tank pair. Figure 4.5 is a demonstration of the area reduction of cyclic work output from the piston assembly.

Pre-charge pressures and available temperature differences will affect the number of piston revolutions, and relatively on number of power-cycles per operation period. The following equations show how these variables change the performance of the MHE.

As mentioned earlier, the compression and expansion processes in the MHE are assumed isothermal and air is assumed to be an ideal gas. Thus, the ideal gas law is used to find the air properties.

$$PV = mRT$$

The MHE is a closed cycle; therefore no gas enters or leaves the system during operation. The amount of leakage in the MHE is negligible; hence, the value of *n* is constant. Thus, it is concluded that $C = nRT$. Here *C* is a constant for each revolution. By substitution of *C* in the ideal gas equation:

$$P = \frac{C}{V} \tag{4.32}$$

The work output of the piston as the result of one expansion can be found as:

$$W = \int_{Vi}^{V_f} P_v \, dV \tag{4.33}$$

Substituting (4.32) into (4.33) yields:

$$W = \int_{Vi}^{V_f} \frac{C}{V} \, dV = C \int_{Vi}^{Vf} \frac{1}{V} dV \tag{4.34}$$

Thus:

$$W = Cln\left(\frac{Vf}{Vi}\right) = Cln\left(\frac{Vi+\Delta V}{Vi}\right) = Cln(1+\frac{\Delta V}{Vi}) \quad (4.35)$$

The piston surface is constant during operation and during each revolution, but the length is changed. Hence, $\Delta V = A\,\Delta L$. By using this value in Equation (4.35),

$$W = Cln\left(1+\frac{A\,\Delta L}{Vi}\right) = Cln(1+C_{avi}\Delta L) \quad (4.36)$$

Here C_{avi} is a constant that is defined as $C_{avi} = \frac{A}{Vi}$

Equation (4.36) shows the work output of the piston as the result of one revolution. After the first revolution, some air mass is transferred to the other tank. Thus, the pressure on the other side is changed and the value of *C* will be changed accordingly. When the work output of the next stroke of the piston is calculated by Equation (4.35), the work performed by the compression of the piston is negative.

After testing the engine several times and simulating different temperatures and pressures, the time required for each revolution was found to be around 1 sec. This timing will be evident in experimental graphs of power output in chapter five.

4.1.8 Mass Balance of Tank 2

When tank 2 is connected to the cold reservoir, water flows through the copper tubes and cools down the air inside the heat exchanger. The air pressure inside the heat exchanger drops. The thermodynamic analyses for this heat exchanger are similar to the analyses for tank 1. The following analysis shows the main equations and conditions in tank 2, when it is used as the heat sink.

In the present experimental setup, the temperature range of the heat sink is between 282.15 K to 298.15 K. Similar to tank 1, tank 2 is an unmixed heat exchanger. Water flows through the system at steady flow rates. Thus mass balance equation for the water stream is given as:

$$\dot{m}_{w3} = \dot{m}_{w4} \quad (4.37)$$

The gas inside tank 2 is not in a steady state condition like tank 1. Thus, Equation (4.8) can be applied to show the air mass balance. In this heat exchanger, unlike tank 1 for the working fluid, in Equation (5.8), tank 2 ($\Delta\dot{m}$) has positive values. The reason is because the air flows to the cold heat exchanger and accumulates within this heat exchanger to be cooled down.

$$\Delta\dot{m} = \dot{m}_6 \tag{4.38}$$

Equation (4.25), for the piston assembly, shows that the mass accumulation in tank 2 is equal to the mass leaving tank 1. Thus, similar equations are used for mass balance of the working fluid in tank 2.

$$\dot{m}_6 = \frac{m_{a,in}}{dt} \tag{4.39}$$

Considering Equations (4.38), (4.39) and Equation (4.13), the total mass accumulation in tank 2 is:

$$\sum \frac{\dot{m}_6}{dt} = (m_{initial} - m_{final}) \tag{4.40}$$

When tank 2 is being charged, all values of Equation (4.8) are zero and no mass flow exists in the system. When the operation starts, air accumulates in tank 2. When the operation stops, no air transfers to tank 2. Air leakages from valves and joints are neglected in the calculations. Similar to tank 1, to keep the compression process almost isothermal, water flows through the system during the piston operation period.

4.1.9 Energy Analysis of Tank 2

After leaving the piston, air will expand and its temperature will decrease. It will be stored in heat exchanger 2. After multiple strokes, the working fluid pressure and temperature in heat exchanger 2 starts increasing. Water from the heat sink goes through the heat exchanger to cool down the air and decrease the temperature and

pressure. In the current calculations, it is assumed that the engine works continuously. For the first step of operation of tank 2, the energy balance for a water stream of tank 2 in this step is defined as:

$$\dot{m}_{w3}h_{w3} = \dot{m}_{w4}h_{w4} + \dot{Q}_{fa} + \dot{Q}_{l} \tag{4.41}$$

where h_{w3} and h_{w4} are the enthalpy of water at the inlet and outlet of the copper tubes. Hence, $\dot{m}_{w3}h_{w3}$ is the energy of the water stream that enters the heat exchanger, and its value is assumed to be constant with time. Also $\dot{m}_{w4}h_{w4}$ gives the energy of the water stream that goes to the heat sink. It is decreases over the period of time until the temperatures of water to the inlet and outlet of tank 2 are very close to each other. $\dot{Q}_{fa}$ represents the amount of heat absorbed by the water stream through the heat exchanger. $\dot{Q}_{l}$ is the energy lost to the ambient from the air. When the temperature of the heat exchanger is lower than the ambient, this value is negative because heat is coming into the system. $\dot{Q}_{l}$ is negligible when the heat sink and ambient have similar temperatures.

During the operation, heat transfer to the system occurs due to air movement into the heat exchanger. The energy balance equation in this condition can be solved for the water stream, or the heat exchanger shell as the system boundary. When the area inside the shell is the system boundary, the heat coming to the system by air and the heat removed by the exit-water stream are transient. A way to find the heat removed from the system is to consider the heat exchanger copper tubes inside heat exchanger 2, as the control volume.

$$\int_0^t \dot{Q}_{from\ air}\ (dt) = mc\,\Delta T \tag{4.42}$$

When the copper tube is the control volume, c is the specific heat capacity of water, *m* is the water mass and ΔT shows the water temperature changes. When the water mass flow rate is known, readings from the water inlet and outlet thermometers are used.

4.1.10 Exergy Analysis of Tank 2

The exergy balance equations for tank 2 are similar to the exergy equations for tank 1. Equation (4.24) for tank 1 shows the exergy transfer from the water stream to the gas due to heat transfer. However, in tank 2, exergy of the air will be transferred to the water due to heat transfer. When the water stream in the copper tubes is used as the control volume, the exergy balance equation can be written as:

$$\dot{m}_3(ex_3 - ex_4) - \dot{Ex}_{fa} - \dot{Ex}_d = 0 \quad (4.43)$$

where ex_3 is the exergy of point 3 for the water inlet, and ex_4 is the exergy of point 4 for the water outlet. These two values are calculated by Equation (4.20), considering properties of water at these points. $\dot{Ex}_{fa}$ is the exergy associated with heat that is transferred from the air to the water. The value of $\dot{Ex}_{fa}$ can be calculated from Equation (4.21). Unlike heat exchanger 1, the value of $\dot{Ex}_d$ in the calculations of tank 2 is either negative or close to zero. The reason is because the temperature of this tank is either less than or close to the ambient temperature; hence, exergy associated with heat will flow into the system.

4.2 Transmission System

In this section, the relative calculations of the transmission system are presented. The equations are presented so it is possible to study the effects of applying different piston and flywheel dimensions for the next MHE.

The information about the torque output for the piston used in the assembly is available from the manufacturer's catalogue. Based on the conditions for the piston, losses from the piston can be different. The torque output for the series used in this assembly is presented in Table 3.4. To find the rotational velocity of the piston, the following correlation can be used:

$$RPM_p = \frac{(NSP)(SRDR)}{360} \tag{4.44}$$

where RPM_p is the piston shaft rotation per minute, *NSP* is the number of strokes per minute and *SRDR* is the shaft rotation degrees per revolution. In the current piston assembly, the pinion rotates 270 degrees after each revolution, thus Equation (4.44) can be written as:

$$RPM_p = (0.75).(NSP) \tag{4.45}$$

The rotational direction is changed after each piston revolution. To find the power output for the piston, RPM_P is multiplied by the torque output from the piston assembly.

$$Power_p = \tau_P.(RPM_p) \tag{4.46}$$

where τ_{Piston} is the torque output of the piston assembly. Equations (4.44) and (4.46) can be combined as follows:

$$P_p = \tau_P \frac{(NSP)(SRDR)}{360} \tag{4.47}$$

Equation (4.47) calculates the power output from the two-way piston assemblies. For this specific assembly, Equation (4.45) can be substituted into Equation (4.46) to calculate the power output. τ_P in the MHE is changed after each revolution, because the pressure differences after each stroke decrease. A way to find the value of τ_P is to connect a torque meter to the piston assembly. In order to estimate the power output from the piston assembly, the output kinetic energy from the piston to the flywheel can be calculated. Considering the losses in chains and bearings, the energy output from the piston can then be estimated.

In the current system, the thickness of the disc is negligible in comparison to its diameter. Thus, to find the kinetic energy from the flywheel, Equation (4.48) can be used:

$$KE = \frac{1}{2}.Jm.\omega^2 \quad (4.48)$$

where *KE* is the kinetic energy of the flywheel, *Jm* is the rotational mass moment of inertia, and ω is defined as the angular velocity. To find *Jm*, Equation (4.49) is used,

$$Jm = \frac{W}{g}.\frac{k^2}{2} \quad (4.49)$$

where *W* is the weight load, *g* is the gravitational constant, and *k* is the radius of gyration. The value of ω to be substituted in Equation (4.48) is calculated by Equation (4.50).

$$\omega = \frac{AD}{Rt}.(0.035) \quad (4.50)$$

AD is the angular distance and *Rt* shows the rotational time. In the present setup, the angular velocity of the flywheel was not measured. Thus, to find the kinetic energy of the flywheel, it is assumed that the flywheel and piston are connected directly. Hence, the *AD* value is 270^o and the *RT* value is the required time for one revolution.

4.3 Efficiencies

There are different types of efficiencies that will be discussed in this section. Theoretical and experimental data from the heat engine under pre-defined conditions is obtained to calculate the system efficiencies.

4.3.1 Thermal (Energy) Efficiency of the Cycle

A limitation on the performance of the systems is indicated from the Kelvin-Planck statement of the second law [41]. The thermal efficiency of the system can be defined as:

$$\eta_{th} = \frac{W_{cycle}}{Q_H} \quad (4.51)$$

where W_{cycle} is the work output of the cycle, and η_{th} is the thermal efficiency of the system (varies between 0-1). The variable W_{cycle} can be calculated using Equation (4.33). Q_H is the amount of heat entering into the system from the heat source. Q_H can be defined in two different ways. In the first method Q_H is defined as the total heat coming into the system from the hot water stream. In the second method, the Q_H can be calculated by substituting Q_{ta}, which is the amount of heat transferred to the air, into Equation (4.51). The efficiency in the second method is independent of the heat exchangers effectiveness, as well as losses in that section. Both methods will be used to show the efficiency drop that occurs through the system because of the heat exchangers.

4.3.2 Overall Efficiency of the Engine

The entire system performance can be evaluated, by the total efficiency of the system. The final goal of the MHE is to generate electricity efficiently. Hence, in the calculations, only the electric work from the generator is considered as the work production. The overall efficiency of the system (η_t) can be defined as:

$$\eta_t = \frac{W_e}{Q_H} \tag{4.52}$$

where W_e is the electric work output from the engine, and Q_H was discussed in section 4.1.2. W_e has significant fluctuations, therefore, in order to have reasonable calculations in the whole time period, the operation of one tank pair must be considered for energy consumption and electricity generation.

4.3.3 Carnot Efficiency

The Carnot efficiency or ideal efficiency is the maximum possible efficiency of a heat engine, when no irreversibility exists in the processes. Experimentally, reaching the Carnot efficiency is not possible in heat engines. The Carnot efficiency gives a

prediction of the thermodynamic performance of the heat engine in varying temperature ranges. The ideal efficiency of the MHE can be defined as follows:

$$\eta_{Ideal} = 1 - \frac{T_C}{T_H} \tag{4.53}$$

where the values of T_C and T_H are the temperatures of the heat sink and heat source, respectively.

4.3.4 Exergy Efficiency

The second law provides an indication of the irreversibilities within the system. The amount of decrease in system performance due to heat and mechanical losses is characterized by this law. In this study, the efficiency of the MHE based on the second law is defined as:

$$\eta_{\text{II}} = \frac{\eta_t}{\eta_{Ideal}} \tag{4.54}$$

This can be calculated by substituting the overall efficiency of the engine and Carnot efficiency into Equation (4.54). The efficiency can be increased by minimizing the mechanical and heat losses within the system. For instance, these losses can be minimized by preventing heat losses from the heat exchanger shells, and increasing the heat exchanger performance.

The exergy efficiency is based on the second law of thermodynamics. The exergy efficiency provides an alternative understanding of performance. In evaluating the energy efficiency, the same weight is assigned to energy whether it is electric, shaft work or low-temperature thermal energy. Exergy efficiency weights the energy flows by accounting for each in terms of exergy [60]. From the exergy efficiency, it can be understood how internal and external irreversibilities affect the performance of the engine. The exergy efficiency (η_{Ex}) for the MHE is defined as:

$$\eta_{Ex} = \frac{W_e}{Ex_{in}} \tag{4.55}$$

where Ex_{in} is the exergy entering into the system. In this system, it is assumed that no chemical reaction occurs in air as the working fluid. In the MHE, it is assumed that the heat that entering the system is waste heat and no combustion is required to generate this heat.

There are two ways to calculate Ex_{in}. In the first method, the exergy of hot water can be obtained from Equation (4.20) (point 5 in Figure 4.1). Thus, the value of Ex_{in} is the exergy of the hot water stream that goes through the hot heat exchanger. In the second method, Equation (4.24) is used to find Ex_{in}. Thus, Ex_{in} is the exergy transferred through the system associated with heat. Considering Equation (4.24), the denominator of Equation (4.55) is smaller than the denominator of Equation (4.52). Hence, the exergy efficiency of the system is higher than the system energy efficiency. This can be explained by converting low grade energy in the MHE to high grade energy of electricity.

4.4 Uncertainty Analysis

Uncertainty analysis is needed whenever an experiment is preformed, to determine the errors associated with the experimental values. The uncertainty in the experimental values has two components; bias and random variations. Bias is the error associated with the inaccuracy of the measuring equipment, and it provides us with a measure of the degree of closeness of the measured experimental values to the actual true values. Random variations are the errors that occur due to the uncontrolled parameters when making repeated measurements. They are related to the precision of the experimental readings, and can be determined by finding the deviation of the readings.

The bias value for the experimental readings is equal to the accuracy of the sensors used in the experiment, which are taken from the manufacturer's catalogues. Determining the random variations of the experimental readings requires finding the standard deviation (σ), using the following equation:

$$\sigma = \sqrt{\frac{\sum(X-M)^2}{n-1}} \tag{4.56}$$

where X is each individual experimental reading, M is the mean value of the experimental readings, and n is the number of recorded experimental readings for each variable. Then the precision can be found using the following equation:

$$P = \frac{2\sigma}{M} \tag{4.57}$$

To reduce the systematic errors, gauges were calibrated before carrying out the experiments. The experiment was done several times for each set of data, and an uncertainty analysis was carried out for each set of experiments. The main source of inaccuracy is the measuring equipment. For example, the accuracy of the pressure sensors is ± 6.9Pa, and the accuracy of the thermometers is ± 0.01ºC. The ambient temperature during each test is non-uniform. For each case, the average temperature of the surroundings was measured for the calculations.

The uncertainty (U) for experimental data is calculated by the following equation:

$$U = \sqrt{B^2 + P^2} \tag{4.58}$$

where B is the bias limit, and P is the precision limit for the experimental readings.

Chapter 5:

Results and Discussion

In this chapter, the theatrical, predicted, and experimental results of the MHE are presented. In the first section, effects of changing the pressures and temperatures on the system are presented. By analyzing these results, it is possible to determine the performance of the system in different conditions, and select the best components for the heat engine.

5.1 Effects of Increasing the Pre-charge Pressure inside the Tanks

Increasing the pre-charge pressure inside the tanks affects the structure and performance of MHE. Moreover, raising this pressure will result in higher capital and maintenance cost of the heat engine. Thus, to increase the pressure to higher levels, proper economic and thermodynamic analyses need to be performed. Figure 5.1 shows how the pressure differentials vary with higher pre-charge pressures. Each line in this figure belongs to a certain heat source and sink temperature. *T1* is the initial temperature and *T2* is the final gas temperature. The trends of variations of pressure differences in three different initial and final temperatures in the range of 273.15 K to 373.15 K are demonstrated. When the pre-charge pressure increases, at a certain temperature (Figure 5.1), the same final temperature will result in higher pressures. Hence, at low-temperature differences, high pressure systems have to be built to obtain high enough pressure differences for continuous operation. Figure 5.2 shows the variations of pressure differences in the MHE heat exchangers at different initial pressures.

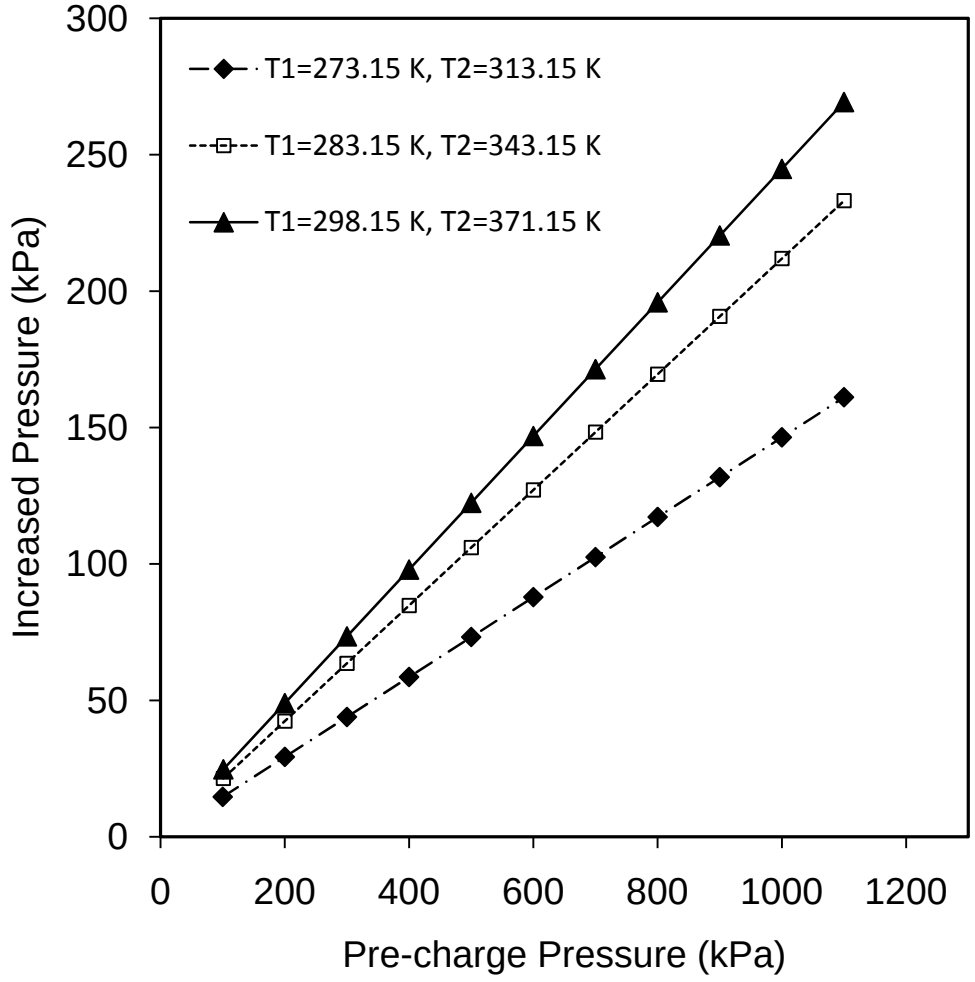

Figure 5.1: Maximum pressure differences with varying pre-charge pressures

In this thesis, tests and simulations were performed for pressure differences of 344.7 kPa to a maximum of 1034.21 kPa on this heat engine. Figure 5.3 shows the heat source temperatures that can create these pressure differences, when the heat sink temperature is 298.15 K. The solid line presents the pre-charge pressure of 344.68 kPa. It is located on top of the broken line that represents the pre-charge pressure of 689.48 kPa. From this trend, the high-temperature heat sources have to be available to create these pressure differences when the pre-charge pressure is not high. In such cases, water at ambient pressures (101.3 kPa) cannot be the heat carrier through the heat exchangers.

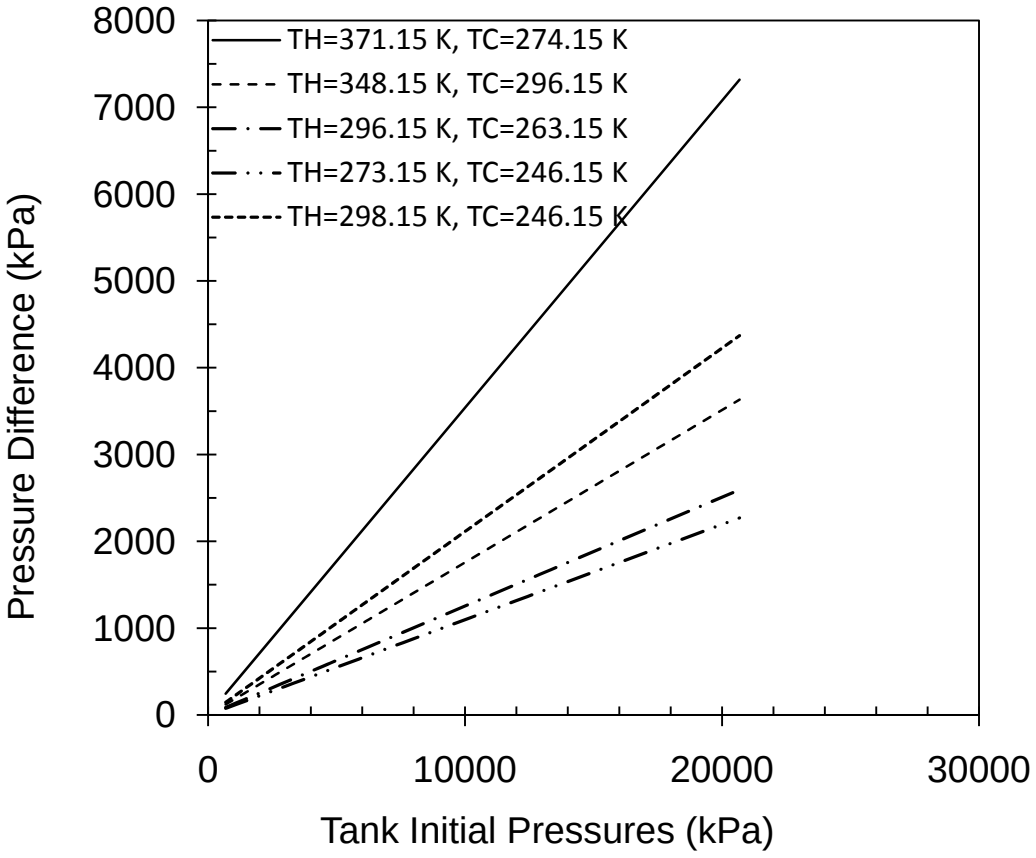

Figure 5.2: The variation of created pressure differences in MHE with different initial pressures

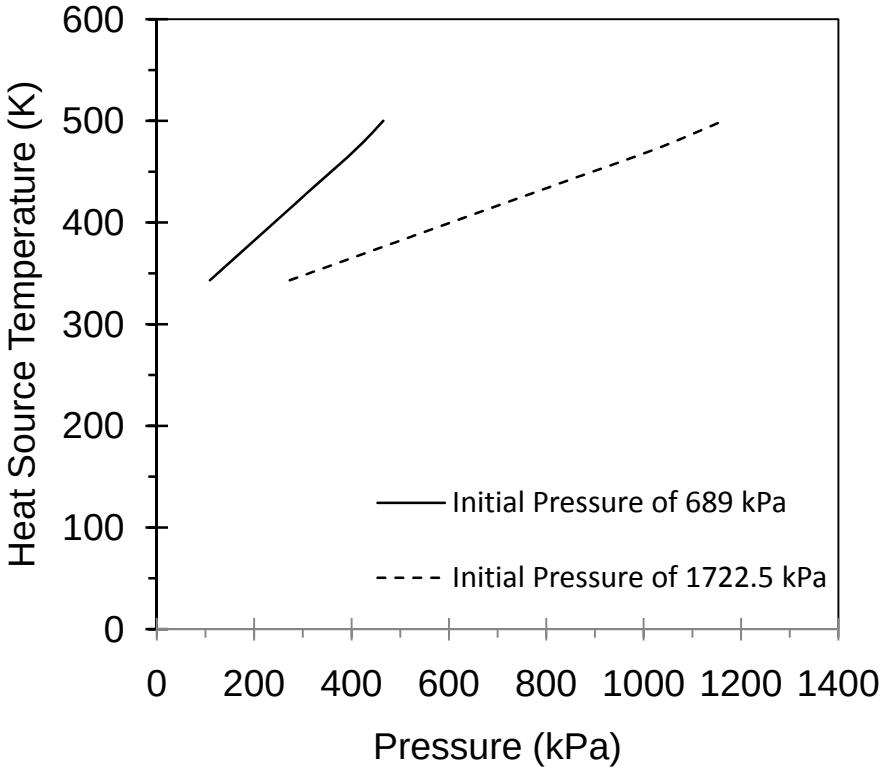

Figure 5.3: Relation of pressure differences with heat source temperatures

5.2 Mechanical Efficiency of Transmission System

To find the transmission efficiency, the engine was operated and tested five times [62]. In each test, the number of piston strokes and power output from the generator was found. The actual torque produced from this piston assembly, for a 689.48 kPa pressure differential, is 42 Nm [59]. From Equations (4.45) and (4.46), the power output from the piston is calculated. The mechanical power outputs were compared with the electric power outputs from the generator. With that data, the summation of losses that occurred through the transmission system and generator was calculated. The average efficiency of the system in these experiments was 40%.

Table 5.1: Transmission and generator efficiency

	Peak Power (W)	Stokes Per Minute	RPM	Piston Power (W)	Mechanical Efficiency
Run 1	81	59	44.25	195	0.42
Run 2	92	61	45.75	201	0.46
Run 3	81	60	45	198	0.41
Run 4	63	58	43.5	191	0.33
Run 5	72	59	44.25	194	0.37
Average	77.8	59.4	44.55	195.8	0.4

Source: [62]

The efficiency found for the transmission system is more accurate for pressure differentials that are closer to the pressure differential of the test (689.48 kPa). This is because the speed of the flywheel is less at lower pressures. When higher pressure differentials exist in the tanks, the flywheel speed is higher. Therefore, it is predicted that for low pressure differentials, the efficiency of the system is higher than 40%, and at higher pressure differentials, the efficiency is lower.

The fourth column of Table (5.1) shows the engine speed. It has an average of 44.55 RPM. The standard deviation of this column is 0.85. Considering this number, the precision limit (P) is 0.04. The bias limit is estimated as half of the smallest scale

of the forth column which is 0.003. This precision limit and bias number result in a 3.85% uncertainty in the power calculations.

5.3 Efficiency of Mechanical Components in the MHE

To calculate the mechanical efficiency of the MHE, two major parts of the system were considered. The first part was losses in the piston assembly sealing, and friction between the rack and pinion of the piston cylinder assembly. The second portion of losses occurs in the transmission system. From the manufacturer's specifications, the losses in the current assembly are in the range of 13-20% of energy output from the pinion. In this study in order to consider losses due to pressure drops, a maximum of 20% was considered in calculation [59].

As mentioned in the section 5.2, the efficiency of the transmission in the current system has an average of 40%. The piston assembly and transmission system function in series, thus, when both are operating in series, the overall efficiency is found by multiplying them. Hence, the overall mechanical efficiency of these two systems is about 32%.

5.4 Pressure Measurements of MHE

In this section, experimental readings obtained from the pressure sensors are presented. To achieve accurate results, the engine was operated several times. Some observed results were not useful because of problems with the installation of pressure tubes for sensors. Accurate readings were obtained from the first pair of tanks.

Figure 5.4 shows how the pressures vary in one pair of heat exchangers (hot and cold) during the operating period. To perform this experiment, one tank was filled with a pressure of 882.53 kPa, and the pressure of the other tank was 103.42 kPa.

Before starting the operation, there was a 160 second delay. Within this period, as demonstrated in Figure 5.4, the pressure inside tank 1 dropped. This happened since the temperature of the compressed air was higher than the ambient temperature initially, and shells of the heat exchangers were not completely insulated. Thus, heat transfer from the air to the shells, and from the shells to the surroundings, occurred. In tank 2, the initial pressure inside the shell was close to the ambient pressure, hence within the first 160 seconds, no considerable pressure change was observed in tank 2.

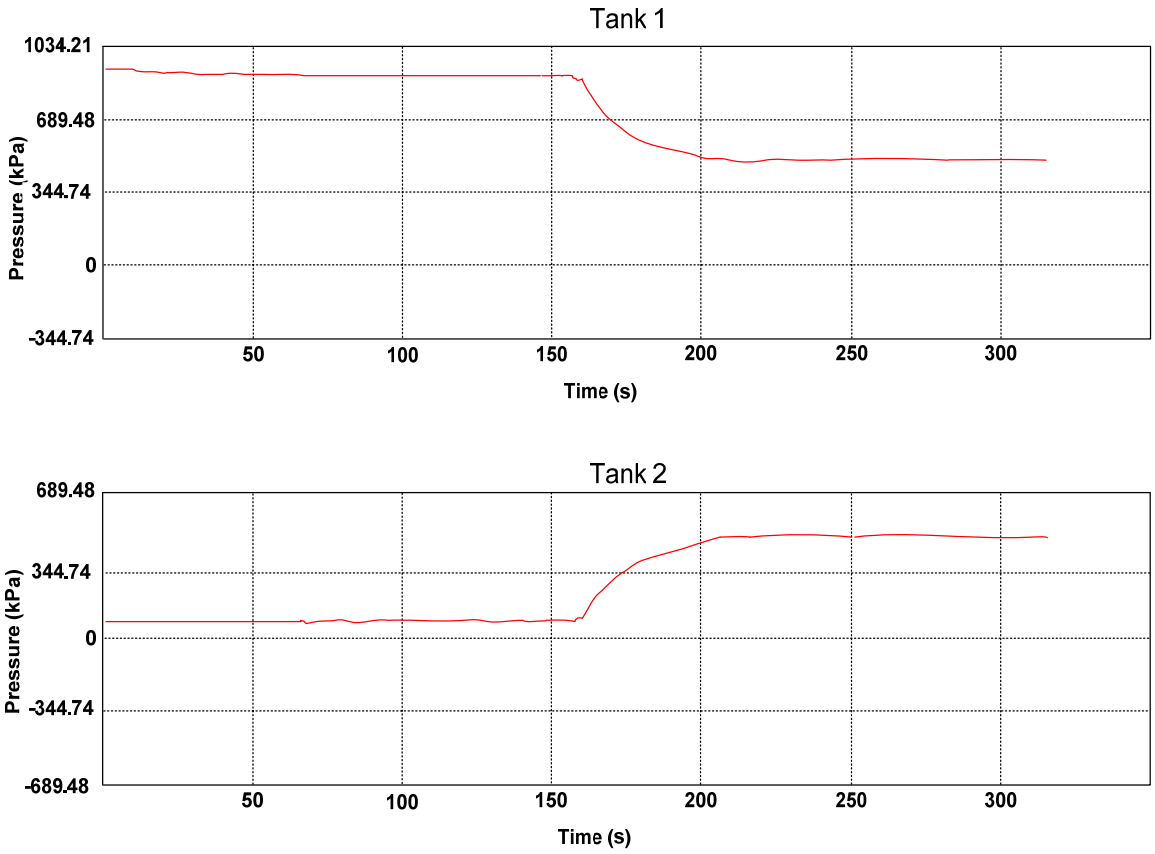

Figure 5.4: Pressure variations in one pair of heat exchangers during the operation period.

When the engine operation starts, due to heat and mass transfer from tank 1 into tank 2, the pressure of tank 1 decreases and the pressure of tank 2 increases simultaneously. The curved sections in Figure 5.4 represent this period. When the piston operation finished, the pressures inside the tanks did not equalize. The

remaining pressure difference was about 20.68 kPa in the experiment. The reason is because of friction losses in the piston assembly, so the remaining pressure difference could not move the piston.

5.5 Power Output Measurements from MHE

In this section, the measured power outputs from the piston assembly and generator are presented. The desired pressure differences were simulated for the tests. Before these tests, tanks were filled with compressed air at different pressures in each. During the experiments, hot and cold water passed through the heat exchangers, in order to heat up and cool them down. To find the power output from the heat engine, the engine was run several times at the same pressure differential and ambient conditions. Figure 5.5 shows the total power output from the electric generator during one cycle. The horizontal axis in this figure shows the initial pressure difference between the tanks. The separate points in this graph show the summation of power outputs from the MHE under specific initial pressures. To obtain reasonable values for each pressure differential, the engine was operated at least three times for each initial pressure differential. The results shown in Figures 5.5 - 5.9 were the closest results to the average readings of one set of experiments.

From the trend line in Figure 5.5, when the engine works under higher pressure differences, the electricity generated from the system is increased.

Figure 5.6 shows the total mechanical power output from the piston assembly at certain pressure differences. The mechanical power outputs are calculated by measuring the number of piston revolutions, within a certain time period, and the piston specifications from the manufacturer's catalogue. The numbers of piston revolutions were found by measuring the number of changes (open/close) of the

pneumatic valve. Comparing Figure 5.5 and 5.6, shows the amount of power loss within the transmission system of the MHE.

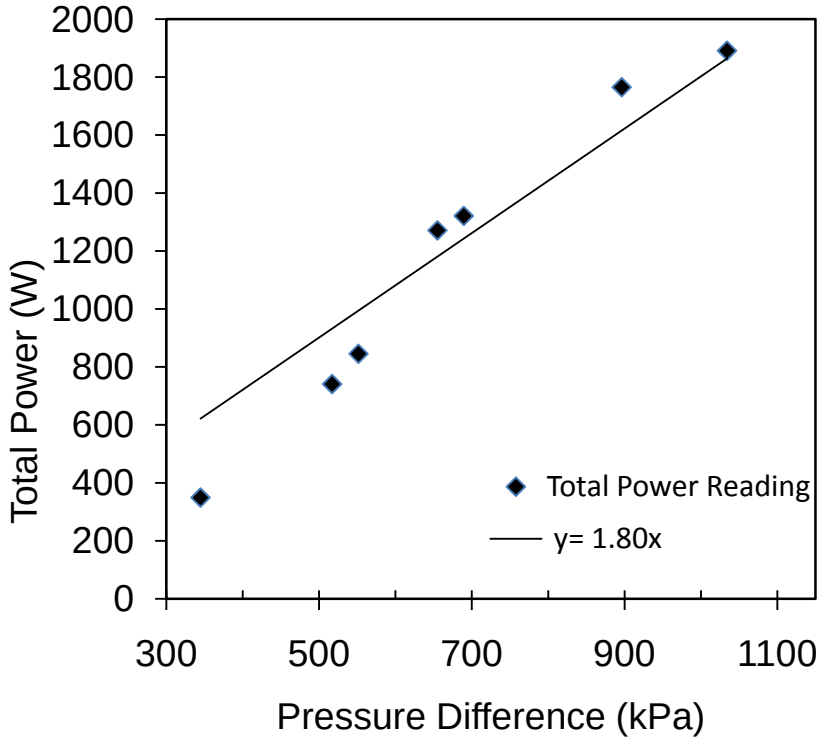

Figure 5.5: Total power output from the generator at varying pressure differences.

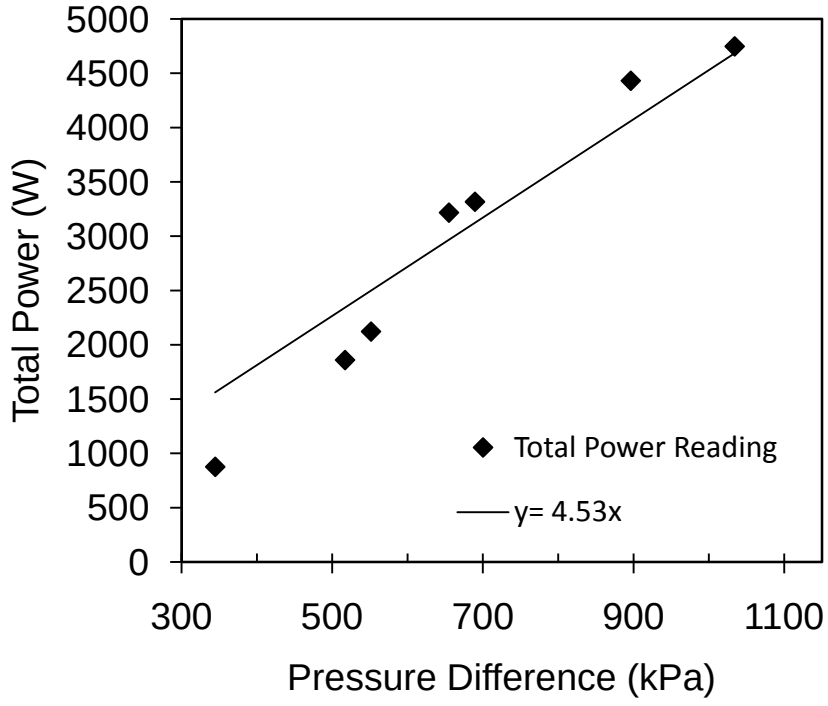

Figure 5.6: Total power output from the piston assembly at varying pressure differentials.

Figure 5.7 shows the measured power outputs from the generator during one cycle of operation. The power is measured after each piston revolution [62]. The minimum pressure differential for these tests was 344.74 kPa and the maximum was 1034.21 kPa. The power outputs from the generator show considerable fluctuations during the operation cycle, due to losses occurring in the flywheel. The flywheel in this system is fairly light; hence, during operation at certain times, the speed of the flywheel is higher than the piston speed. Consequently, the energy output of the piston is not added to the flywheel energy at these times. When the flywheel speed decreases, the power of the piston can be added to the system again.

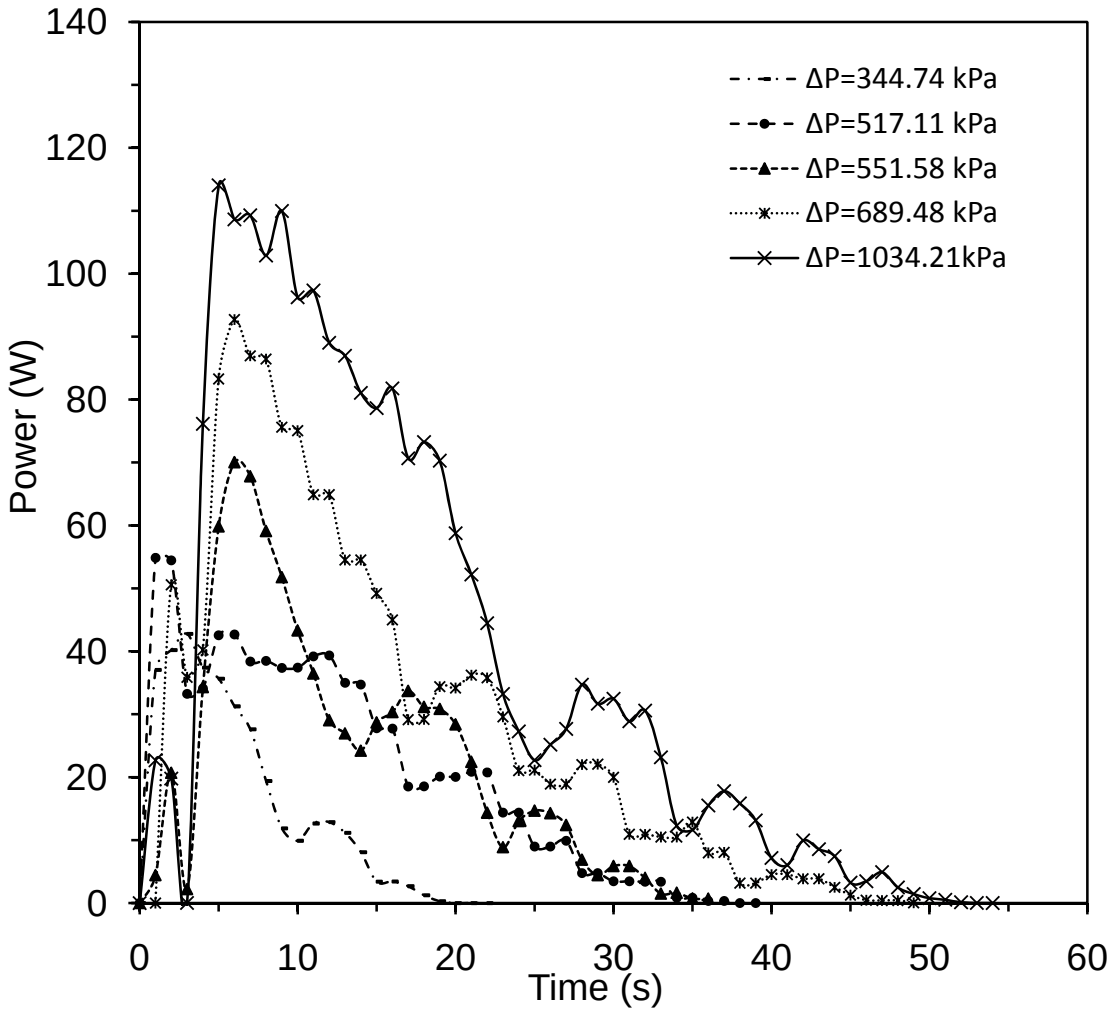

Figure 5.7: Measured power output from the generator from one tank pair at varying pressure differentials.

In Figure 5.8, the points represent the measured power outputs from the generator at two different pressure differentials. The continuous line shows the predicted power output from the generator at an 779.11 kPa initial pressure differential. The experimental pressure readings for this power prediction are presented in Figure 5.4. At this specific pressure differential (779.11 kPa), no power output reading was available from the generator. To validate the predicted power output from the generator, the power output measurements from the upper and lower pressure differentials were used. As expected, this line is located between the power output readings of the initial pressure difference of 689.48 and 1034.48 kPa.

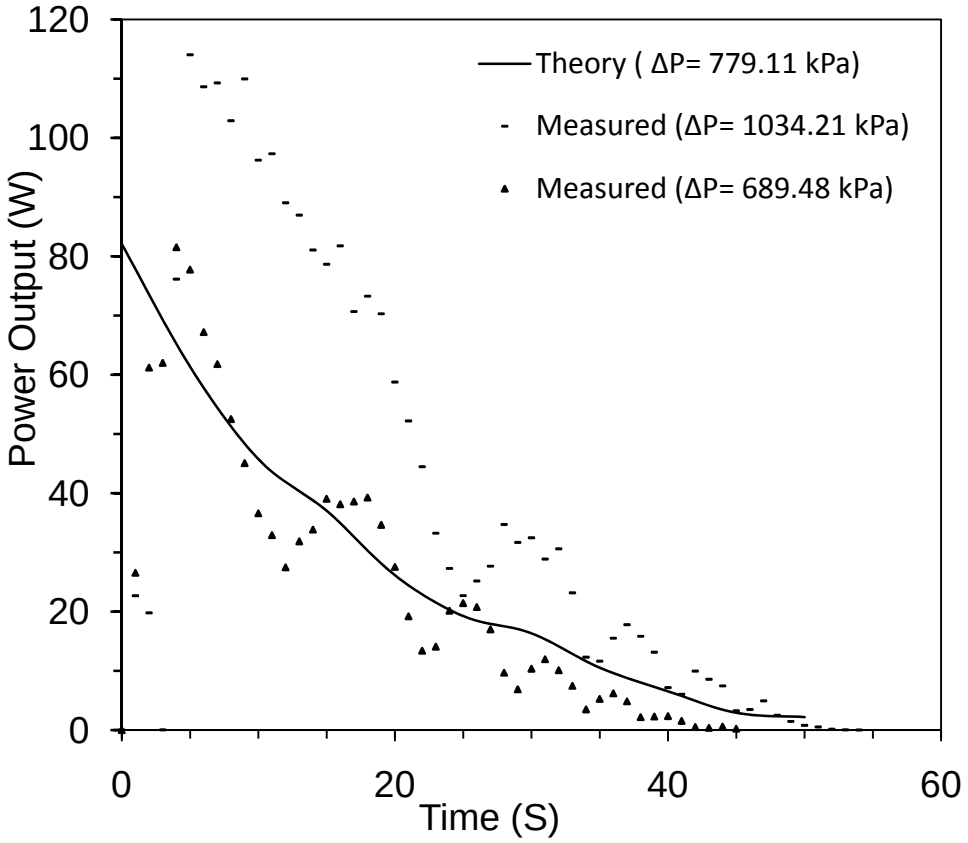

Figure 5.8: Comparison of measured and predicted power outputs from the generator for varying pressure differentials during one operation cycle.

The line that predicts the power output starts from a maximum value and drops over time gradually. However, the practical power measurements start from

almost zero, go higher, drop drastically and the power reaches its maximum. The reason for this trend is the initial energy required to rotate the flywheel. The first stroke is so powerful that afterwards, for about 2 seconds, no power is added to the flywheel. This trend is visible in almost all measured data from the MHE (Figure 5.7). Figures (5.7) and (5.8) show that the power output from the generator in the current prototype is not uniform. Sections (5.7.2) and (5.7.3) show the configurations of the MHE that can generate steady power output.

Figure 5.9 shows a comparison of measured and predicted peak power outputs from the generator for varying pressure differentials. Seven observed peak power outputs at certain initial pressures are shown in this graph. The continuous solid line shows the predicted peak power outputs from the generator. The closest match between the model and observed data occurs between the initial pressures of 600 and 700 kPa. At pressures around 1000 kPa, the model predicts higher power outputs from the system than the observed numbers. This is because the transmission efficiency was measured at 689.48 kPa. At higher pressure differentials, the rotary speed of the flywheel increases. Thus, more energy from the piston revolutions cannot be captured. Therefore, at high pressure differentials, the mechanical efficiency of the transmission system is less than 40%.

5.6 System Efficiency

The Carnot efficiency of the heat engines was discussed in chapter four. Figure 5.10 shows the Carnot efficiency of the system. The temperature ranges for the heat source and the heat sink in this study are between 272.15 K to 372.15 K. Practical applications; typically reside within this temperature range. In addition, in many areas of industry, waste heat in this temperature range is freely available. If solar source is

used to heat up the hot heat exchanger, the gas temperature can reach up to 472 K in certain hours during the day. In Figure 5.10, each line demonstrates the change of Carnot efficiency by changing the heat source temperature at a constant heat sink temperature. The trend of the lines shows an increase in Carnot efficiency by elevating the source temperature. For instance, at the temperature of 293.1 K and 298.15 K, for heat sink and source temperatures, the Carnot efficiency of a heat engine is 1.68% and when the temperature of the source is 353.15 K, the Carnot efficiency reaches 22.48%.

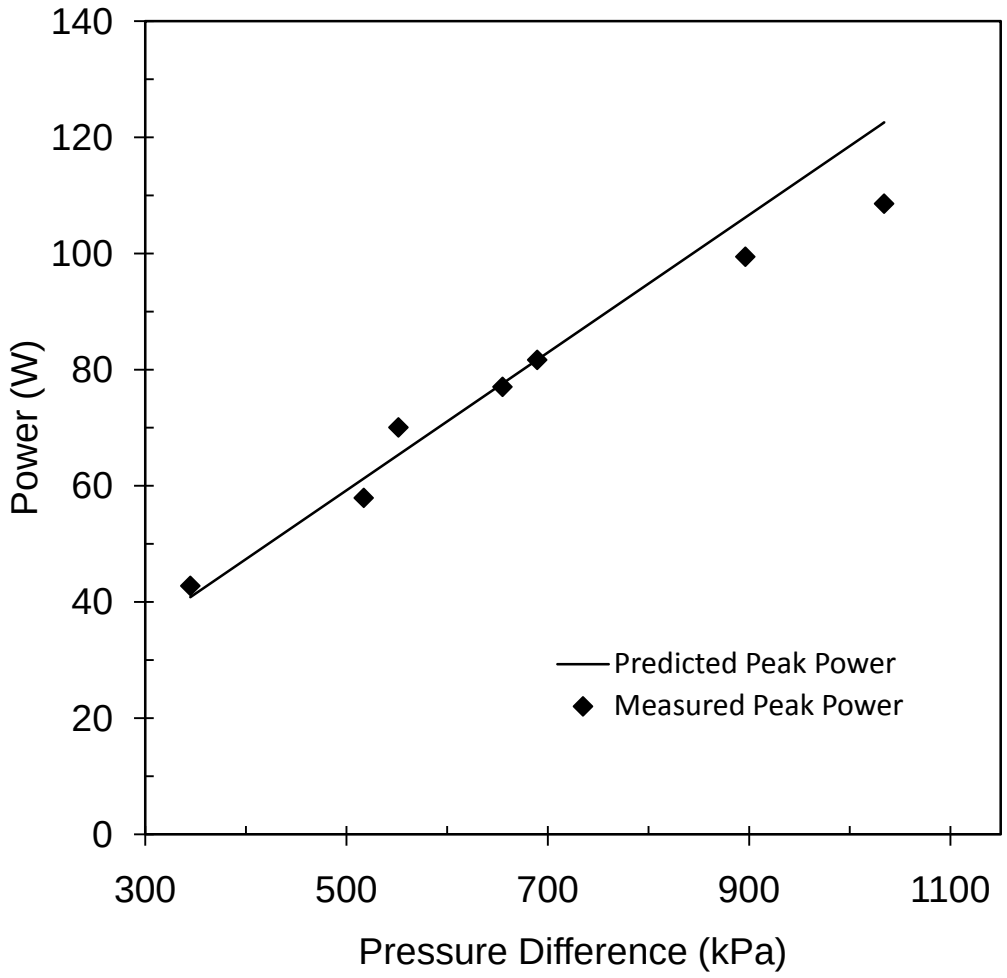

Figure 5.9: Comparison of measured and predicted peak power outputs from the generator for varying pressure differentials.

Figure 5.12 shows the variation of Carnot efficiency for certain temperature differentials. From this figure, having the same temperature differences in lower temperature ranges gives higher Carnot efficiencies of the heat engine. When the heat sink temperature is 273.15 K, the efficiency of the heat engine is higher than 283.15 K and 293.l5 K. This trend is valid for temperature differentials below zero as well. Also in Figure 5.9, the maximum possible efficiency achievable from this system in temperature ranges of 273.15 K to 373.15 K is 27.77%. Consequently, when water is used to bring and remove heat from the system, the thermal efficiency of the system cannot exceed 27.77%.

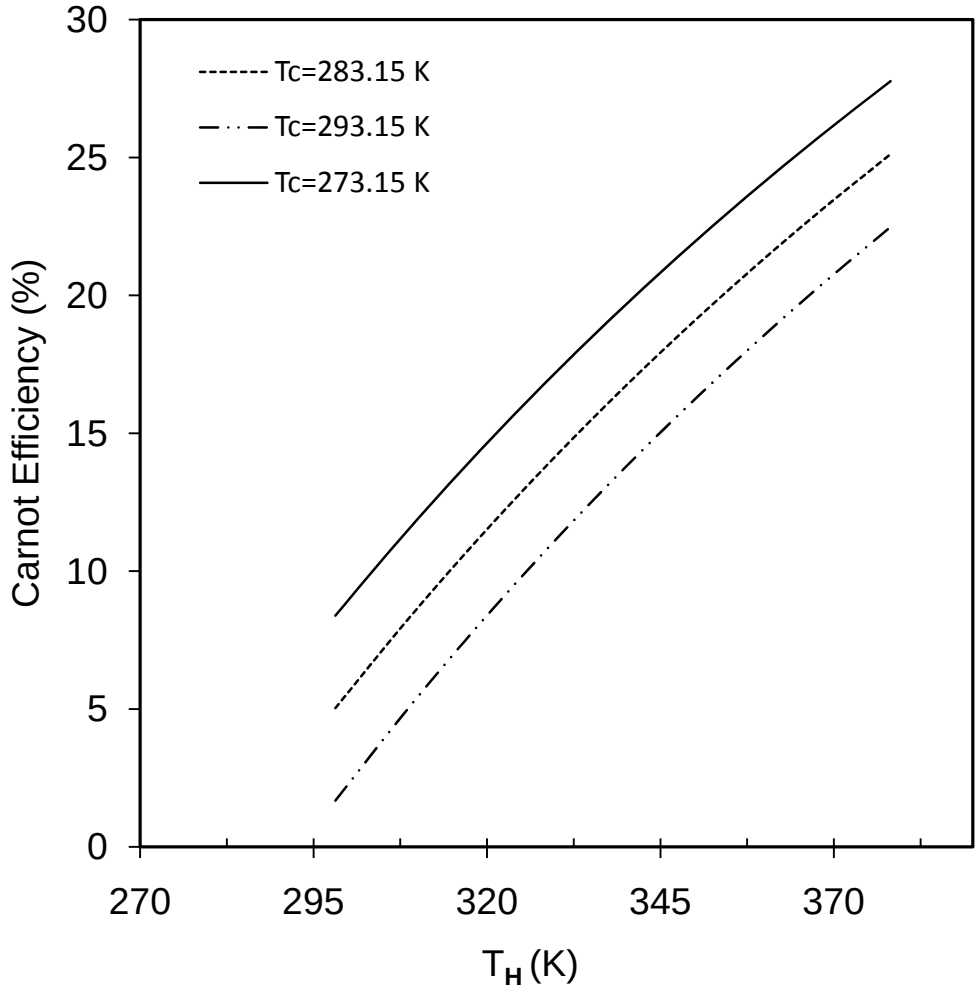

Figure 5.10: Variations of Carnot efficiency at different source temperatures.

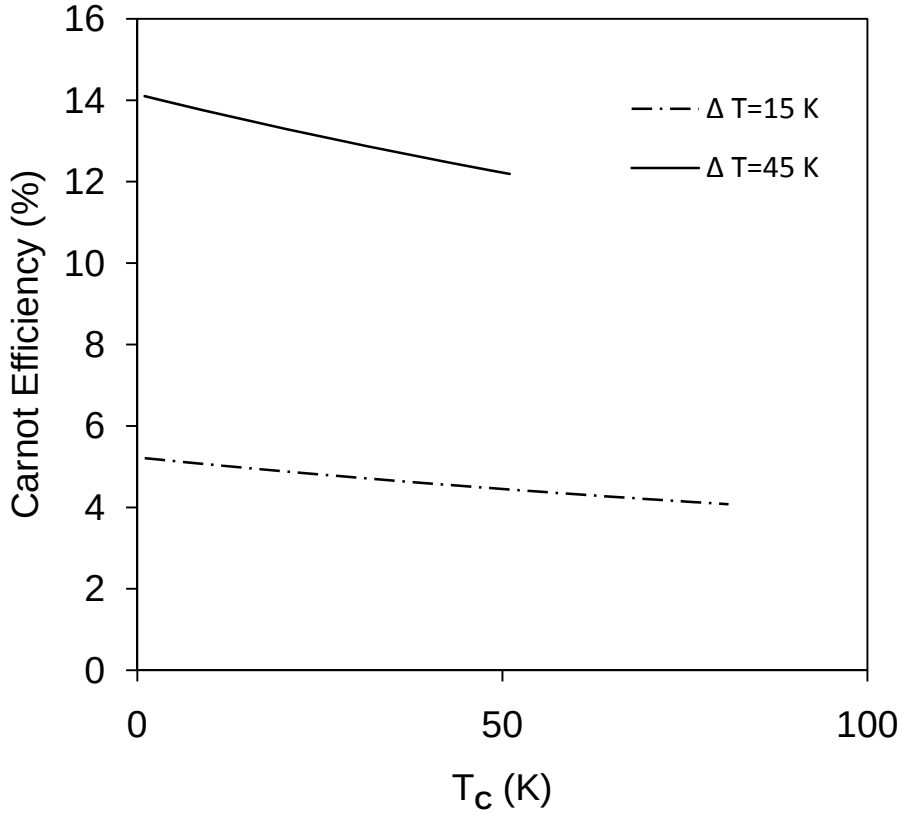

Figure 5.11: Variations of Carnot efficiency with different temperature ranges.

Figure 5.12 shows the energy and exergy efficiency of the system at varying pressure differentials. In this figure, the heat source and heat sink temperatures are 298.15 K and 342.15 K, respectively. The results are based on models and experimental mechanical efficiency of the system. From Figure 5.11, at higher initial pressures, the energy and exergy efficiencies of the system increase. Exergy and energy efficiency of the MHE with the heat sink and source temperatures of 273.15 K and 289.15^{o}K, are presented in Figure 5.11. When the air mass inside the tanks increases, the amount of heat that is transferred from the water stream to the air will raise. Therefore Increasing initial pressure of the MHE raises the energy and exergy efficiencies of the system Comparing Figures 5.12 and 5.13 clearly demonstrates that the effect of the temperature differential of the heat source and sink on the MHE is

significantly higher than the effect of initial pressure.

An interesting point in both Figures 5.12 and 5.13 is that the exergy efficiency of the MHE is significantly higher than the energy efficiency of the system. The reason is because calculations assumed that the system is using heat recovery and converting low grade heat to high grade energy [63]. Thus, no combustion or chemical reaction occurs for heat production. In addition, comparing Figures 5.12 and 5.13 demonstrates the effect of pressure increase for higher temperature differentials is higher than low pressure differences.

Figure 5.15 shows the variation of energy and exergy efficiency versus heat source temperature. In this plot the temperature of the heat sink is 298.15K. As this figure shows, the energy and exergy efficiency of the MHE increase when the temperature of the heat source increases. The other noticeable point in Figure (5.15) is that when heat is being recovered from low-temperature heat sources the exergy efficiency is higher than energy efficiency of the MHE.

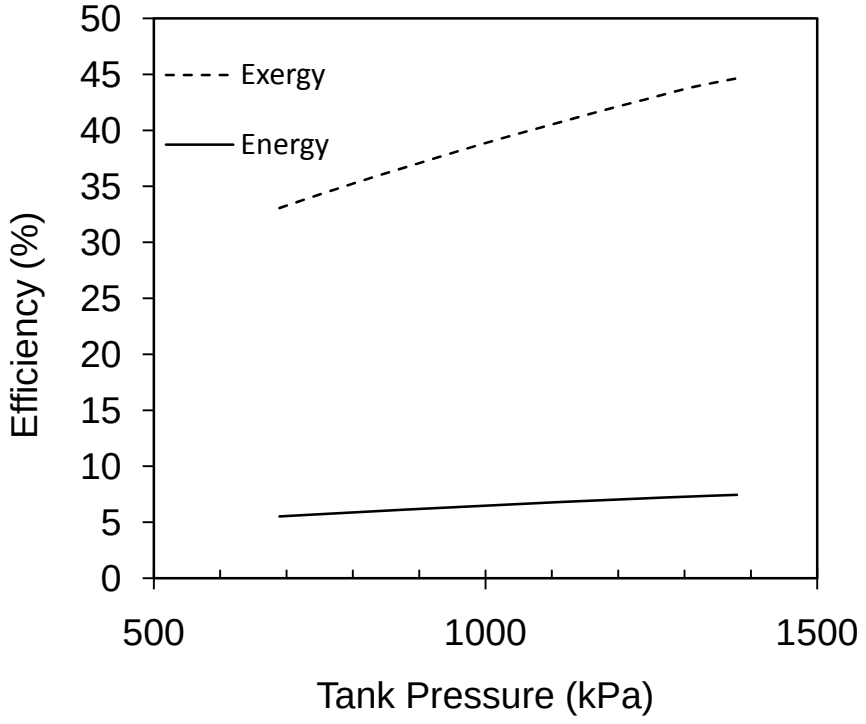

Figure 5.12: Energy and exergy efficiency versus system pressure (T_C=298.15 K and T_H=343.15 K).

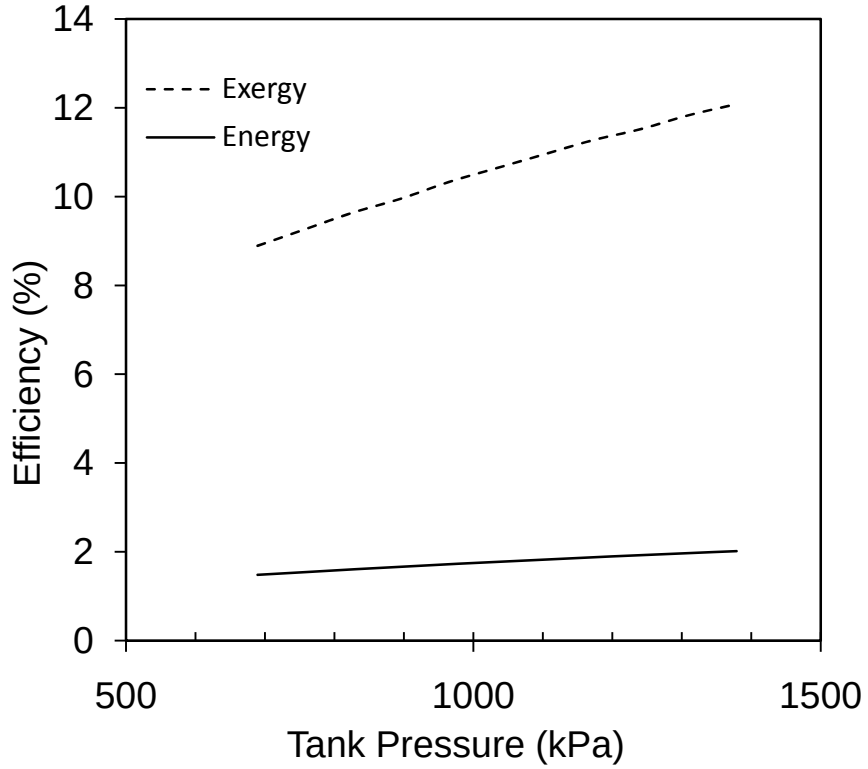

Figure 5.13: Plot of Energy and exergy efficiencies versus system pressure. (T_C=274.15 K and T_H=289.15 K).

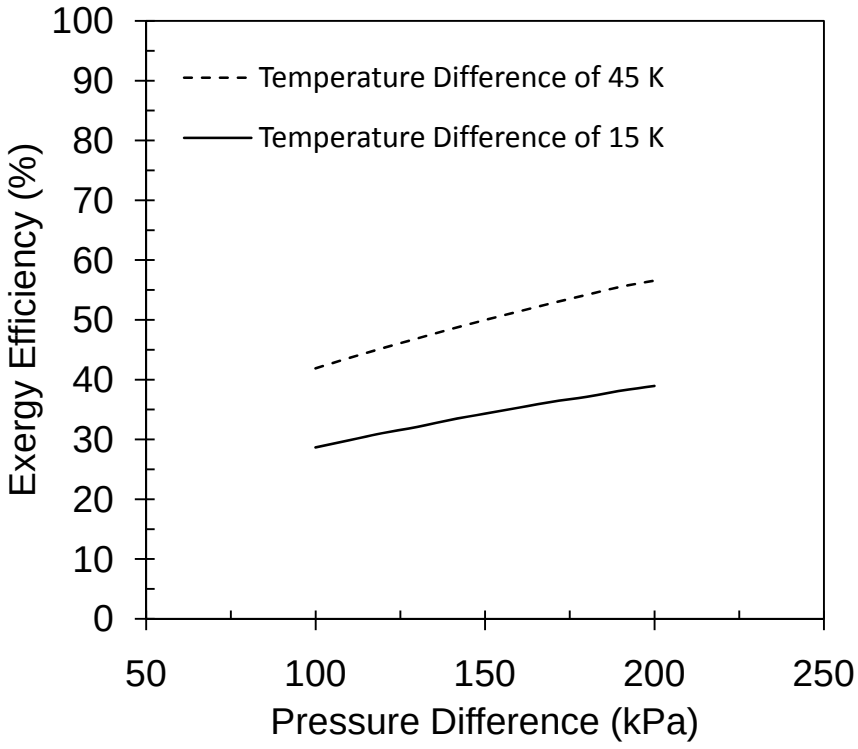

Figure 5.14: Effect of increasing the initial pressure on the exergy efficiency of the MHE.

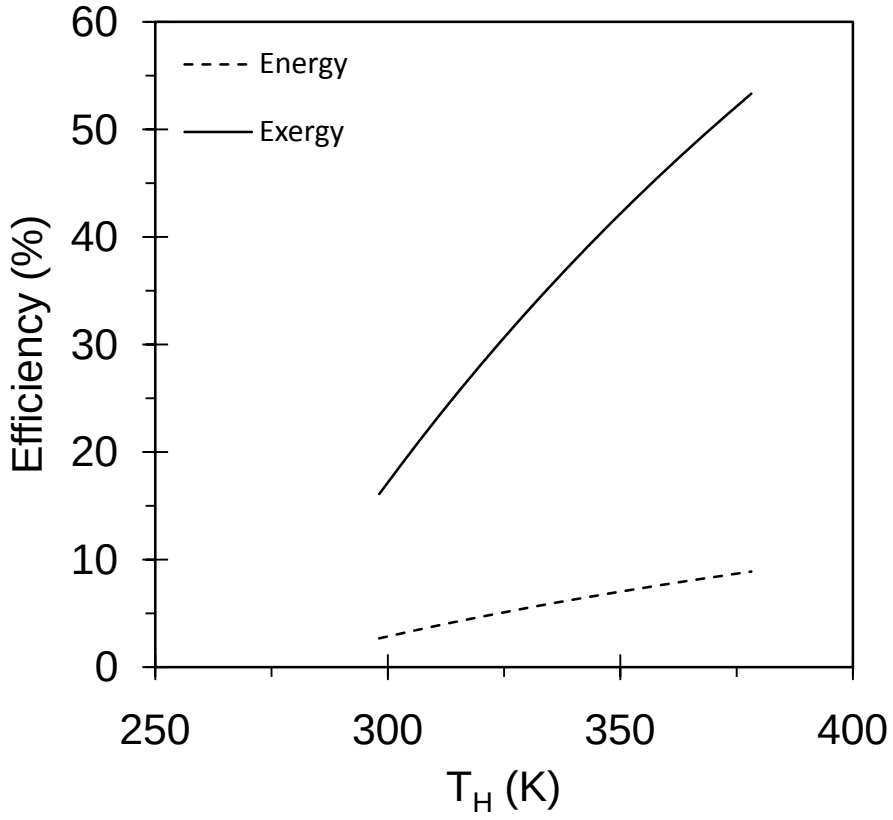

Figure 5.15: Effect of increasing the heat source temperature on the energy and exergy efficiency of the MHE.

5.7.1 Possible Improvements of the Current System

In the current system, two pairs of heat exchangers are used to create pressure differences. As shown in Chapter Five, the efficiency of the transmission system is about 40%. This efficiency can be increased by altering some parts. Figure 6.1 shows a schematic of the transmission system in the current MHE.

In this system, a poly V type belt is connecting the flywheel to the electricity generator. The pulley for the generator was grooved; however, the flywheel had no groove on the edge. Due to the speed variations of the flywheel, the connecting belt slips on the pulley while it drives the generator. These slippery movements will result in kinetic energy losses.

Furthermore, when the belt is tightening strongly, the force on the bearings increases and the rate of friction losses will be higher. When the belt is not tight enough, the pulley slippage will increase. To overcome this problem, the tightness of the belt has to be checked frequently, to maintain good performance of the heat engine.

A possible substitute for the poly V type belt is a toothed belt, a toothed pulley, and a flywheel. In this case, the down time of the machine will be reduced, and the amount of energy lost as a result of slip will decrease. Another way to reduce the losses and the maintenance cost is by changing the belt with a chain. There are two potential disadvantages that may occur with this replacement.

1. The chain transmission is noisier than the belt system.
2. The life of the shaft keys will be reduced due to sudden speed changes of the pulley.

In the current system, the diameter of the flywheel is 36cm and the diameter of the connected pulley to the generator is 5 cm. The speed of the pulley generator is about seven times more than the flywheel speed, and the diameter of the generator pulley is too small compared with the flywheel. Therefore, to avoid a sudden speed change, the speed change can be done in two steps. This rapid speed change can be improved by using another pulley, which has a ratio between the current generator pulley ratio and the flywheel ratio.

5.7.2 Possible Designs for the Next Marnoch Heat Engine Prototype

In the previous section, possible improvements of the current system were discussed. The proposed changes in section 5.7.1 required no major cost. In this section, three

possible configurations for the new prototype are suggested. To achieve these designs, the system must be rebuilt completely.

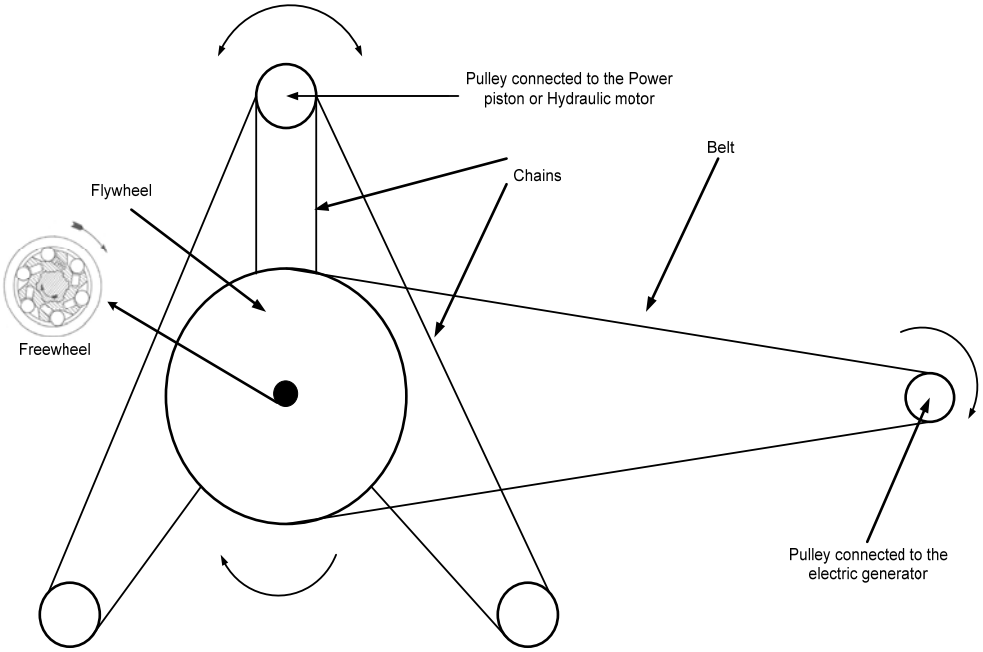

Figure 5.16: Schematic of the transmission in the current system.

5.7.2.1 Application of Multiple Tank Pairs

As discussed earlier, one of the major issues of the current system is that the power output of the engine is uneven, because pressures inside the tanks are equalizing rapidly with the present configuration. Where enough space is available for instalment of the heat engine, it is possible to use multiple tank pairs to overcome this problem.

Figure 5.17 shows a MHE that operates with 8 pairs of tanks. In this design, one or more tank pairs can operate simultaneously. Hence, kinetic energy from their flywheels can be added together. With this assembly, when the power output of one tank pair is decreasing, the other pair is at the beginning of operation. Thus, the other pair will add more power to the system, and the exit electric power output will not fluctuate drastically. The other benefit of this system is that there will be more time

vacant for each tank pair to be charged. Figure 5.18 shows the trend of the possible power output of a MHE with two and multiple pairs of tanks.

The lines in Figure 5.18 show the trend of power output from the generator. Lines in Figure 5.18a are not connected to each other and they have dramatic ups and downs with time. The gaps between vertical lines in that graph represent the time gaps where no power is generated by the heat engine. This time gap exists because of the required time for switching the tank pairs. If the valves that switch the tanks can operate faster, this gap will be reduced and more power will be generated by the MHE.

In Figure 5.18b, the line, which shows the power output, is a continuous line and has minor fluctuations in comparison to Figure 5.18a. The curved lines at the bottom of Figure 5.18b represent the power generated by each pair of tank. The overall electric power output in this graph is located at the top of the graph (represented by a continuous line). It is the summation of individual curves. In the next section, effects of using one generator for all heat exchangers and separated generators for each tank pair, in a multiple tank pair configuration will be discussed.

5.7.2.1.1 MHE with Multiple Pairs of Tanks and One Electric Generator

When the MHE operates with multiple pairs of tanks, more than one pair of heat exchangers are operating at the same time, and the torque output from their pistons does not have the same value. This occurs because some are at the beginning of their operation period, and the others are in the last steps of the discharging mode. When the piston energy output is converted to rotary kinetic energy in the flywheel, the angular speed of each flywheel is different. Freewheels can be used to connect each pulley to the shaft. In this way, when the speed of one flywheel reduces, it does

not break the momentum of the other flywheels.

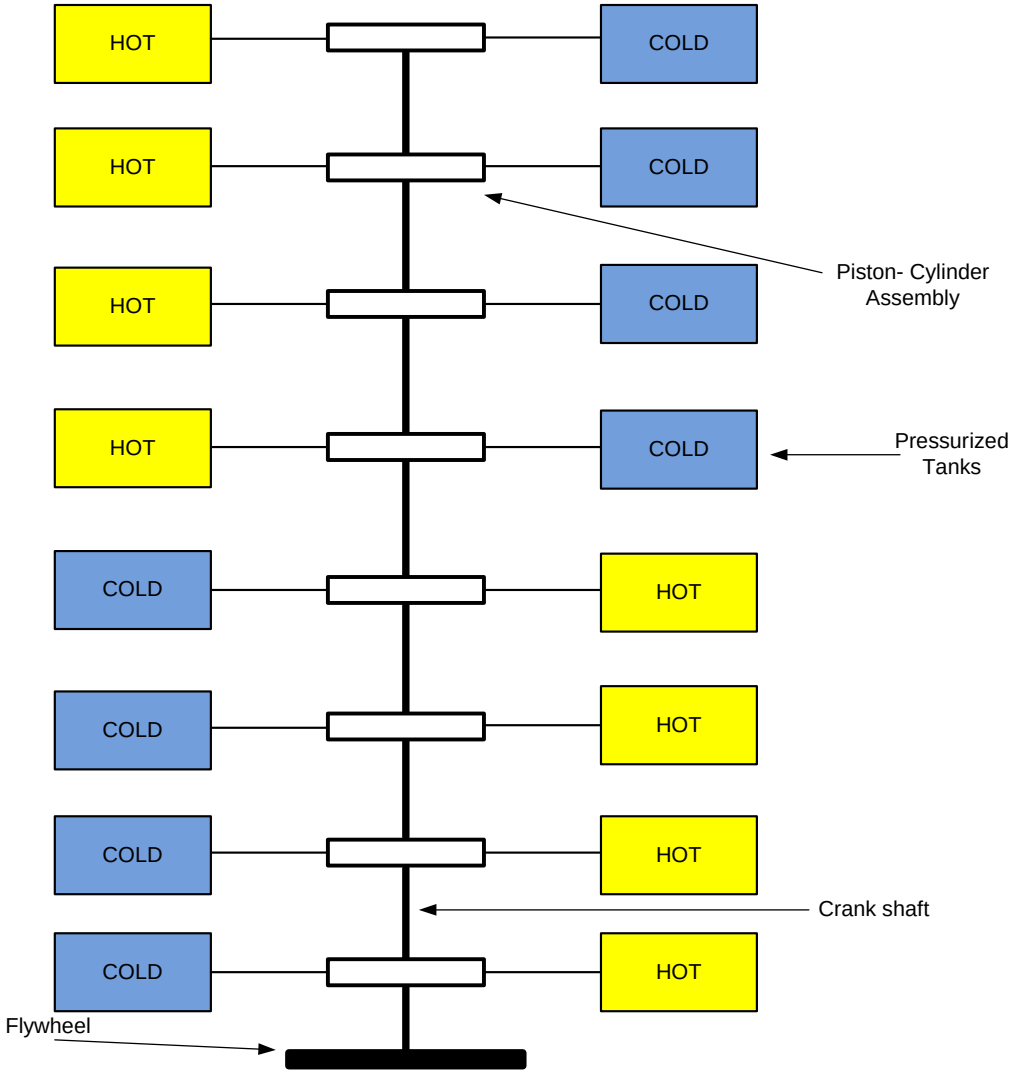

Figure 5.17: MHE with 8 tank pairs.

In this configuration, when the speeds of the individual pulleys are less than the main flywheel speed, no energy is added from that tank pair to the main shaft. In this case, it can be observed that pistons are acting and the connected flywheels are rotating. Nevertheless, no energy is being transferred through the shaft to the flywheel. The weight of the main flywheel, which is connected to the generator, must be optimized in the way that the maximum possible energy from each tank pair is captured.

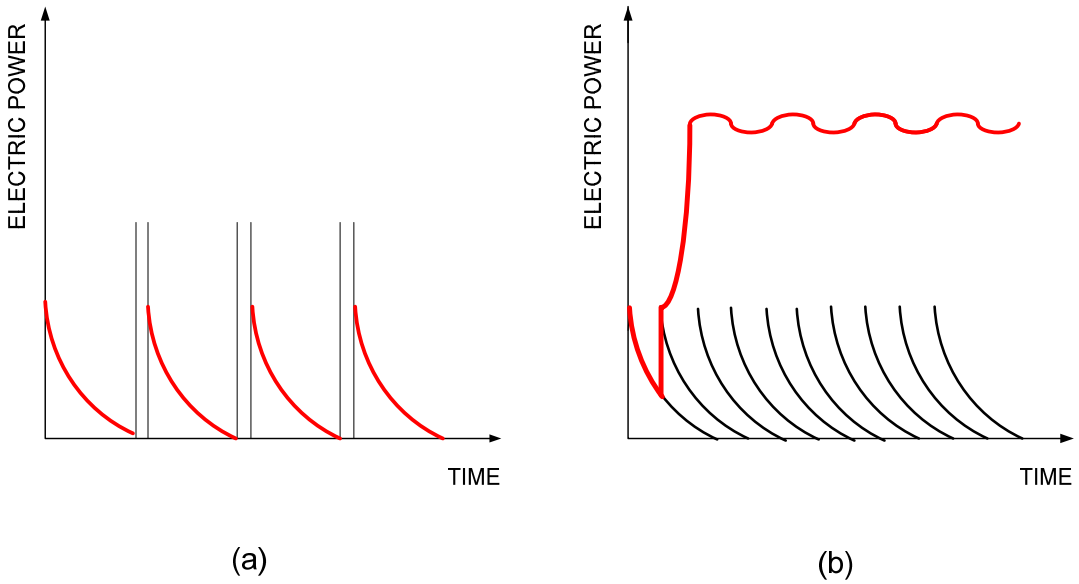

Figure 5.18: Trend of power outputs of an MHE with (a) two and (b) multiple pairs of tanks.

Figure 5.19 shows the transmission system that is required for the MHE with three pairs of tanks. The angular velocities of the pulleys are represented by *W*. When the values of *W1*, *W2*, and *W3* are less than *W*, no power will be added to the main flywheel by that pair. To utilize this wasted energy, an alternative configuration is recommended in section 5.7.2.1.2.

5.7.2.1.2 MHE with Separated Generators

In all configurations of the MHE, it is preferable for heat and mass transfer from the heat source to the heat sink to occur as much as possible. When the cold side with more mass is heated in the next cycle, the resulting pressure differences of the tanks will be higher for the next cycle. Consequently, the torque output of the piston will increase.

With respect to the previous assembly (section 5.7.2.1.1), the last strokes of the piston cannot add to the power output of the main flywheel. A solution to maximize the output energy from the pistons and flywheels is to use separate electric generators for each tank pair. In this design, each piston assembly produces electricity

until the last revolution of the piston. Figure 5.20 shows a schematic of this design. In this figure, only the major transmission components of the assembly are shown.

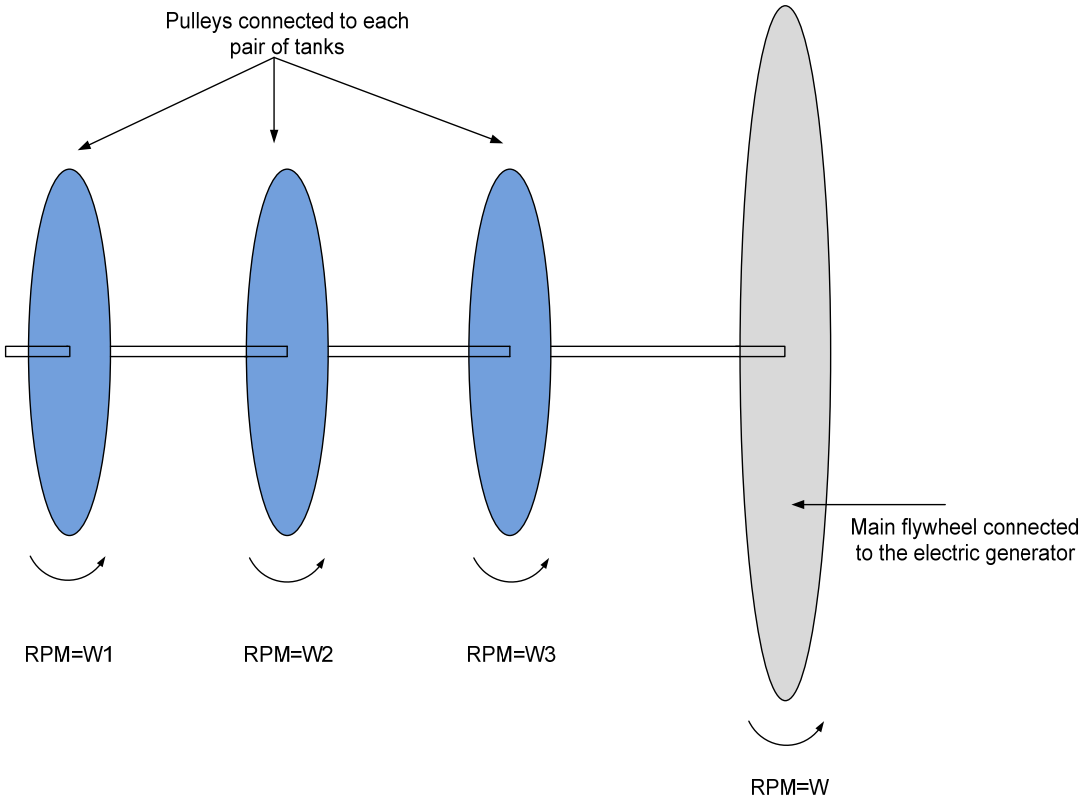

Figure 5.19: Required transmission system for three pairs of tanks.

In addition to energy loss reduction, the other advantage of this system is that the mass of the flywheels can have more variations in comparison to the design specifications in section 5.7.2.1.1. One disadvantage of this design is that due to separate generators, the capital cost of the unit and the maintenance costs are high. The other issue is space limitation, as this system requires larger space for installation.

5.7.3 Marnoch Heat Engine with Hydraulic Motors

In the current MHE, a pneumatic piston is used to produce power from pressure differentials. Another alternative that can be used to convert pressure differentials to mechanical shaft work is a hydraulic system. In this configuration, two external heat

exchangers collect and transfer the heat from the heat source and sink. They are connected to bladder accumulators. Accumulators are half filled with oil and half with pressurised air. Temperature differences in the heat exchangers cause pressure differentials inside heat exchangers, and consequently the accumulators. Figure 5.21 shows the components and connections for this assembly. In the next step, the valves at the bottom of the accumulators are opened and oil moves from the high pressure side to the low pressure side.

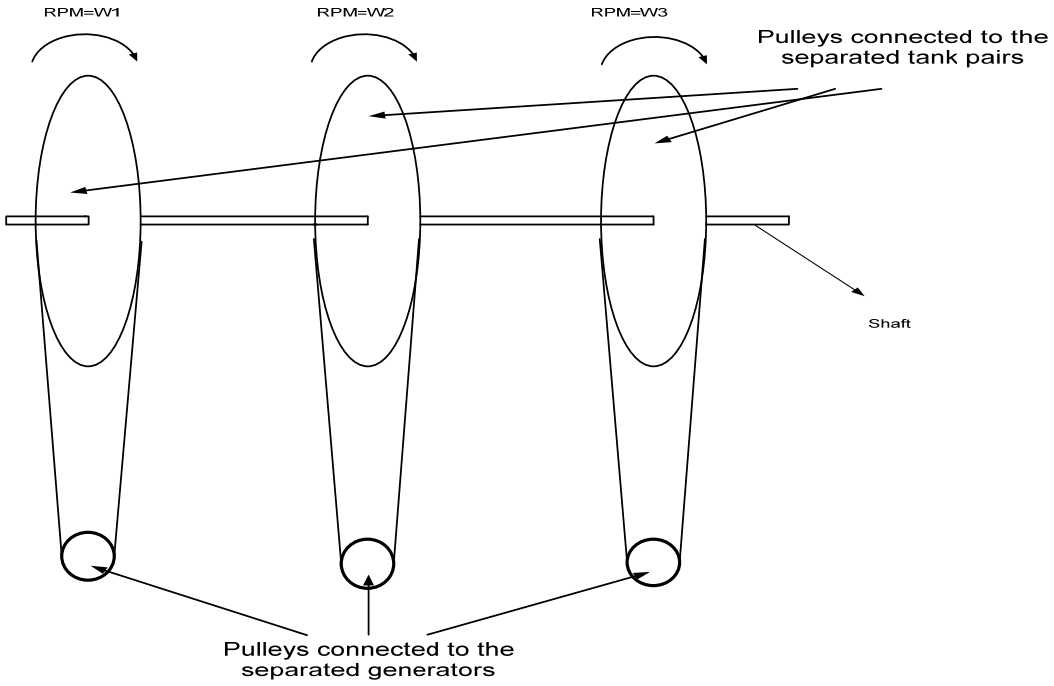

Figure 5.20: Schematic of the MHE with separated electric generators.

A hydraulic motor is installed through the hose, where oil mass transfer is occurring, in order to produce shaft work. This hydraulic motor is connected to an electric generator to produce electricity. With this setup, it is feasible to collect the heat from various sources and to connect each accumulator to more than one heat exchanger.

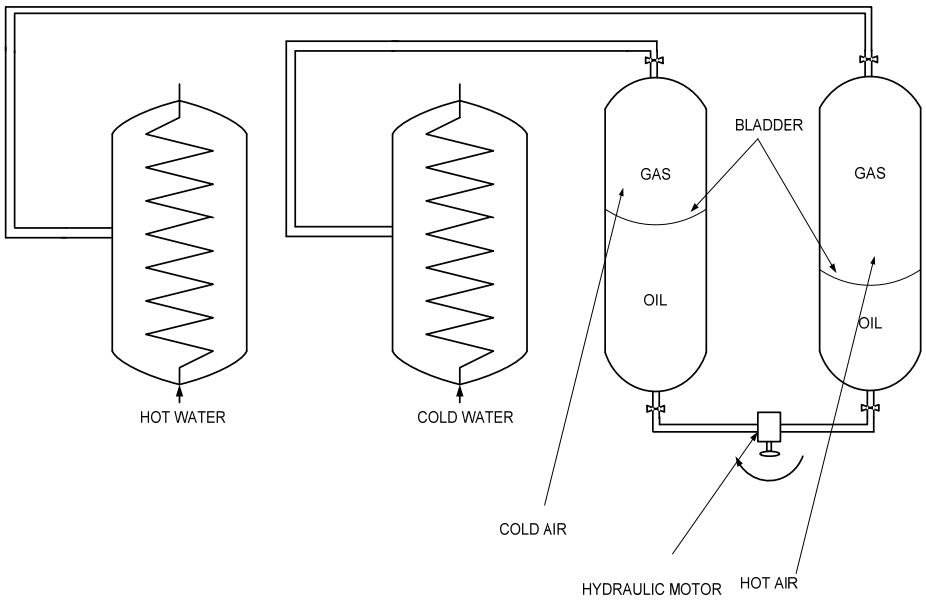

Figure 5.21: MHE with external heat exchangers and hydraulic motor.

In the other alternative setup, heat transfer occurs in the gas section of the heat exchangers. By the application of the internal heat exchangers, the occupied area of the MHE will decrease in comparison to the configuration with external heat exchangers. Thus, for highly compact pressure units, this configuration can be considered.

The advantages of using a hydraulic system in the MHE, in comparison to the pneumatic system, are listed below:

- The noise produced by a hydraulic system is significantly less than a pneumatic system.
- Power consumption by the valves is less than the pneumatic system.
- Durability and operation of valves are better in the hydraulic system.
- It gives a smaller hydraulic system for the same power output.
- Maintaining isothermal expansions and compressions are easier in a hydraulic system, since there is no fast change of mass transfer direction.

- The MHE with a hydraulic system works smoother than an MHE with a pneumatic system. Therefore, it is expected to obtain power output from this system with fewer power fluctuations (Figure 5.23).

Figure 5.23a shows a possible trend of power outputs from the MHE with two pairs of tanks and a hydraulic system. Figure 5.23b depicts the power generation from the MHE with multiple heat exchangers and a hydraulic system.

A preliminary assembly was established in order to observe and study the performance of the hydraulic systems. Figure 5.24 shows an image of the current setup. The maximum pressure that can be used in these bladder accumulators is 20,684 kPa. In the present setup, accumulators were filled with air at 1,034 kPa, since the external heat exchangers were not certified to hold more than 1,034 kPa. The accumulators were filled with five litres of oil. In the current setup, all ball valves were manually operated.

When operation of the system started, the hydraulic motor was rotating smoothly until the existing pressure differential was not able to run the motor. The challenge of this system is friction inside the hydraulic motor. When the pressure difference between tanks was about 68 kPa, the system stopped working. Thus, for further applications, the components of the motor must be altered to reduce the motor friction.

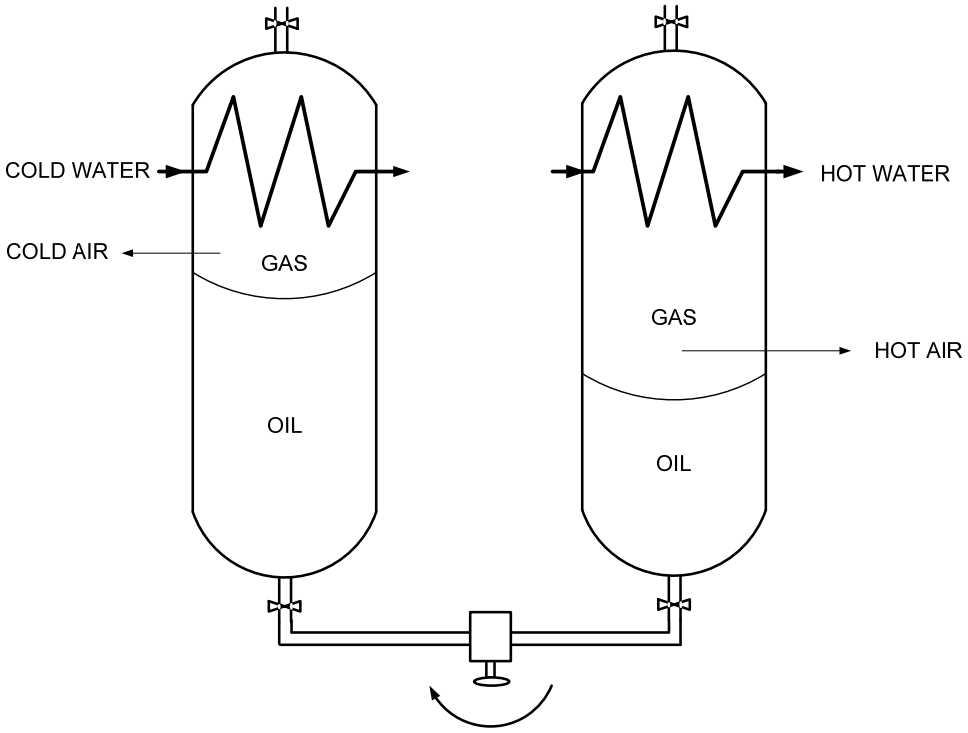

Figure 5.22: Hydraulic assembly of the MHE with internal heat exchangers.

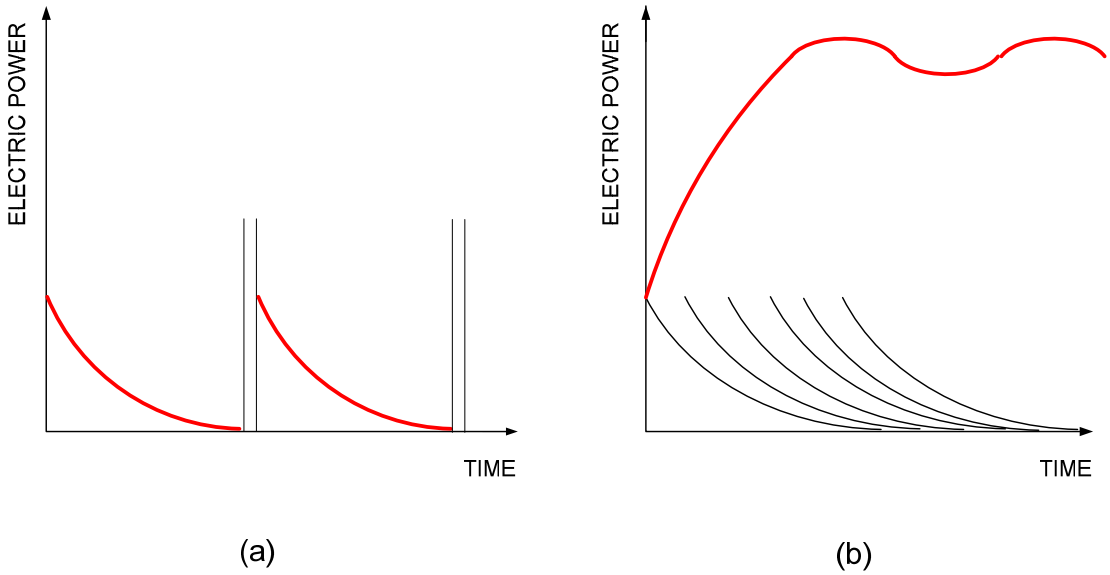

Figure 5.23: Power output of the MHE with accumulators and hydraulic motor.

Figure 5.24: Preliminary assembly of the MHE with accumulators.

Chapter 6:

Conclusions and Recommendations for Future Research

6.1 Conclusions

The Marnoch heat engine is an energy conversion device that has the capability to convert low grade heat to electricity. As described in this thesis, MHEs have good potential for being used in many applications. Its commercialization for stationary applications is promising. The engine can utilize waste heat from nuclear, fossil fuel or renewable fuelled power plants. The main conclusions of this thesis are listed below:

- The engine can operate continually when a suitable heat source and heat sink are available;
- Having higher temperature differentials increases the power output from the MHE;
- For a higher initial pressure in the heat exchangers, there is higher power output; and
- The Marnoch heat engine is commercially viable.

6.2 Recommendations for Future Research

A thorough design optimization is recommended for the system, using computing facilities, to find the optimum parameters such that the best system performance. It is

also recommended to build a flexible prototype to study the system in practice, and validate the theoretical studies in another way as well.

Potential modifications were presented in section 5.7. The following list shows suggested studies to be performed to achieve better performance from the MHE. Moreover, some recommended modifications for the components are also listed below:

- Increasing the piston-cylinder volume when the piston is used for energy conversion;
- Optimizing the flywheel weight for each piston assembly and pressure differential;
- Perform a detailed study on the hydraulic motors for energy conversion;
- Study of different accumulators;
- Finding faster valves using less energy;
- Use of better hoses and joints to decrease the pressure drops as much as possible;
- Use of higher ratio elbows to decrease the friction losses;
- Replacing air with other working fluids which have higher heat transfer coefficients;
- Perform tests with low-temperature differentials to test the performance of the engine;
- Performing a detailed thermo-economic analysis of the MHE.

References

1. Dincer, I., "Renewable energy and sustainable development: a crucial review", *Renewable and Sustainable Energy Reviews*, Vol. 4, pp. 157-175, 2000.

2. Dincer, I., Rosen M. A., "Thermodynamic aspects of renewables and sustainable development", *Renewable and Sustainable Energy Reviews*, Vol. 9, pp. 169-189, 2005.

3. Rasthal, J. E., Drennen,T. E., *Pathways to a Hydrogen Future,* 1st ed., UK: Elsevier, 2007.

4. Etcheverry, J., "Comments Regarding the Ontario Power Authority's (OPA)", Supply Mix Advice Report, David Suzuki Foundation, Toronto, February 2006.

5. EIA, "Emissions of Greenhouse Gases", Report by the Energy Information Administration (EIA), *US Department of Energy,* "http://www.eia.doe.gov/", August 22, 2008.

6. Rahm, D., *Sustainable Energy and the States*, Essay on Politics Markets and Leadership, 1st ed., North Carolina: McFarland, 2002.

7. Anon, A., "World Energy Council, Technical Report", *Global energy perspectives to 2050 and beyond*, London, 1995.

8. Randolf, J., Masters, G. M., *Energy for Sustainability*, 1st ed.,Washington: Island Press, 2008.

9. Tester, J. W., Drake, E. M., Golay, M. W., Peters, W. A., *Sustainable Energy Choosing Among Options*, 1st ed., Massachusetts: MIT Press, 2005.

10."http://www.dauphine.fr/cgemp/Publications/Articles/PAPER%20MOSCOW%20CPZ.pdf", Contribution of coal and nuclear to sustainable energy, supply: perspectives and problems, Dauphine University of Paris, Paper presented at the Russian Academy of Sciences, Academies of Sciences, President's meeting of G8 countries, Brazil, China, India and South Africa, Moscow, April 2006.

11. Caldicott, H., *Nuclear Power is Not the Answer to Global Warming or Anything Else*, 1st ed., New York: The New Press, 2006.

12. Turner, W. C., *Energy Management Handbook*, 5th ed., Washington: The Fairmont Press, 2005.

13. OECD, "http://www.oecd.org/document/", Report by the Organization for Economic Co-opration and Development, Economic, Environmental and Social Statistics, May 12, 2009.

14. Spiro, T. G., Stigliani, W. M., *Environmental Issues in Chemical Perspective*, 1st ed., New York: State University of New York Press ,1980.

15. Beer, J. M., “High efficiency electric power generation, The environmental role”, *Progress in Energy and Combustion Science*, Vol. 33, pp. 107–134, 2007.

16. Ehrlich, K., Konys, J., Heikinheimo, L., “Materials for high performance light water reactors”, *Journal of Nuclear Materials*, Vol. 327, pp. 140–147, 2004.

17. Viswanathan, R., Henry, J. F., Tanzosh, J., Stanko, G., Shingledecker, J., Vitalis, B., Purgert, R, “U.S. program on materials technology for ultra-supercritical coal power Plants”, *ASM International*, Vol. 14, pp. 281-292, 2005.

18. “http://www.berr.gov.uk/files/file30703.pdf”, Brochure, Advanced Power Plant Using High Efficiency Boiler/Turbine, September 25, 2006.

19. Hardel, J., Kassfeldt, E., Prakash, B., “Friction and wear behaviour of high strength boron steel at elevated temperatures of up to 800 ^{o}C”, *Wear*, Vol. 264, pp. 788–799, 2007.

20. Zamrik, S. Y., Renauld, M. L., “Thermo-mechanical out-of-phase fatigue life of overlay coated IN-738LC gas turbine material”, *Thermo-mechanical Fatigue Behavior of Materials*, Vol. 3, pp. 119-137, 2000.

21. Tan, L., Ren, X., Sridharan, K., Allen, T. R., “Corrosion behavior of Ni-base alloys for advanced high temperature water-cooled nuclear plants”, *Corrosion Science*, Vol. 50, pp. 3056–3062, 2008.

22. Was, G. S., Ampornrat, P., Gupta, G., Teysseyre, S., West, E. A., Allen, T. R., Sridharan, K., Tan, L., Chen, Y., Ren, X., Pister, C., “Corrosion and stress corrosion cracking in supercritical water”, *Journal of Nuclear Materials*, Vol. 371, pp. 176–201, 2007.

23. Brown, L. F., “A comparative study of fuels for on-board hydrogen production for fuel-cell-powered automobiles”, *International Journal of Hydrogen Energy*, Vol. 26, pp. 381–397, 2001.

24. Nojoumi, H., Dincer, I., Naterer, G. F., “Greenhouse gas emissions assessment of hydrogen and kerosene-fueled aircraft propulsion*”, International Journal of Hydrogen Energy,* Vol. 34, pp. 1363-1369, 2009.

25. Sesto, E., Casale, C., “Exploitation of wind as an energy source to meet the world's electricity demand”, J*ournal of Wind Engineering and Industrial Aerodynamics*, Vol. 74, pp. 375-387, 1998.

26. Cassedy, E. S., *Prospects for sustainable energy: a critical assessment*, 1st ed., Cambridg: University Press, 2000.

27. Maegaard, P., Bassam, N., *Integrated Renewable Energy for Rural Communities: Planning Guidelines, Technologies and Applications*, 1st ed., UK: Elsevier Science, 2004.

28. Nojoumi, H., “Investigation of a New Bipolar Design for PEM Fuel Cells”, Thesis (MASc), Faculty of Engineering and Applied Science, *University of Ontario Institute of Technology*, Oshawa, Canada, July 2009.

29. MacPhee, D., "Performance investigation of various cold thermal energy storages", Thesis (MASc), Faculty of Engineering and Applied Science, *University of Ontario Institute of Technology*, Oshawa, Canada, July 2008.

30. Reilly, R. W., Zaloudek, F. R., "An assessment of second- generation compressed air energy storage concepts.", Thechnical report for the for the U.S. Department of Energy, Pacific Northwest Laboratory, *Battelle Memorial Institute*, Washington, July 1982.

31. Jubeh, N. M., Najjar, Y. S. H., "Comparison of performance of compressed-air energy-storage plant with compressed-air storage with humidification", Institution of Mechanical Engineers (IMechE), *Power and Energy*, Vol. 220, pp. 581-588, 2005.

32. Gardner, J., Haynes, T., "Overview of compressed air energy storage", Technical Report, *Boise State University*, Boise, Idaho, December 2007.

33. Vieira, F., Ramos, H., "Covas and almeid, pump-storage optimization with renewable energy production in water supply systems", *BHR Group*, Vol. 34, pp. 928-936, 2008.

34. Turnur, R. H., Cengel,Y. A., *Fundamentals of Thermal-Fluid Science*, 2nd ed., New York: Mc Graw Hill, 2006.

35. Daley, J. G., "Stirling engine performance optimization with different working fluids", *Intersociety energy conversion engineering conference*, San Diego, August 25, 1986.

36. Züttel, A., "Materials for hydrogen storage", *Marterials Today*, Vol. 6, pp. 24-33, 2003.

37. Weigel, C., "Alternative Working Fluids for the Marnoch Thermal Energy Conversion Device", *University of Ontario Institute of Technology*, Thesis (BSc), Faculty of Engineering and Applied Science, Oshawa, Canada, April 2008.

38. Rolle, K. C., *Thermodynamics and Heat Power*, 6th ed., Virginia: Pearson/ Prentice Hall, 2005.

39. Sonntag, R. E., Borgan, C., Wylen, G. J., *Fundamentals of Thermodynamics,* 6th ed., New York: Wiley, 2003.

40. Cengel, Y. A., Boles, M. A., *Thermodynamics, An Engineering Approach*,6th ed., New York: McGraw-Hill, 2006.

41. Moran, M. J., Shapiro, H. N., *Fundamentals of Engineering Thermodynamics*, 6th ed., New York: Wiley, 2007.

42. Organ, A. J., Finkelstein, T., *Air engines: the history, science, and reality of the perfect engine*, 1st ed., Michigan: American Society of Mechanical Engineers Press, 2001.

43. www.stirlingengine.com, September 24, 2009.

44. ”http://wood-pellet-ireland.blogspot.com/”, Stirling Engine Reference, Guide and Catalog, September 24, 2009.

45. Kongtragool, B., Wongwises, S., “A review of solar-powered Stirling engines and low temperature differential Stirling engines”, *Renewable and Sustainable Energy Reviews*, Vol. 7, pp. 131–154, 2003.

46. Andersen, Kildegard, S., “Numerical Simulation of Cyclic Thermodynamic Processes”, Thesis (Ph.D), Department of Mechanical Engineering, Energy Engineering, *Technical University of Denmark*, Lyngby, Copenhagen, March 2006.

47. Berchowitz, D. M., Shonder, J., “*Estimated size and performance of a natural gas fired duplex stirling for domestic refrigiration applications*”, Technical report, Oak Ridge National Labs, Oak Ridge, Tennessee, U. S. A, October 2008.

48. Karabulut, H., Aksoy, F., Ozturk, E., “Thermodynamic analysis of a Betta type Stirling engine with a displacer driving mechanism by means of a lever”, *Renewable Energy*, Vol. 34, pp. 202-208, 2009.

49. Eid, E., “Performance of a beta-configuration heat engine having a regenerative displacer”, *Renewable Energy*, Vol. 34, pp. 2404-2413, 2009.

50. Parlak, N., Wager, A., Elsener, M., Soyan, H. S., “Thermodynamid analysis of a gmma type stirling engine in non-ideal adiabatic conditions*”, Renewable Energy*, Vol. 34, pp. 266-273, 2009.

51. Abdullah, S., Yousif, B. F., Sopian, K., “Design consideration of lowtemperature differential double-acting Stirling engine for solar application”, *Renewable Energy,* pp. 1923–1941, 2005.

52. Kongtragool, B., Wongwieses, S., “A four power-piston low-temparature differential Stirling engine using simulated solar energy as heat source”, *Solar Energy*, 2008, Vol. 82, pp. 493-500.

53. Senft, J. R., *Mechanical Efficiency of Heat Engines.,* 1st ed., New York: Cambridge University Press, 2007.

54. Marnoch, I., Naterer, G., Rosen, M. A., Weston, J., “Marnoch engine Performance for multiple pressure vessel configurations”, *International Conference on Efficiency, Cost, Optimization, Simulation and Environmental Impact of Energy Systems*, Istanbul, July 2008.

55. Chukwu, C. C., Naterer, G. F., Rosen, M. A., Dahlquist, E, Marnoch, I. A., “Thermal optimization and economic analysis of a Marnoch heat engine” *Swedish National Energy Convention,* Toronto, March 12-13, 2008.

56.“http://www.potashcorp.com/media/pdf/about/brochure/PCS_Mini_Mine_Tour_brochure.pdf”, Down Under, A mini tour, May 14, 2009.

57. Marnoch, I. A., *Thermal conversion device and process,* Patent Number 4389858, Canada, Jun 5, 2008.

58. Munson, B. R., Young, B. J., Okishi,T. H., *Fundamentals of Fluid Mechanics*,5th ed., New York: Wiley, 2005.

59. *Pneumatic Automation Products*, Manufacturer Catalogue, USA: Parker Hannifan Corporation, 2001.

60. Dincer, I., Rosen. M.A., *Exergy: Energy, Environment and Sustainable Development* , 1st ed., Elsevier, 2007.

61. Armstrong, A., Haseen, F., Marnoch, I., Weston, J., Naterer, G. F., Lu, L., Rosen, M. A. "Thermodynamic Design and Control of a Marnoch Thermal Energy Conversion Device*", Proceedings of 21st Canadian Congress of Applied Mechanics*, Toronto, Canada, pp. 284-285, June 2007.

62. Self, S., "Power Testing of the Prototypical Marnoch Thermal Energy Conversion Device", Thesis (BSc), Faculty of Engineering and Applied Science, *University of Ontario Institue of Technology*, Oshawa, Canada, April 2008.

63. Naterer, G. F., "Second law viability of upgrading waste heat for thermochemical hydrogen production", *International Journal of Hydrogen Energy*, Vol. 33, pp. 6037-6045, 2008.